A MAGNETIC FIELD ENERGY HARVESTER FOR ENERGIZING WIRELESS SENSORS IN ELECTRIC RAILWAYS

HERATH MUDIYANSELAGE DINUSHA DILHAN NAWARATHNE

MPhil

The Hong Kong Polytechnic University

2025

The Hong Kong Polytechnic University

Department of Electrical and Electronic Engineering

A Magnetic Field Energy Harvester for Energizing Wireless Sensors in Electric Railways

Herath Mudiyanselage Dinusha Dilhan Nawarathne

A thesis submitted in partial fulfilment of the requirement for the degree of Master of Philosophy

April 2025

CERTIFICATE OF ORIGINALITY

I hereby declare that this thesis is my own work and that, to the best of my knowledge and belief, it reproduces no material previously published or written, nor material that has been accepted for the award of any other degree or diploma, except where due acknowledgement has been made in the text.

(Signed)

Herath Mudiyanselage Dinusha Dilhan Nawarathne

(Name of student)

DEDICATION

I wholeheartedly dedicate this thesis to my parents, my pillars of success

Amma and Appachchi

ABSTRACT

Advancements in technology have encouraged modern railway transportation systems to adopt real-time monitoring solutions to enhance operational efficiency, reliability, and passenger safety. Among these, condition monitoring systems play a critical role by utilizing sensor networks to detect faults and degradation proactively. The accuracy and effectiveness of such systems depend heavily on the availability of comprehensive sensor data. Wireless sensor networks (WSNs) offer an optimal solution for deploying diverse amounts of sensors in remote locations, enabling wireless data transmission without extensive infrastructure.

However, the large-scale deployment of WSNs faces a significant limitation due to the finite energy capacity and lifespan of conventional electrochemical batteries used to power sensor nodes. Energy harvesting techniques present a promising alternative to powering autonomous devices in WSNs by utilizing ambient energy sources to sustain their continuous operation. In electric railways, the magnetic fields generated around current-carrying conductors represent a particularly viable energy source. Unlike alternative energy sources, magnetic field energy is independent of weather conditions and can be harvested by employing non-intrusive methods without interfering with railway operations.

This study presents a comprehensive investigation into the design, development, and validation of a free-standing magnetic field energy harvester (MFEH) for powering autonomous sensors and devices in WSNs deployed in electric railways. The research contributes two key advancements to the magnetic field energy harvesting field: (1) Development of a practical MFEH capable of being deployed adjacent to rail tracks while delivering sufficient power for wireless sensors, and (2) Implementation of a power management circuit that maximizes power delivery to DC loads under varying operating conditions.

The design of the MFEH was optimized through parametric finite element method (FEM) simulations, focusing on optimizing core geometry and coil parameters while minimizing associated loss mechanisms. The design process incorporated strategies to minimize core losses and eddy current losses induced by proximity to ferromagnetic rail tracks. Simulation results provided critical insights into loss reduction and output power enhancement. Following the conclusions derived using simulation analyses, a prototype MFEH was fabricated and validated

under AC load conditions, achieving a maximum power output of 4 W. Since WSN loads operate in DC mode, a power management unit was designed, comprising a full-bridge rectifier and a four-switch buck-boost (FSBB) converter. The conditions for maximum power extraction through the FSBB converter were derived through a theoretical analysis, which was experimentally verified through integrated MFEH system testing. The final implementation demonstrated a maximum DC power output of 3.27 W at a rail current of 450 A. The FSBB converter showcased its power management capacity by delivering maximum power output across varying load and rail current conditions by adjusting its duty cycle.

This thesis successfully presents an efficient, free-standing MFEH unit developed capable of energizing wireless sensors and autonomous devices employed in electric railway applications. The study demonstrates significant improvements over existing solutions and provides actionable guidelines for further advancing magnetic field energy harvesting in railway environments.

ACKNOWLEDGEMENTS

I would like to express my deepest gratitude to my chief supervisor, Professor C.Y. Chung for providing me with the invaluable opportunity to undertake this research and for his unwavering guidance and mentorship throughout this study. I am also sincerely grateful to Dr. Liu Junwei for his continuous support and constructive advice, which greatly contributed to achieving the objectives of this research. My sincere thanks also go to Professor H.Y. Tam for his recommendation and encouragement, which made this research journey possible.

I extend my wholehearted gratitude to my parents for their unwavering support through every step in my life. I am forever grateful for all their sacrifices made to ensure my success.

I express my heartfelt appreciation to my beloved wife, Dineshi, for her stedfast support throughout this endeavour. Her encouragement has been my greatest strength.

Lastly, I am forever grateful to my alma mater, Kingswood College Kandy for shaping me into the individual that I am today.

KFE

TABLE OF CONTENTS

LIST OF FIGURES

LIST OF TABLES

CHAPTER 1 INTRODUCTION

1.1 Background

1.1.1 Energy Harvesting

Energy harvesting, also referred to as energy scavenging, is the process of capturing energy from the surrounding environment and converting it into usable electrical energy. Although energy harvesting shares conceptual similarities with large-scale renewable energy generation, they serve distinct applications and operate in significantly different power levels. Utility-scale renewable energy systems generate megawatt-scale power for electrical grid distribution, while energy harvesting systems are designed to power autonomous microelectronic devices such as wireless sensors, wearables and IoT devices. Even in most optimized configurations, energy harvesting systems typically generate power in the milliwatt to watt level, with the primary objective of enabling battery-free operation of low-power applications.

The concept of energy harvesting gained popularity with the widespread adoption of wireless sensors across various industries. The rapid advancement of technology has elevated data to a valuable commodity, driving increased use of sensors to capture richer datasets. Unlike conventional sensors, wireless sensor networks (WSNs) consist of distributed nodes that communicate, collaborate, and aggregate information. This networked approach provides end users with significantly enhanced information, data intelligence and system flexibility [1].

By definition, wireless sensors cannot rely on conventional wired power sources and instead require localized energy solutions. While electrochemical batteries are conventionally used to fulfil the energy requirement of WSNs, their limited capacity, frequent need for replacements, accessibility requirements for replacements and maintenance introduce operational complexities and usability issues. Furthermore, accessibility requirements may compromise optimal sensor positioning and performance. The environmental impact arising from the proliferation of electrochemical batteries and their disposal presents further concerns. Energy harvesting techniques offer a sustainable alternative to address these issues by extracting ambient energy from the environment to power these systems autonomously.

Energy harvesting systems are designed to extract ambient energy from diverse environmental energy sources and convert it to usable electrical energy. Most commonly used energy sources for energy harvesting include kinetic, solar, wind, thermal, and magnetic field energy. Kinetic energy represents one of the omnipresent energy sources that exist in various forms such as structural vibrations, human motion and fluid flows. Various transduction mechanisms have been developed for kinetic energy harvesting, including piezoelectric, turboelectric, and electromagnetic conversion techniques [2]. Solar energy harvesting primarily relies on photovoltaics at a smaller scale, though its applicability depends on the availability of sunlight. Wind energy harvesting systems typically use micro-turbines to capture naturally occurring wind or process-induced airflow. Thermoelectric energy harvesting offers potential for utilizing waste thermal energy, converting thermal gradients into electrical energy through the Seebeck effect [3,4]. Magnetic field energy harvesting extracts energy from magnetic fields generated by current-carrying conductors, enabling power generation for a wide range of applications [5,6]. As extensively documented in the literature, energy harvesting is poised to become a fundamental enabler of wireless sensing across various systems. The growing demand for these systems over time is driven by the continuous development of ultra-low-power sensors, advanced instrumentation, and emerging wireless technologies.

1.1.2 Electric Railways and Wireless Sensor Networks

Transportation networks serve as a critical foundation for economic development that directly influences the operational efficiency and productivity of a country. As an essential component of modern society, transportation systems should accommodate sector-specific requirements. For example, manufacturing industries depend on reliable logistics for the distribution of goods, the service sector prioritises transportation requirements of their employees, and construction industries seek cost-effective material transportation facilities. Amongst various transportation modes, railways emerge as a vital system that offers scalable solutions to these multifaceted global transportation demands.

Multiple compelling factors, including improved efficiency, better operational reliability, greater flexibility, simplified maintenance requirements and improved environmental sustainability, have driven the global transition from conventional fossil fuel-based railways to electrified railway systems. According to Forbes [7], leading economies including China, India,

Japan, Australia and European nations have electrified more than 50% of their railway networks. Electric railways typically employ independent power supply systems utilizing either alternating current (AC) or direct current (DC) configurations selected based on specific service requirements and operational parameters. However, despite the technological advancements, railway systems remain susceptible to frequent faults and breakdowns due to their dynamic operating conditions. These undetected faults and anomalies in railroads not only disrupt normal operations but also pose significant risks, potentially escalating into disastrous consequences and jeopardizing passenger safety. Therefore, proactively identifying and addressing anomalies, faults, and degradations in railway systems is essential.

Generally, preventive maintenance is conducted in railway systems to detect and mitigate equipment defects. This time-based or usage-triggered approach follows a predetermined schedule, which includes systematic inspection sequences such as lubrication, component replacement and cleaning, all carried out by qualified technicians [8]. In contrast, smart maintenance technologies that have been introduced to the railway industries utilize data-driven methodologies in fault detection, anomaly identification and predictive trend analysis that indicate potential malfunctions [9,10]. Modern smart maintenance systems employ condition-based monitoring strategies by deploying sensor networks to track critical parameters such as vibration spectra, thermal profiles, strain/stress distributions, displacement metrics, etc., across key infrastructure components [11–13]. This data-driven narrative has put WSNs under the spotlight in the field of condition monitoring in the railway industry, as they inherit a network that can provide a continuous supply of data with attractive cost benefits [14]. In addition, the interest demonstrated by some of the railway authorities in implementing advanced condition monitoring techniques to improve operational safety and service reliability has provided the opportunity for integration of WSNs in railway systems across the globe [15,16].

However, WSNs face a major challenge in ensuring a stable, reliable and continuous power supply as conventional use of electrochemical batteries is constrained by their finite energy availability [17,18]. The reliance on batteries for powering WSNs fundamentally compromises their deployment flexibility as battery-powered nodes require placement in easily accessible locations for periodic maintenance and replacement. Furthermore, reliance on electrochemical batteries imposes a significant maintenance burden and an additional cost, as they require regular inspections and timely replacements to ensure uninterrupted operation [19,20].

Therefore, these limitations can be addressed by implementing energy harvesting techniques to power WSNs deployed in railway systems. As illustrated in Fig. 1-1 various components in WSNs can be powered by sustainable local power supplies using energy harvesting mechanisms to enable continuous autonomous operation. This approach eliminates the requirement for periodic maintenance and reduces the environmental impact through reduced disposal of electrochemical batteries, thereby ultimately aiding in reducing the carbon footprint.

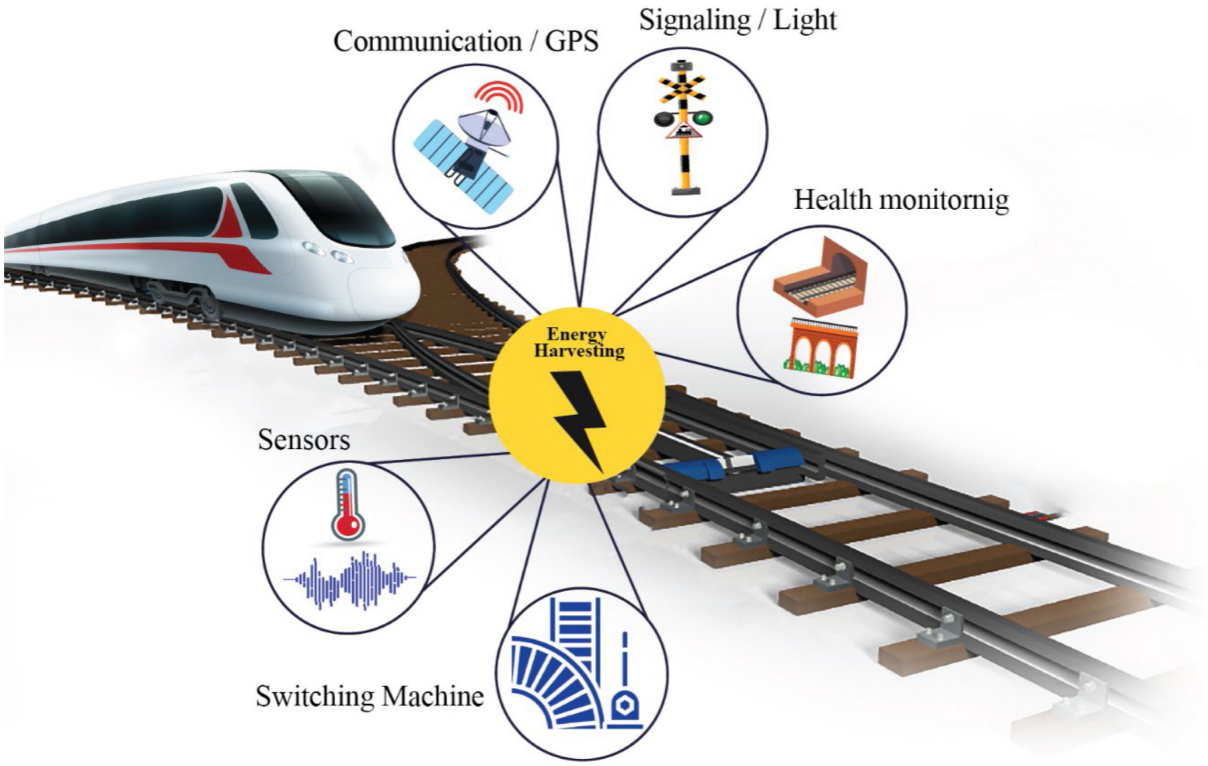

Fig. 1-1: Requirement of energy harvesting in the railway industry [21]

1.2 Energy Harvesting in Electric Railways

1.2.1 Energy Harvesting Methods Used in Electric Railways

Electric railway systems, widely deployed in urban areas, provide an efficient and reliable transportation service for commuters. To ensure their continued productivity, efficiency, and reliability, these systems require extensive maintenance. With technological advancements, traditional maintenance approaches have evolved into condition monitoring systems equipped with numerous sensors to track various parameters across railway infrastructure. As a result, WSNs have emerged as a critical technology enabling real-time condition monitoring in electric railways [22].

In recent years, the growing interest in employing WSNs in railway networks has inspired significant research towards applying various energy harvesting techniques that aim to address the power requirement of WSNs by scavenging ambient energy sources present in railway environments, such as solar, wind, vibration and magnetic field energy [23]. Given the variety of renewable energy sources present in these settings, energy harvesting presents a promising solution for providing a sustainable power supply to WSNs.

While there are numerous studies that have explored energy harvesting in railways, a few of the recent studies are compared in this section to establish a foundational understanding. Solar energy, being the most abundant energy source globally, has also been utilized for powering small-scale autonomous applications in railways. For instance, Cii *et al.* [24] (2020) demonstrated a solar powered wireless sensor node for freight trains, enabling autonomous operation. Hao *et al.* [25] (2021) proposed a foldable photovoltaic unit mounted alongside railroads to power trackside equipment in outdoor environments. However, despite its high energy yield, solar energy harvesting in electric railway networks faces significant limitations due to its dependence on weather conditions, diurnal variability and incompatibility with underground sections. Although integration of energy storage can mitigate nighttime shortages, the inherent inability to harvest solar power in tunnels and subterranean networks restricts its applicability. Given that railway systems often span both aboveground and underground segments, this poses a critical challenge for relying solely on solar energy.

Similar to solar energy, wind energy harvesting in railway systems faces inherent limitations due to its reliance on weather conditions and the absence of natural wind in subterranean sections. However, recent research has explored innovative solutions to harness wind energy generated by train motion, converting it into electrical energy through mechanical propellers. For example, Pan *et al*. [26] developed a novel rotor mechanism to capture train-induced wind energy within tunnels and convert it to electrical energy, enabling self-powered railway applications. In a subsequent study, Pan *et al*. [27] introduced an energy harvesting system that consists of a porous barrier wall equipped with multiple wind turbines (Fig. 1-2) to optimize wind energy harvesting in railway systems. To further enhance the reliability and power output, a hybrid energy harvesting system that consists of both solar and wind energy harvesting techniques was presented by Tairab et al. (2023) [28]. Despite these advancements, a major drawback of wind energy harvesting systems is the susceptibility of wind turbines to wear and tear, which requires frequent maintenance and operational oversight.

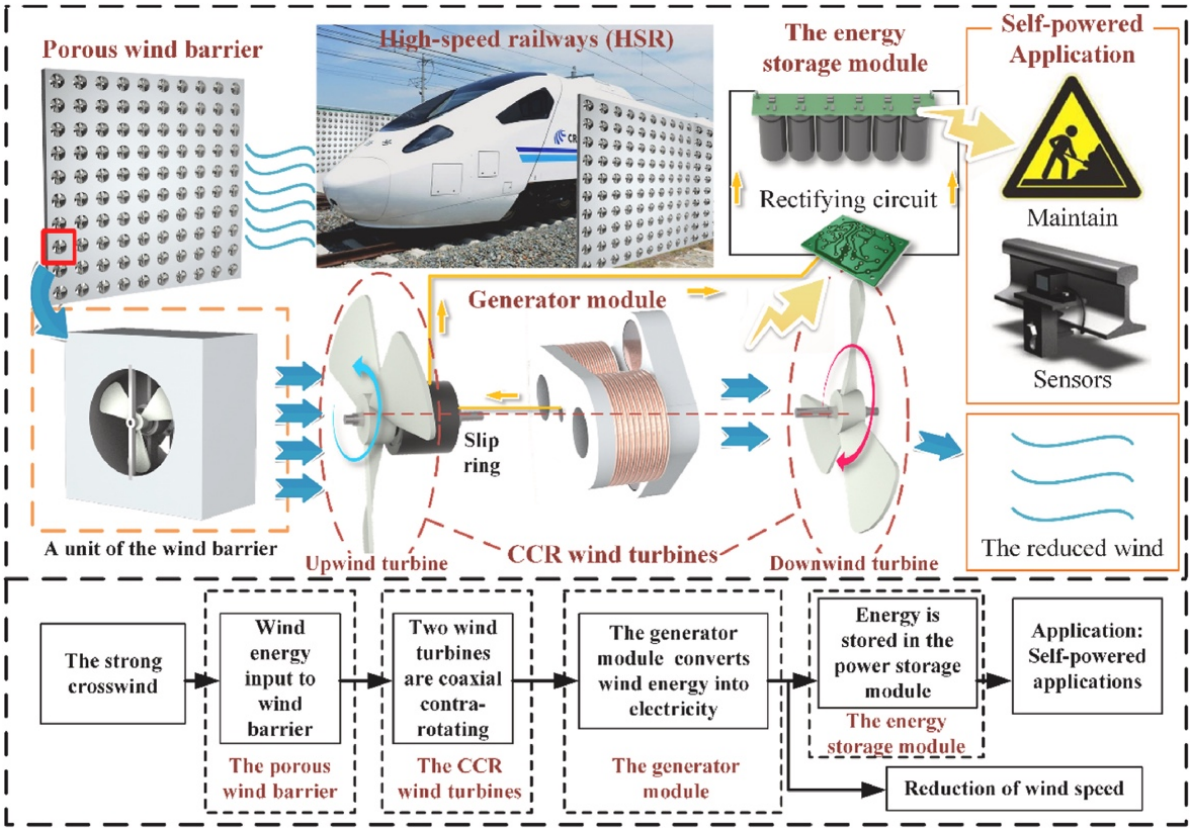

Fig. 1-2 Flow chart of a wind energy harvesting system proposed in [27]

Some recent studies have explored extracting vibration and thermal energy from railway systems. Vibration and thermoelectric energy harvesting are promising alternatives, particularly suited to dynamic railway environments. Train-induced vibrations, which are consistently present in rail systems, offer a reliable energy source for harvesting. Various transduction mechanisms have been investigated, including electromagnetic, piezoelectric, and triboelectric approaches.

Electromagnetic vibration harvesters operate on Faraday's law of induction, where flux variations are induced by mechanical vibrations via permanent magnets coupled to linear or rotational generators [29–32]. For instance Fig. 1-3 and Fig. 1-4 illustrate a linear [33] and a rotary [34] electromagnetic energy harvesting system, designed to harness vibration energy from railroads. The linear electromagnetic energy harvesting system operates on vertical displacement principles, where a permanent magnet oscillates within a coil to induce flux variations directly from rail vibrations. In contrast, in the rotary energy harvesting system, the rail vibrations are converted into rotational motion through a gear assembly, which then drives an electrical generator. While these systems demonstrate promising results and provide future research directions, their effectiveness is constrained by reliance on complex mechanical structures, which may limit practical deployment.

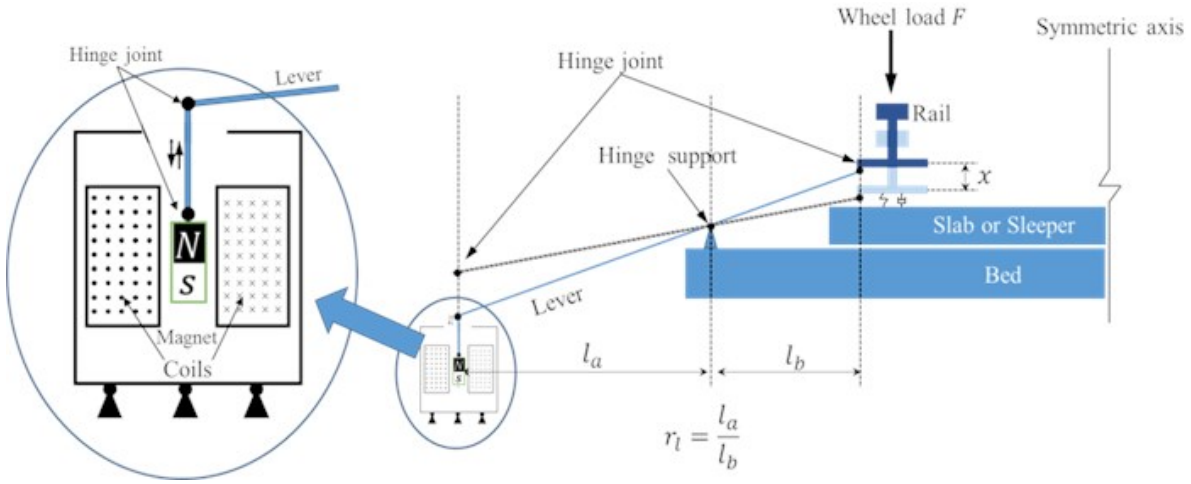

Fig. 1-3 A linear electromagnetic energy harvesting system [33]

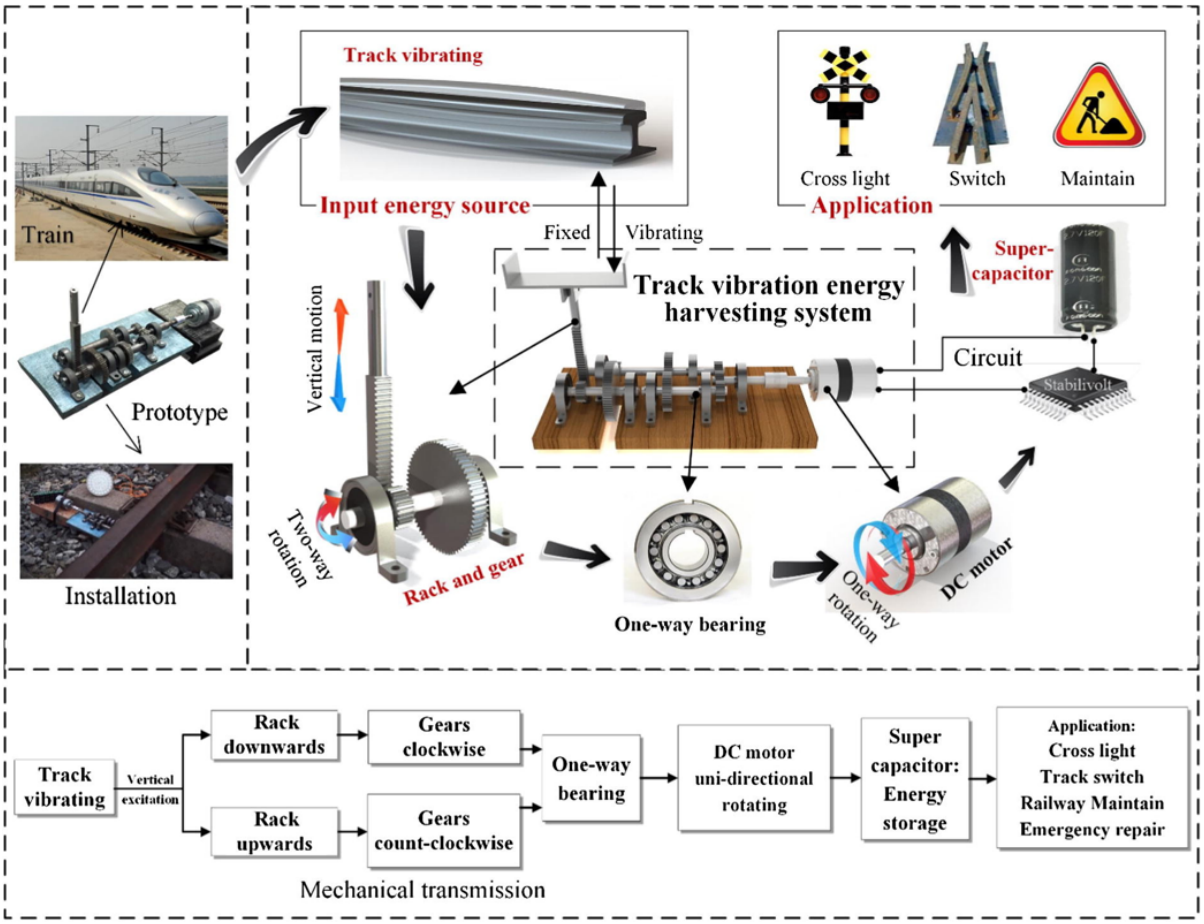

Fig. 1-4 Rotary electromagnetic energy harvesting system [34]

The piezoelectric energy harvesting method uses the direct piezoelectric effect, where certain materials generate an electrical charge when subjected to external mechanical stress from vibrations or movements. This approach has been implemented using several harvester configurations designed to optimize the energy conversion efficiency, including cantilever type, stacked type, circular type and bilateral fixed type harvesters [35–38]. For instance, Wang *et al*. [39] developed a piezoelectric stack energy harvesting device, illustrated in Fig. 1-5. As shown in the figure, the device requires direct physical contact with rail infrastructure, significantly complicating installation and potentially limiting practical deployment in operational railway environments.

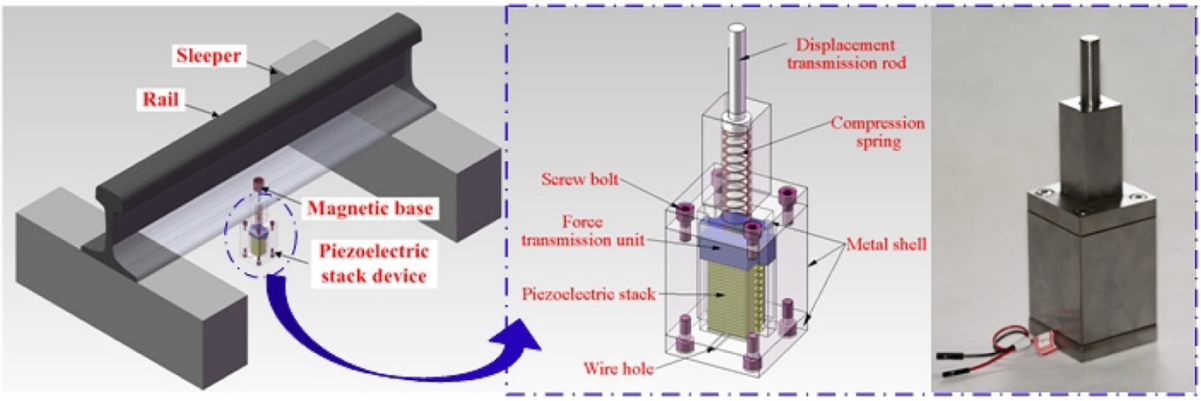

Fig. 1-5 A stacked type piezoelectric energy harvesting device [39]

Apart from the aforementioned two main popular transduction mechanisms employed in vibration energy harvesting, there are other mechanisms, such as triboelectric harvesters and hydraulic harvesters, that utilize vibration energy in railroads [40]. Triboelectric energy harvesters operate based on the triboelectric effect, wherein two distinct materials generate opposite electrical charge through repeated contact and separation cycles. Fundamentally, these energy harvesting systems utilize mechanical movements induced by vibrations to drive relative motion between triboelectric layers and convert resulting charge separation to electrical energy via triboelectric nanogenerators (TENG) [41–43]. Fig. 1-6 illustrates two fundamental TENG configurations and their operational modes: one employing a double-electrode design for three distinct types of motion, and the other utilizing a single-electrode configuration.

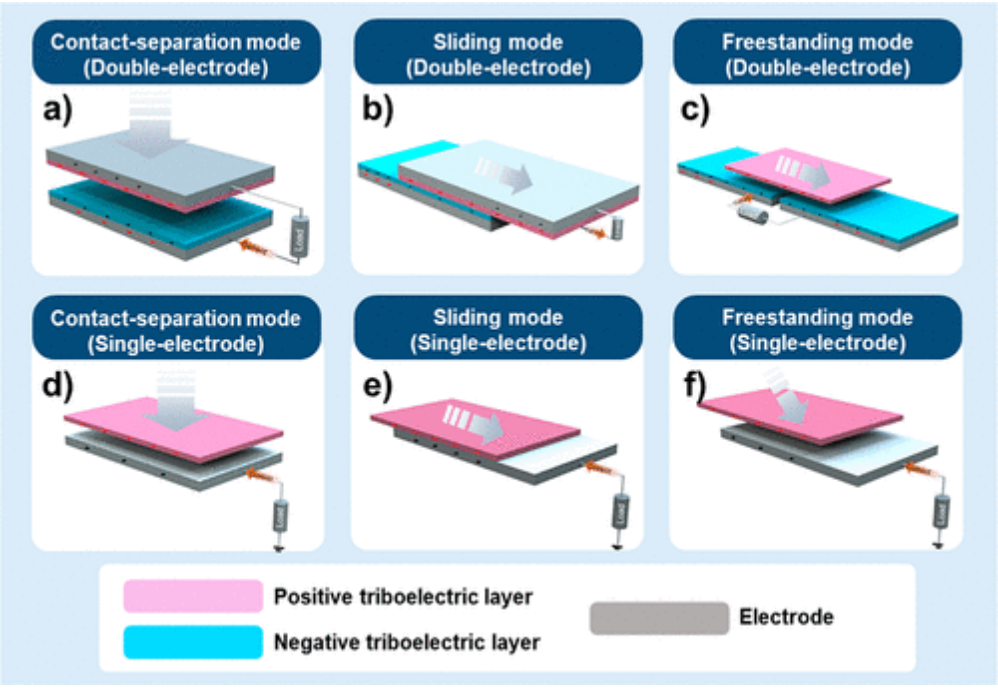

Fig. 1-6 Two basic structures for triboelectric nanogenerators with three working modes [43]

Although railway environments provide abundant vibration energy sources, all vibration energy harvesting techniques share fundamental limitations. Vibration energy harvesting techniques require a mechanical coupling to the infrastructure to transfer train-induced vibration energy to an electrical form. The requirement of structural integration adds installation complexity to the energy harvesting system. In addition, the complex mechanical structures and moving components employed in various vibration energy harvesting systems require regular maintenance due to wear and tear. Furthermore, some of these systems demonstrate low energy conversion efficiency under operational conditions, while the lifecycle costs associated with installation and maintenance often exceed the energy benefits obtained.

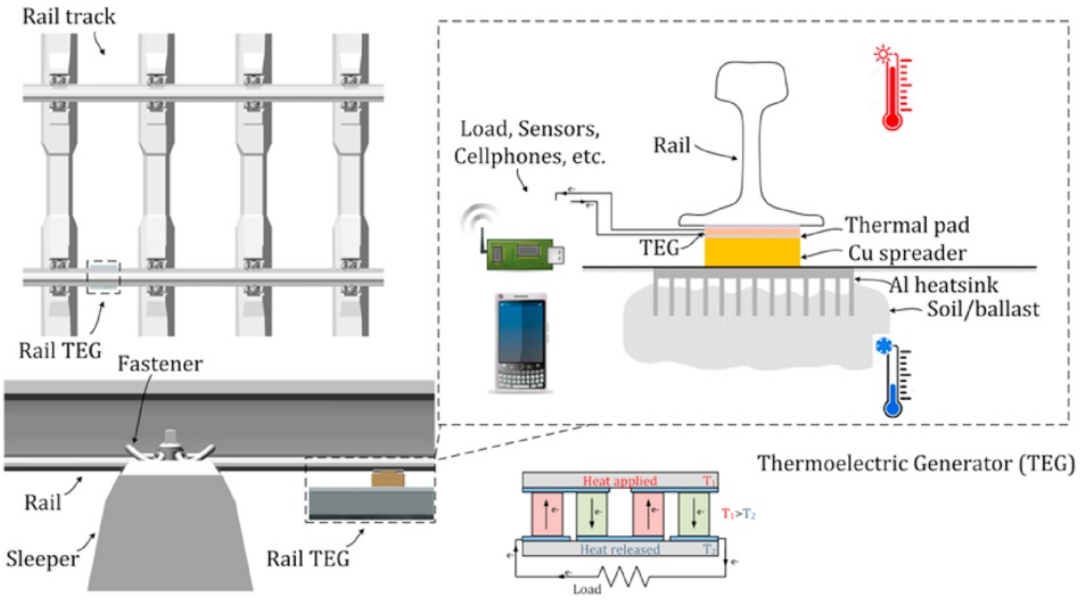

Fig. 1-7 Thermoelectric energy harvesting using the temperature gradients in railway infrastructure [44]

Thermoelectric energy harvesting is another energy harvesting technique that has been documented in literature for powering wireless components. This approach utilizes the Seebeck effect to convert thermal gradients into electrical energy. In typical railway environments, temperature gradients formed between heated rail tracks due to sun exposure and cooler underlayment are extracted by using a thermoelectric generator as illustrated in Fig. 1-7. However, similar to vibration energy harvesting methods, the thermoelectric energy harvesting technique also requires physical integration with the railway infrastructure, introducing installation complexities and ongoing maintenance requirements to maintain optimal thermal contact. In addition, the practical implementation of this technology faces significant limitations due to comparatively low power outputs [45,46]. The intermittent nature of

thermally induced power generation, dependence on environmental conditions and cost of efficient thermoelectric material further worsen the limitations of this energy harvesting method.

In addition to solar, wind, vibration and thermal energy sources present in electric railways, another promising yet often overlooked energy source is magnetic field energy. Magnetic fields are inherently generated around current-carrying conductors, which are typically present in electric railway environments, such as close to overhead power lines, third rails and return current rail tracks. When traction currents are in the form of AC, the fluctuating magnetic fields produced in the vicinity of these current-carrying conductors can be converted into usable electricity. The fundamental principle behind this technique lies in converting magnetic field energy into usable electrical energy through inductive coupling techniques that follow Faraday's laws of induction. Magnetic field energy harvesting has been explored in various other domains, such as overhead transmission lines, power distribution substations, domestic power lines, power conducting busbars, etc. [47–51]. Given the diversity of potential application scenarios, various magnetic field energy harvesting methods have been developed with distinct characteristics and advantages. A thorough examination of these techniques is essential to identify optimal strategies for maximizing output power and increasing the feasibility of harnessing magnetic field energy that can be implemented in electric railway systems.

The techniques used for scavenging magnetic field energy offer several significant advantages that make them particularly suitable for electric railway applications. A key benefit lies in their non-intrusive nature, as the energy harvester operates without direct contact with railway infrastructure, ensuring minimal interference with the normal operation of the railway network. Additionally, the abundance of magnetic field energy in electrified railway environments allows for efficient energy harvesting, which can in turn provide a continuous power supply to connected loads. The absence of moving parts in magnetic field energy harvesters (MFEHs) further enhances their practicality by reducing maintenance demands and operational costs. Given these advantages, further in-depth investigation into the mechanisms employed for magnetic field energy harvesting is necessary to better understand their potential and optimize their performance within electric railway systems.

1.2.2 Magnetic Field Energy Harvesting in Electric Railways

In electrified railway systems, electric power is used for the propulsion of locomotives. These systems typically purchase electricity from electric utility providers, which is then transmitted through the railway network and distributed to trains. The dedicated power supply systems in various electric railway systems may vary between AC and DC systems due to various technical and operational requirements. AC traction power systems exhibit variations in both voltage magnitude and frequency across different regions and countries. For instance, Finland uses a 25 kV, 50 Hz system while Switzerland operates using a 15 kV, 16.7 Hz system. In contrast, DC traction power systems operate at different voltage levels ranging from 750 V to 3000 V across the world [52,53]. For example, Belgium, Spain and Italy employ 3000 V DC traction power supply systems, while some Japanese railways use a 1500 V DC system [54,55].

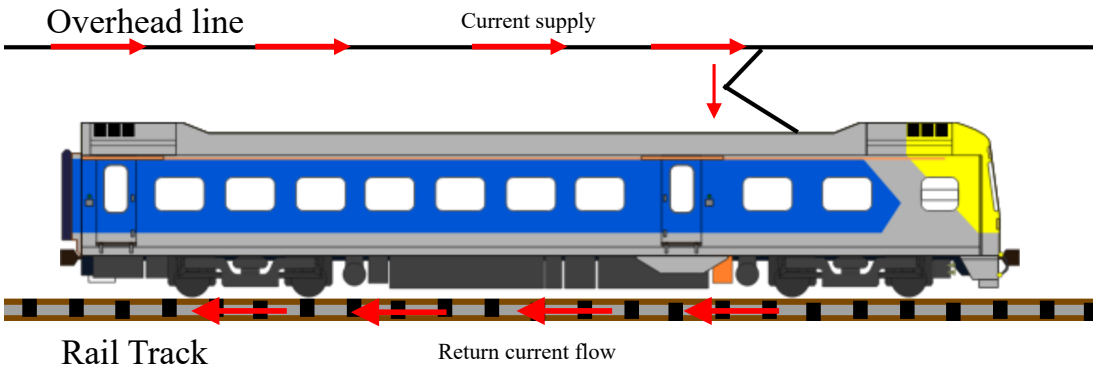

Fig. 1-8 Overhead power supply to a freight train in an electric railway system

Power delivery to moving trains in electric railways is usually accomplished through conductors running alongside the rail track that takes one of two forms: via overhead catenary line, suspended from poles and towers contacted through a pantograph or via a third rail mounted at track level, which interfaces with the train through a pickup shoe [56]. A typical overhead electric railway power supply mechanism illustrated in Fig. 1-8, demonstrates that rolling stock draws power from the overhead catenary line through the pantograph, with the return current flowing back to the primary power supply station via the rail track, thereby completing the electrical circuit [57]. This current flow throughout the traction power supply network generates substantial amounts of magnetic fields around the conductors, including the overhead power lines and the rail tracks that carry the return current. In DC power systems,

these magnetic fields remain almost static, whereas AC traction power systems generate time-varying magnetic fields. Although these magnetic fields are considered stray magnetic energy, which represents a form of wasted energy, they constitute a viable energy source that can be converted to usable electricity by employing MFEHs.

Magnetic field energy harvesting is primarily based on Faraday's law of induction, which states that an electromotive force (EMF) is induced in a conductor placed in a fluctuating magnetic field. In this process, a copper coil wound around a high permeability ferromagnetic core, which is referred to as a magnetic field energy harvester (MFEH) in this study, is exposed to a fluctuating magnetic field, and a voltage is generated across its coil. The ferromagnetic core enhances energy harvesting efficiency by concentrating the magnetic flux through the coil, thereby increasing the induced EMF. The voltage induced across the coil can be put to practical use once the reluctance of the circuit, primarily caused by coil inductance, is effectively minimized.

MFEHs can be classified into two categories based on their installation technique: cable-mounted and free-standing configurations. In the cable-mounted technique, the energy harvesting device is directly clamped around the current-carrying conductor, such as the overhead line. In contrast, free-standing energy harvesting devices are placed in an open environment in the vicinity of a fluctuating magnetic field source without a physical attachment to the current-carrying conductor. The following sections provide a comprehensive analysis of each of the energy harvesting techniques.

1.2.3 Cable mounted Magnetic Field Energy Harvester

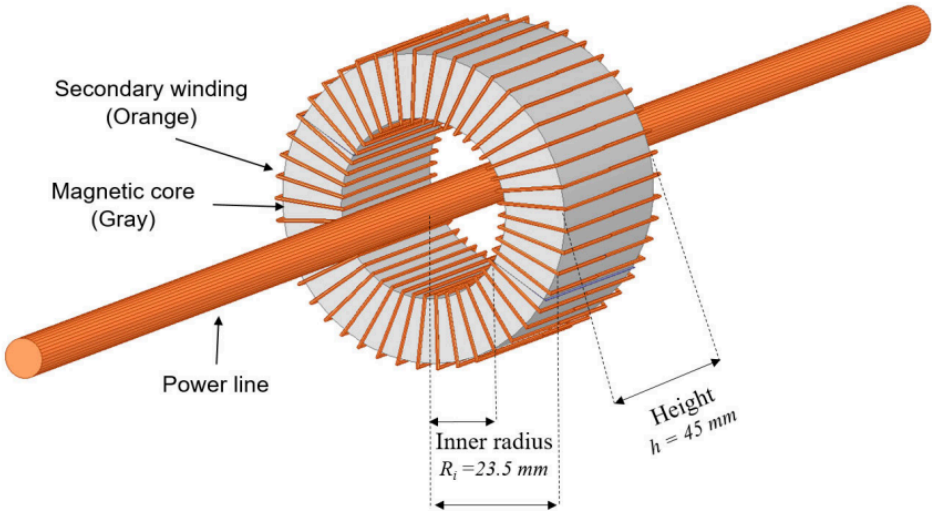

Fig. 1-9 Cable-mounted magnetic field energy harvester [58]

A conventional cable-mounted, toroidal-shaped MFEH that is clamped around a current-carrying conductor is illustrated in Fig. 1-9. When a time-varying current passes through the power line, it generates a corresponding fluctuating magnetic field around the conductor. The toroidal-shaped core serves two purposes: it confines and concentrates the magnetic flux generated by the conductor within its structure and provides a low reluctance path that directs the concentrated magnetic flux through the coil winding. This flux linkage induces an EMF across the coil terminal according to Faraday's law of induction, where the induced voltage is proportional to the number of coil turns and the rate of change of the magnetic flux [59]. The induced voltage can be calculated by:

$$V_{coil} = N\frac{d\phi}{dt} = NA_e\frac{dB_C}{dt} \qquad 1\text{-}1$$

where, N denotes the number of coil windings, ϕ denotes the magnetic flux passing through the coil, A_e denotes the effective cross-sectional area of the coil and B_C denotes the magnetic flux density inside the core.

Cable-mounted magnetic field energy harvesters, which are also referred to as cable-clamped and current transformer (CT) energy harvesters, have been explored for applications in transmission and distribution power systems to power wireless sensors and other monitoring devices. For instance, a Rogowski coil proposed by Du *et al*. (2010) [60] demonstrated the feasibility of harnessing magnetic field energy induced by transmission line currents to power online monitoring systems. However, the maximum power that can be extracted from cable-mounted energy harvesters is fundamentally constrained by the magnetic flux density threshold of the core material. As the current through the conductor increases, the induced magnetic field through the core increases proportionally, potentially driving the core into saturation. Under saturation conditions, the relative magnetic permeability of the core drops significantly, resulting in reduced magnetic flux variation within the core and consequently diminishing the energy extraction capacity [61]. Several innovative approaches have been proposed in the literature to mitigate the core saturation in cable-mounted MFEHs. Zhuang *et al*. [61] proposed an active compensation technique employing an additional coil to manipulate the magnetic field generated by the power line, thereby maintaining the magnetic flux density levels in the core. Paul *et al*. [62] proposed a novel dual-core configuration designed to prevent magnetic saturation through implementing air gaps strategically while simultaneously addressing the challenge of magnetic flux leakage. The magnetic flux density passing through the core of an MFEH can be generally expressed as:

$$B_C = \mu_{eff}\mu_0 H_{ex} \tag{1-2}$$

where μ_0 represents the magnetic permeability of free space, μ_{eff} represents the effective permeability of the core and H_{ex} denotes the magnetic field generated by the current-carrying conductor. However, for a toroidal core, as the magnetic flux is fully enclosed, effective permeability equals the relative magnetic permeability of the core material. Therefore, selecting a ferromagnetic material with a high permeability can significantly enhance the magnetic flux density through the coil. Material selection optimization, particularly through high permeability ferromagnetic materials with elevated magnetic flux density thresholds, has also been documented in the literature as a design consideration to maximize the output power of the energy harvester [63]. Equation 1-2 also indicates that the magnetic flux density within

the core can be further improved by optimizing the effective permeability, which depends on the geometry of the core [64].

Although numerous studies have explored cable-mounted MFEHs for transmission lines, their application in electric railways has received less attention. A key limitation in electric railways is the presence of the moving pantograph, which maintains continuous contact with the overhead power line, which makes cable-clamped energy harvesters impractical. Additionally, for installing cable-clamped devices in overhead lines, the power lines should be de-energized. The added weight of cable-clamped MFEHs may also lead to undesirable sagging in overhead lines. For these reasons, free-standing MFEHs present a more viable solution, as they avoid physical interference with the pantograph and eliminate the need for direct attachment to current-carrying conductors in electric railways.

1.2.4 Free-Standing Magnetic Field Energy Harvester

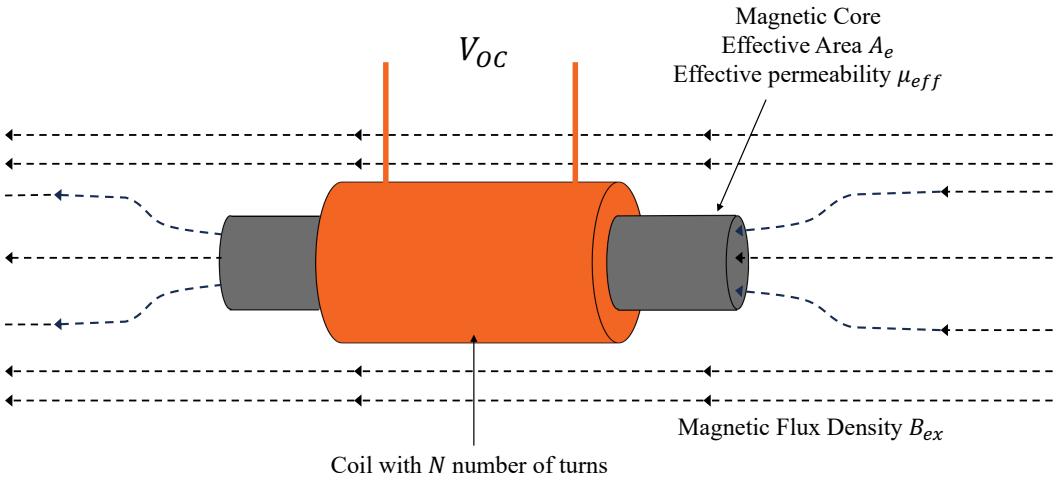

Fig. 1-10 Free-standing magnetic field energy harvester

A basic solenoid-type energy harvester used in free-standing magnetic field energy harvesting is illustrated in Fig. 1-10. The device typically consists of a ferromagnetic core wound with a copper coil of N turns. When exposed to an external magnetic field, an EMF is induced across the coil according to Faraday's law of induction. Unlike cable-mount MFEH, the free standing variant is portable and versatile enabling deployment in remote locations. Therefore, this MFEH can be easily deployed in traction power systems along rail tracks, where it can efficiently harvest magnetic field energy generated from current flowing conductors. The

induced open circuit voltage in the coil can be calculated using Eq. (1-3), where ω represents the angular frequency of the alternating current flowing through the nearby conductor and B_{ex} denotes the magnetic flux density generated due to the current flow in the conductor.

$$V_{OC} = A_e B_{ex} \omega \mu_{eff} \quad 1\text{-}3$$

By exploiting the ubiquity of magnetic fields in electrified railway environments, MFEH provide a sustainable means of powering devices in WSNs without requiring direct physical contact with the railway infrastructure. The simplicity of MFEHs owing to the absence of complex moving parts further enhances reliability while minimizing maintenance needs.

Magnetic field energy harvesting using free-standing energy harvesting devices has been explored in limited studies across various fields. For instance, Gupta *et al*. (2010) [65] conducted an early feasibility study using an inductor to harvest electromagnetic energy generated from domestic current-carrying conductors. Despite the miniature scale of their setup, which yielded a modest 1-2 mW of power, their work demonstrated the potential of magnetic field energy extraction using non-intrusive mechanisms. Building on this, Roscoe *et al*. (2013) [51] developed a 50 cm long solenoid type free-standing MFEH with a cast iron core of 5 cm diameter to harness magnetic field energy in substations. Their device generated a maximum output power of 300 μW when exposed to a magnetic flux density of 18 μT. Although they had developed a bulky core structure to enhance the magnetic flux density penetration, use cast iron core which is prone to high eddy current losses resulted in the low output power. This underscores the critical importance of selecting core materials with high relative permeability and low electrical conductivity to minimize energy losses within the core. Further advancements emerged with Maghe *et al*. [66] who first investigated the use of flux collectors in MFEHs. Their design employed an X-shaped core wound with 300 coil turns and mounted directly on a current-carrying conductor. The proposed design achieved a comparatively higher output power of 257 mW by optimizing the proximity to the magnetic field source and enhancing flux concentration which is a notable milestone in the field.

Yuan *et al*. (2015) [67] introduced a novel bow-tie coil shown in Fig. 1-11 for harvesting magnetic field energy beneath overhead power lines, aiming to power autonomous sensors. MnZn Ferrite was selected as the core material for its high relative permeability and low electrical conductivity properties which are critical in enhancing the magnetic flux penetration

and mitigating eddy current losses. With 40,000 coil winding, the device achieved a maximum output power of 360 µW under a magnetic flux density of 7 µT. Building on their previous work, the same research team later proposed a novel helical core design illustrated in Fig. 1-12 for magnetic field energy harvesting [68]. This configuration too utilized MnZn Ferrite as the used as the core material where just 400 turns of copper winding turns were used. Despite the reduced coil winding turns, the design generated a power output of 0.61 mW under the same magnetic flux density of 7 µT, demonstrating significant advancements compared to their previous study. Reaching further advancements Wang *et al*. [69] developed an I-shaped MFEH to scavenge electromagnetic energy generated by large alternating currents. The proposed MFEH consisted a MnZn Ferrite core wound with 40,000 coil turns. The device achieved a maximum power output of 5.2 mW when exposed to a magnetic flux density of 6.5 µT. These studies collectively highlight the critical role of core geometry and material properties in optimizing energy harvesting efficiency.

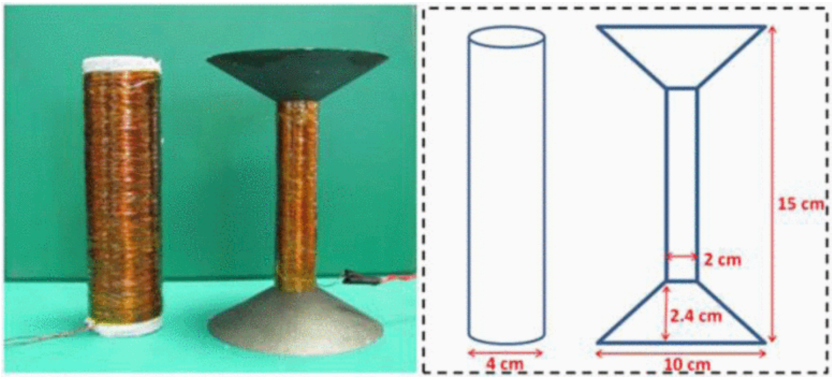

Fig. 1-11 Solenoid and the bow-tie coil [67]

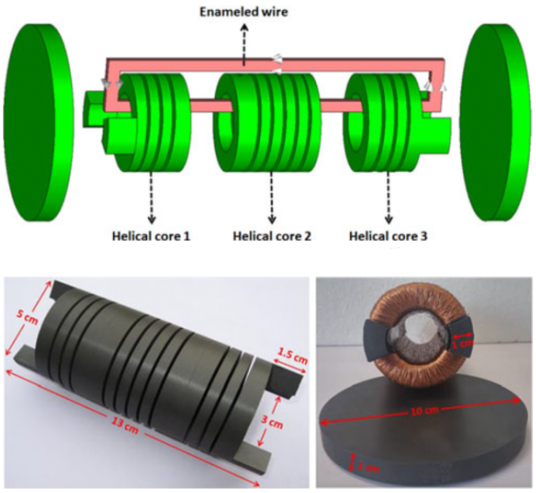

Fig. 1-12 Design and fabricated helical core proposed in [68]

The application of free-standing magnetic field energy harvesting techniques in electric railway systems was initially explored by Espe *et al*. [70] in 2020. Their feasibility study focused on harvesting magnetic field energy generated from rail tracks that carry return currents in electric railways. Building on this work, the same research group later developed an MFEH consisting of an I-shaped core fabricated from Ferroxcube 4B1 material, a specialized magnetic alloy. The MFEH measuring 15 cm in length was wound with 80,000 turns of copper coil. The device achieved a maximum output power of 40.5 mW when the device was placed 0.25 m away from a rail track conducting a 200 A current at 50 Hz in a laboratory setting. However, the power output dropped significantly to 4.5 mW when the frequency of the current flowing through the rail track was changed to 16.7 Hz. This underscores the critical dependence of the energy harvesting mechanism on the frequency of the magnetic field source. Further in-situ testing of the developed MFEH as illustrated in Fig. 1-13 revealed its practical performance under real-world conditions. When positioned 0.5 m away from the rail track, the MFEH generated a maximum instantaneous output power of 1.01 mW. Over the duration of a single train passing by, the device successfully harvested 109 mJ of energy. [71]. Findings of this study demonstrates both the potential and limitations in free-standing magnetic field energy harvesting techniques in electric railways particularly in its sensitivity to proximity to the magnetic field energy source.

Fig. 1-13 In-situ experimentation of the magnetic field energy harvester developed in [71].

Zhang *et al*. [72] investigated the impact of proximity of magnetic field energy harvesting by positioning the MFEH near the web of the rail track. Their coreless hollow-coil type free-standing MFEH achieved a maximum power output of 9.2 mW when a 600 A current was flowing through the rail track at 50 Hz. This study demonstrates the benefits of minimizing the distance between the MFEH and the magnetic field energy source. However, a significant limitation can be identified from the study. Despite having 2000 coil turns and enhanced magnetic flux density due to its proximity to the source, its efficiency was likely constrained by the absence of a magnetic core. A magnetic core could have further enhanced the magnetic penetration of magnetic flux density through the coil.

Kuang *et al*. conducted a comprehensive investigation into magnetic field energy harvesting from return currents in rail tracks [73,74]. The study included a theoretical analysis, numerical simulations and experimental verifications. The study identified various parameters that impact the final power output of the energy harvesting system and suggested optimization methods and recommended parameter trade-offs. The MFEH designed in their study shown in Fig. 1-14 was fabricated using a 230 mm long MnZn Ferrite rod (diameter of 31.5 mm) flanked by two large flux collector plates to enhance magnetic flux concentration. Experimental verifications by placing the MFEH beneath the rail track showcased a maximum power output of 5.05 W when a 520 A current was applied through the rail track at 50 Hz. While the results of the study highlight the effectiveness of optimized core design and flux collection techniques, they also raise practical implementation concerns.

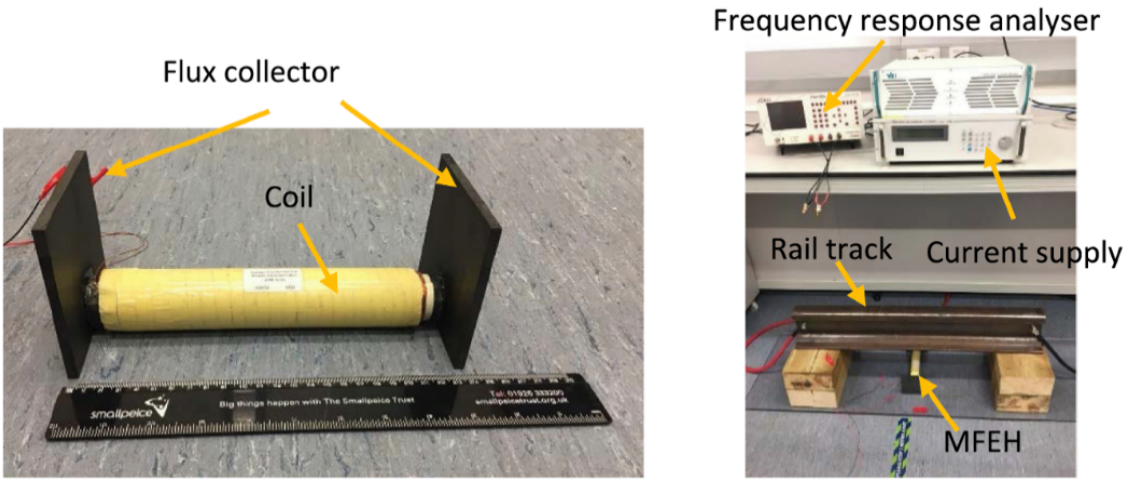

Fig. 1-14 A prototype of the MFEH device proposed in [73] and their experiment setup

Existing research on magnetic field energy harvesting in traction power systems remains limited. While studies demonstrate feasibility of the energy harvesting technique in electric railways, several challenges can be identified from literature. Many reported devices produce relatively low outputs and many designs rely on bulky core designs with thousands of coil windings, which increase fabrication cost and complicate practical implementation. Although free-standing MFEHs offer advantage of flexibility in placements, certain studies have positioned harvesters in impractical locations. Furthermore, while researchers emphasize the potential of MFEH for powering autonomous devices and sensors in WSNs, a critical gap in current research is the lack of analysis regarding power delivery to practical DC loads. These loads typically include various WSN components such as sensors, microcontroller and communication modules. The variable power demands of these devices make it essential to thoroughly investigate the MFEH system's performance across different load levels to ensure reliable operation in real-world railway applications

A comparison of various energy harvesting techniques from different sources of energy in railway environments are given in Table 1-1. The evaluation reveals that magnetic field energy harvesting offers distinctive advantages that outweighs its limitations compared to alternative energy sources. Despite this potential, research on harnessing magnetic field energy present in electric railways to energize WSNs remains relatively unexplored. The ubiquity of current carrying conductors in electric railway networks which generate time varying magnetic fields presents a promising opportunity for magnetic field energy extraction. Unlike most of the other energy harvesting mechanisms, magnetic field energy can be harnessed through non-intrusive techniques and operates independently of weather and mechanical wear. These characteristics make magnetic field energy harvesting uniquely suited for powering autonomous devices in railway environments offering both implementation advantages and reduced maintenance requirements.

Table 1-1:Comparison of energy harvesting techniques in Electric railways

Energy source	Advantages	Disadvantages
Solar Energy	• High power density • Non-intrusive energy harvesting technique	• Highly dependent on weather conditions • Daytime availability • Unavailability in underground conditions

Wind Energy	• Non-intrusive energy harvesting technique	• Reliant on environmental conditions • Requires complex mechanical apparatus • Requires regular maintenance
Vibration Energy	• High availability due to consistent generation of vibration energy in railways	• Requires complex mechanical apparatus • Requires regular maintenance • Requires direct integration with the railroad infrastructure
Thermoelectric Energy	• Converts waste heat energy to electrical energy	• Highly dependent on weather conditions • Low power output • Requires direct integration with the railroad infrastructure • Limited application scenarios
Magnetic Field Energy	• Abundant availability of magnetic field energy in electric railways • Requires minimal maintenance • Utilize non-intrusive energy harvesting techniques	• Energy losses in the ferromagnetic core • Magnetic saturation of the core • Intermittent generation of magnetic field energy

1.3 Motivation for the Study

Transportation sector serves as an important pillar in national economy of each and every country, where reliability, efficiency and safety are amongst the main priorities. Railway networks, as one of the primary modes of mass transportation, play a critical role in global mobility serving millions of passengers daily. In these dynamic systems ensuring a reliable, punctual and safe transportation service is highly dependent on efficient maintenance. With advancements in technology, maintenance practices have evolved significantly through the adoption of online monitoring systems, which equip the user with early detection of degradations and anomalies. For example, condition monitoring of key parameters such as vibrations in rail tracks or sleepers, thermal gradients along rail tracks and stress-strain forces exerted on rails provides maintenance teams with advanced insights into potential malfunctions or deterioration trends.

The accuracy of these online monitoring systems relies heavily on access to comprehensive data, often collected via wireless sensors deployed in WSNs. In electric railway systems, wireless sensors can be installed in various remote locations to retrieve real-time data. However, providing a reliable power supply for powering autonomous sensors and devices within the WSN remains a challenge. Conventional solutions, such as electrochemical batteries, face limitations due to their finite energy capacity and limited lifespan. These drawbacks introduce an additional maintenance burden, as batteries require regular checks and replacements to sustain the uninterrupted operation of monitoring systems.

To address these limitations, energy harvesting mechanisms offer a promising solution by scavenging ambient energy from electric railway environments to power autonomous sensors and devices. Solar, wind, vibration and magnetic field energy are amongst the potential energy sources present in electric railway environments. Although solar energy is abundant, its dependence on daylight and weather conditions is a major drawback. Moreover, as electric railway networks are also laid in subterranean environments, this limits the universal applicability of solar energy throughout the railway network. Although wind energy harvesting typically depends on environmental conditions, researchers have developed innovative mechanical systems capable of generating electricity from train-induced airflow, even in

underground environments [26–28]. However, such mechanical systems often involve intricate mechanical designs that require regular maintenance to ensure continuous operation.

Vibration energy, abundant in dynamic railway systems, presents another viable energy source. While there are diverse techniques to harvest vibration energy from railway systems, all the mechanisms require direct physical contact with railroad infrastructure for transduction [29–38]. This introduce installation complexities, additional costs and potential vulnerabilities to the railway operation. Furthermore, vibration energy harvesting techniques typically rely on sophisticated mechanical designs and transducers to convert kinetic energy into electrical energy. As with wind based energy harvesting systems, such mechanical apparatus require regular maintenance to maintain functionality which aggravate operational and maintenance burden.

Magnetic field energy is a rich source of energy naturally present in electric railway systems, particularly around current carrying conductors such as overhead lines and return current flowing rail tracks. Leveraging Faraday's law of induction, a voltage can be induced across a coil when exposed to a fluctuating magnetic field in an electric railway. This principle can be further improved by integrating a ferrite core to concentrate magnetic flux through the coil [51]. Two primary magnetic field energy harvesting techniques have emerged in research: cable-mounted and free-standing magnetic field energy harvesting. In cable mounted approach, a ferrite core wound with copper coil is clamped around the current carrying to harvest magnetic field energy [60–62,64]. While effective in overhead power lines such as transmission lines and even domestic power lines, this method faces practical limitations in electric railways. The overhead power supply lines cannot accommodate clamped MFEH due to interference with the sliding pantograph which draws power from the overhead line. By contrast, free-standing MFEHs offer great compatibility with railway infrastructure. Free-standing MFEH employs a finite length of ferrite rod, wound with copper wire and positioned in close proximity to fluctuating magnetic fields generated by nearby conductors [66–69]. Therefore, free-standing MFEH is more suitable for electric railway systems. Unlike cable-mounted designs, free-standing MFEHs require no physical contact with current-carrying components, eliminating risks of obstruction or interference with moving trains. This approach not only aligns with the operational dynamics of railways but also minimizes installation complexity, positioning free-standing MFEH as a practical and sustainable solution for powering autonomous devices in employed in electric railway environments.

While free-standing magnetic field energy harvesting holds potential for powering autonomous devices in electric railways, existing research remains limited and reveals critical gaps. Early investigations conducted by Espe *et al*. [70] first reported the feasibility of the technique in electric railways and later demonstrated experimental validations with an I-shaped MFEH generating a maximum power output of 40.5 mW. Zhang *et al*. [72] achieved a maximum power output of 9.2 mW using coreless MFEH positioned near the rail web. A notable advancement was reported by Kuang *et al.* in 2021 whose MFEH achieved a maximum power output of 5.05 W when positioned 48 mm beneath a rail track carrying 520 A current at 50 Hz. Despite these efforts, significant challenges persist. Many studies rely on bulky MFEH designs with an excessive number of coil windings, and their placement strategies often neglect real-world constraints, such as spatial limitations. More critically, while numerous studies have explored free-standing MFEHs for powering autonomous devices, none have thoroughly analyzed power delivery to DC loads that typically represents components in WSNs. This represents a significant oversight, as both the traction current and the load requirements of autonomous devices in WSNs experience substantial fluctuations. To address these limitations, a comprehensive study is needed to optimize parameters of free-standing MFEHs while considering realistic placement constraints that maximize power extraction. Furthermore, the integration of an efficient power management unit is essential to ensure stable power delivery to varying DC loads. Such advancements would bridge the gap between theoretical potential and practical implementation of MFEH systems in electric railways.

1.4 Objectives

This study aims to advance magnetic field energy harvesting technology for electric railway systems through achieving following objectives:

1. To investigate magnetic field transients in electric railway environments and identify optimal techniques and areas to deploy free-standing magnetic field energy harvesting devices.
2. To design, develop, and systematically optimize a free-standing magnetic field energy harvesting unit specifically tailored for electric railway applications.
3. To design and develop an efficient power management circuit capable of maximizing power delivery to connected loads.
4. To demonstrate the potential applications of the developed energy harvesting system in electric railway systems.

1.5 Thesis Outline

The focus of this study is to design and develop a free standing magnetic field energy harvesting unit that power autonomous devices in WSNs deployed across railway network. By leveraging the fluctuating magnetic fields generated by traction currents, the proposed system aims to provide a sustainable, maintenance-free power source, addressing the limitations of conventional battery dependent solutions. The thesis is organized as follows.

Chapter 1 of this thesis begins by establishing the background of magnetic field energy harvesting in electric railway systems, emphasizing its potential to address the limitations of conventional power supply methods for autonomous devices. A comparison of other energy sources utilized for energy harvesting is presented through a review of relevant literature. This is followed by a detailed literature review of existing magnetic field energy harvesting methods used across various domains, including transmission lines, domestic power lines and traction power systems. It critically examines prior methodologies, highlighting their advancements, and innovations while identifying the shortcomings encountered in electric railway applications. Building on the literature review, the chapter outlines the motivation for the study, emphasizing the requirement for free-standing magnetic field energy harvesters capable of operating under real world railway conditions while delivering power to dynamic loads. The chapter concludes by clearly articulating the objectives of the study which aim to address gaps identified in existing literature and advance magnetic field energy harvesting in electric railways.

Chapter 2 provides a detailed overview of the magnetic field energy harvesting system. The chapter begins with a brief explanation of the overall system architecture. It then explores the magnetic field transients inherent in electric railway systems, presenting a theoretical approach to assess their characteristics. Following this, the fundamental structure of the energy harvesting unit is modelled, supported by a detailed theoretical analysis of the principles governing magnetic field energy harvesting in electric railway environments. The section concludes by identifying key parameters influencing the power output of free-standing MFEHs, derived from an analysis of its equivalent circuit. The effects of demagnetization factor and the effective permeability of the magnetic core and their role in optimizing the power

output of the energy harvesting unit are examined in depth, highlighting their critical influence on flux concentration and power output optimization.

A key focus of the chapter is placed on the losses specific to free standing magnetic field energy harvesting techniques. These include losses caused by hysteresis and eddy current generation which arise due to core's material properties and positioning of the MFEH. A detailed investigation on eddy current losses generated by the proximity of MFEH to ferromagnetic structures such as rail tracks, is included in the chapter. Finally, the chapter emphasizes the necessity of integrating a power management unit into the energy harvesting system, illustrating the proposed system's architecture. The chapter concludes with explaining the role of the power management unit in the proposed energy harvesting system, underscoring its importance in ensuring stable power delivery to dynamic loads under fluctuating railway operating conditions.

Chapter 3 presents the comprehensive design and fabrication process of the MFEH. The chapter begins by detailing the simulation setup and key design parameters. Subsequent sections include discussions on the material selection criteria for the MFEH and the analytical methods employed for parameter optimization. A thorough analysis of core parameter optimization is provided, followed by the results of coil parameter optimization. The chapter included detailed explanation on the selection criteria and design trade-offs implemented to maximize the system's output power, supported by graphical illustrations. Finally, experimental verification results are presented and critically analyzed with corresponding justifications.

Chapter 4 focuses on the design and implementation of the power management unit. It opens with a theoretical analysis establishing the requirements of a power management unit and its expected performance. The subsequent section elaborates on the circuit design methodology and component selection process for the power management system. In the next section the laboratory test results of the fully integrated energy harvesting system is presented, followed by an in-depth discussion of these findings. Efficiency improvement methods employed in the study are discussed later followed by a detailed loss analysis in the proposed energy harvesting unit. The chapter concludes with a discussion on converter control techniques reported in literature and the necessity of employing a well-functioning control technique for the converter proposed in the study.

Chapter 5 provides a comparative performance evaluation of the developed energy harvester against other ambient energy harvesting technologies proposed for railways applications. This is followed by a critical comparison with previous studies in the magnetic field energy harvesting field. The chapter then summarizes the key conclusions derived from the research. Finally, potential directions for future investigations to further advance this field of study are identified.

CHAPTER 2 SYSTEM OVERVIEW

2.1 Introduction

This chapter begins with a detailed explanation of the basic principles underlying magnetic field energy harvesting in electric railways. It is critical to identify the magnetic field transients in electric railways where energy harvesting units can be deployed to effectively capture magnetic field energy. The magnetic flux density distribution in electric railway systems is demonstrated in this chapter through theoretical and simulation analyses, while highlighting the factors impacting it. Although the magnetic fields near overhead power lines are stronger than those near current returning rail tracks due to leakage currents in the rails, this chapter focuses on magnetic field transients close to rail tracks.

The subsequent sections of this chapter present a comprehensive theoretical analysis of magnetic field energy harvester modelling for electric railways. The factors governing the output power of the energy harvester is identified in this section by analyzing its equivalent circuit. The inductance compensation and its representation in the equivalent circuit of the MFEH is described and the conditions for achieving maximum output power is demonstrated. In free-standing MFEHs, a demagnetizing field is generated due to magnetic pole formation at the open ends of the energy harvester. The role of effective permeability in mitigating this field is theoretically explained and supported by literature in the next section. The parameters that can improve effective permeability is identified and later optimized through parametric simulations. In the next section, the losses inherent with free-standing MFEHs are examined. Eddy current losses caused by proximity to ferromagnetic rail tracks are explained and illustrated using finite element method (FEM) simulations. The analysis emphasizes the parameters directly contributing to these losses and underscores the importance of managing them. Simulation results further demonstrate how ferromagnetic rail tracks alter the magnetic flux density distribution of the MFEH. Finally, the chapter concludes by addressing the necessity of an energy conversion circuit and a power management unit to ensure efficient energy extraction and regulation in dynamic railway environments.

2.2 Magnetic Field Transients in Electric Railway Environments

In electric railway systems, fluctuating magnetic fields are generated around current carrying conductors such as overhead lines and rail tracks which return the current drawn by trains to the primary power supply. The spatial distribution of these magnetic fields in a typical railway environment is illustrated in Fig. 2-1 (adopted from [75]). Here, the overhead line carries 500 A current directly into the paper while the rail tracks facilitates its return path in the opposite direction. Although ambient magnetic field energy is abundant in electric railway environments, this study specifically focuses on energy harvesting from magnetic fields generated in return rail tracks, as the pantographs which draw current from overhead power lines obstruct the deployment of cable-mounted MFEHs. Therefore, free-standing MFEHs are considered in this study, which can overcome this limitation and enable energy scavenging in accessible locations along rail tracks.

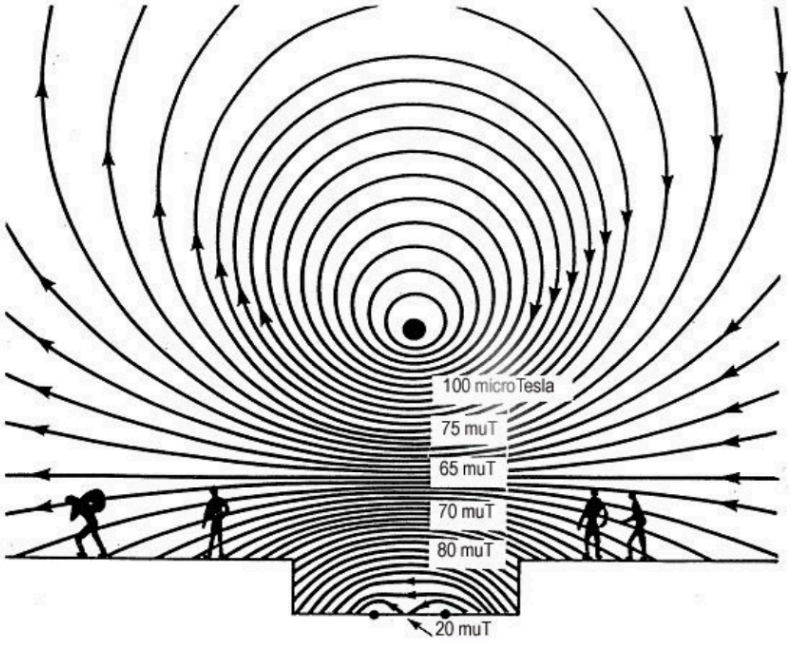

Fig. 2-1 Distribution of magnetic fields in a typical railway environment [75]

For an infinitely long rail track carrying a current I_r along its axis, the magnetic flux density B_{ex} at a radial distance r from the rail track can be calculated using Ampere's law as given in

Eq. 2-1. Here, μ_0 denotes the magnetic permeability of free space, H_{ex} represents the magnetic field intensity at r distance induced by current flowing through the rail track. The equation states that magnetic flux density increases with the magnitude of the current flowing in the rail track but diminishes with increasing distance from the rail track to the point of consideration.

$$B_{ex} = \mu_0 H_{ex} = \frac{\mu_0 I_r}{2\pi r} \qquad 2\text{-}1$$

As the equation indicates, the magnetic field generated by rail tracks is strongest in close proximity to the current carrying rail track. Therefore, understanding the spatial distribution of magnetic flux density around the rail track is critical for optimizing magnetic field energy harvesting. Therefore, a FEM simulation was performed using COMSOL Multiphysics simulation software. The results, illustrated in Fig. 2-2 described the magnetic flux density around a rail track carrying a 300 A, 50 Hz AC current into the paper. The simulation results reveal that magnetic flux density is predominantly concentrated near the edges of the rail. This result implies that a coil positioned near the rail edges will experience significant fluctuations in magnetic flux. According to Faraday's law of induction, such fluctuations induce a higher EMF making these regions optimal for energy harvesting applications.

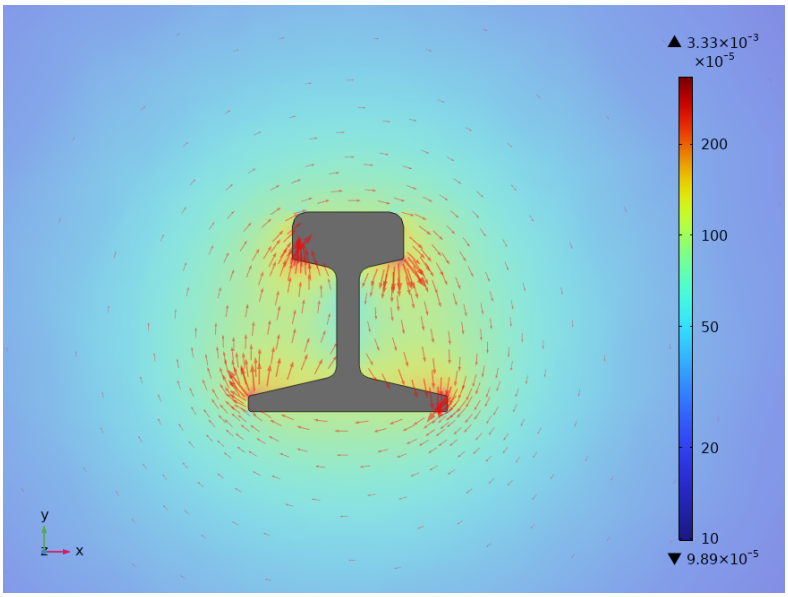

Fig. 2-2 Magnetic flux density distribution around a rail track carrying a 300 A current

2.3 Overview of the Magnetic Field Energy Harvesting System

This section outlines the mathematical framework governing free-standing MFEHs and identifies key parameters impacting their final power output. The importance of the core structure in improving the efficiency of the energy harvester is examined, followed by an analysis of losses inherent to free-standing magnetic field energy harvesting configurations. Finally, the section concludes by outlining the system architecture of the free-standing MFEH, which explains the requirement of rectifiers and power management circuitry to efficiently extract power from the energy harvester and deliver to connect loads.

2.3.1 Modelling of Magnetic Field Energy Harvesting System

Faraday's law of induction serves as the fundamental principle for magnetic energy harvesting across various environment. When a coil is placed within a fluctuating magnetic field, an EMF is induced across its terminals. This effect can be significantly amplified by incorporating a high-permeability ferromagnetic core, around which the coil is wound. Introduction of the ferromagnetic core enhances the magnetic flux density penetration through the coil windings by several orders of magnitude compared to air core configurations [76,77]. Fig. 2-3 illustrates a basic design of a free-standing MFEH employed in such energy harvesting systems, demonstrating the integration of core and coil components.

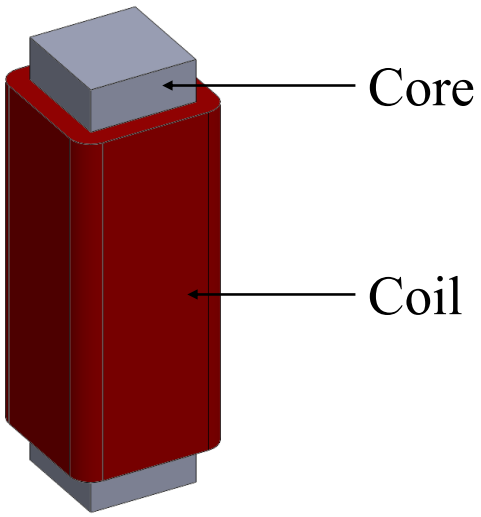

Fig. 2-3 A typical free-standing MFEH

Faraday's law of induction states that the open circuit voltage V_{OC} induced across the terminals of a coil in an MFEH when exposed to a time-varying magnetic field is expressed as:

$$V_{OC} = N\frac{d\phi}{dt} = NA_eB_{ex}\omega\mu_{eff} \quad 2\text{-}2$$

where N denotes the number of coil turns, ϕ represents the magnetic flux through the coil, A_e represents the effective cross-sectional area of the coil (assumed to be the same as the cross-sectional area of the core), ω denotes the angular frequency of the current flowing through the rail track, and μ_{eff} represents the effective permeability of the core.

The induced voltage generated by magnetic flux variation enables power extraction when the system is connected to an external load. The power transfer is governed by the impedance of the load connected and the internal impedance of the energy harvester. According to maximum power transfer theorem, the maximum power output extraction from the MFEH occurs when the load impedance equals the complex conjugate of the source impedance. The reactance introduced by the coil inductance L_C can be compensated by connecting a capacitor in series. Therefore, the compensation capacitance can be calculated as:

$$C = \frac{1}{\omega^2 L_C} \quad 2\text{-}3$$

Fig. 2-4 illustrates the equivalent circuit of the MFEH. R_C and L_C connected represent the coil parameters: coil resistance and coil inductance, respectively. The coil inductance can be estimated by [59]

$$L_C = \frac{\mu_0\mu_{eff}N^2A_e}{l_c} \quad 2\text{-}4$$

where l_c denotes the length of the coil

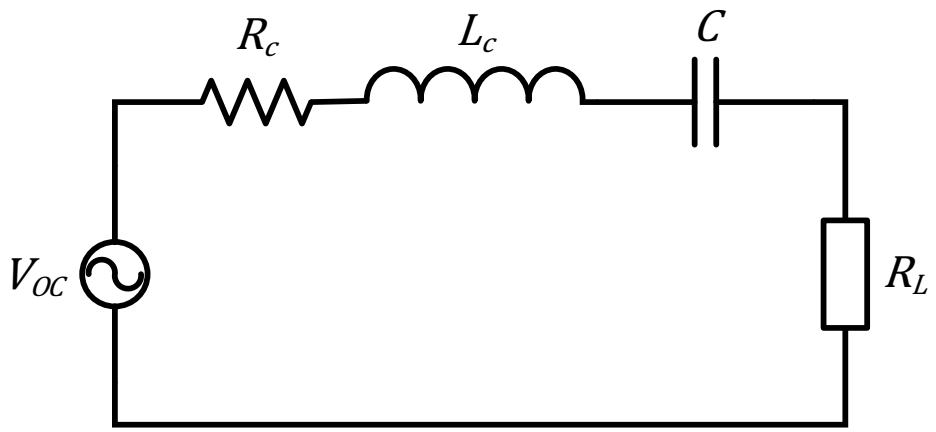

Fig. 2-4 Equivalent circuit of the MFEH system

The coil resistance R_C consists of two distinct components. The inherent ohmic resistance of the copper wire R_W and the resistance component arising due to eddy current losses R_{ac} [78]. A detailed analysis of eddy current losses and their impact on free-standing magnetic field energy harvesting is provided later in this chapter. The apparent coil resistance can thus be expressed as:

$$R_C = R_W + R_{ac} \tag{2-5}$$

As stated in maximum power transfer theory, the maximum power can be extracted from the MFEH when the load resistance R_L matches the coil resistance R_C. Under this condition, the maximum power output of the MFEH P_O is given by:

$$P_O = \left(\frac{V_{OC}}{2\sqrt{2}}\right)^2 / R_L = \frac{{V_{OC}}^2}{8R_C} = \frac{(NA_eB_{ex}\omega\mu_{eff})^2}{8R_C} \tag{2-6}$$

Equation 2-6 highlights the critical parameters governing the output power of free-standing MFEHs. To maximize the output power, the induced voltage should be amplified and coil resistance should be minimized. In order to improve the induced voltage, the flux linkage should be enhanced or the number of coil turns should be increased. At the same time, minimizing the coil resistance involves optimizing the parameters of the coil wire and mitigating eddy current losses. However, these requirements are typically interdependent. For

instance, increasing the number of coil turns to increase V_{OC} raises R_C due to the extended conductor length. Therefore trade-offs between parameters are required for a balanced design approach that harmonizes flux concentration, coil geometry, and core material properties. By optimizing these interdependencies, the energy harvesting system can ultimately achieve optimal power output.

2.3.2 Impact of Effective Permeability and Demagnetization Factor

This study focuses on converting naturally occurring magnetic field energy in electric railway environments to usable electric energy through free-standing magnetic field energy harvesting devices. As previously discussed, the energy harvester is equipped with a copper coil wound around a ferromagnetic core, which attracts ambient magnetic fields and induces a voltage across the coil. The ferromagnetic core plays a crucial role in this process by concentrating magnetic flux and providing a low-reluctance path, thereby enhancing energy harvesting efficiency. Equation 2-6 demonstrates the impact of effective permeability, which relates to the shape of the core [79] on the overall power output of the energy harvesting system. Therefore, understanding the relationship between the shape of the core and its magnetic properties is vital for optimizing the device's performance. In this section, a detailed discussion on the factors related to the shape of the core is provided.

By convention, the magnetic induction B_{ex} in free space produced by current-carrying conductor generating a magnetic field H_{ex} can be expressed as:

$$B_{ex} = \mu_0 H_{ex} \tag{2-7}$$

When a ferromagnetic core is exposed to an external magnetic field H_{ex}, the magnetic flux density within the core B_C consisting of two distinct contributions can be expressed as:

$$B_C = \mu_0(H_{in} + M) \quad 2\text{-}8$$

where H_{in} represents the magnetic field within the core and M represents the magnetization of the material caused by H_{in}. The response of a magnetic material to an external magnetic field can be defined by permeability μ and susceptibility χ of the material which is expressed as:

$$\mu = \frac{B_C}{H_{in}} \quad 2\text{-}9$$

$$\chi = \frac{M}{H_{in}} \quad 2\text{-}10$$

Permeability quantifies the ability of the material to support the formation of magnetic flux, whereas susceptibility characterizes the degree of magnetization of the material in response to an external magnetic field. However, depending on the material type, both permeability and susceptibility may exhibit constant or variable behaviour [59]. Another important parameter in this aspect is the relative permeability of the core material which is expressed as:

$$\mu_r = \frac{\mu}{\mu_0} \quad 2\text{-}11$$

where μ_0 is the permeability of free space $\mu_0 = 4\pi \times 10^{-7}$ Hm^{-1}. Therefore, magnetic flux density within a magnetic core can be further simplified as:

$$B_C = \mu_0\mu_r H_{in} \quad 2\text{-}12$$

However, sometimes determining the resultant magnetic field H_{in} within the core presents practical challenges. Therefore, the concept of effective permeability μ_{eff} is introduced as [79]:

$$\mu_{eff} = \frac{B_C}{\mu_0 H_{ex}} = \frac{B_C}{B_{ex}} \quad 2\text{-}13$$

The effective permeability μ_{eff} directly describes the magnetic flux density induced within the core by external magnetic field H_{ex}. Effective permeability is not an intrinsic material property but a geometry dependent parameter that reflects the ability of the core to concentrate magnetic flux. As established in the previous section, the output of the energy harvesting unit is critically influenced by the effective permeability of the core. Therefore, techniques to optimize effective permeability of the core should be investigated further.

However, deriving analytical expressions for effective permeability for different core geometries remains a formidable challenge due its non-linear complex relationships between different parameters. Therefore, the effective permeability of a cylindrical core was investigated to determine its influencing parameters. The effective permeability of a cylindrical core can be estimated by [80]:

$$\mu_{eff} = \frac{\mu_r}{1 + N_d(\mu_r - 1)} \quad 2\text{-}14$$

where N_d denotes the demagnetization factor. Equation 2-14 demonstrates that effective permeability of a given magnetic core depends exclusively on the demagnetization factor with which it shares an inverse relationship. Therefore, this highlights necessity of identifying means to control the demagnetizing factor to optimize effective permeability for magnetic field energy harvesting applications.

The demagnetization factor quantifies the strength of the demagnetizing field that arises within a magnetic material when subjected to an external magnetic field. As illustrated in Fig. 2-5, when a finite length of a magnetic core is exposed to an external magnetic field H_{ex}, the formation of magnetic poles at its ends, generates an internal demagnetizing field H_d opposing the external magnetic field [59].

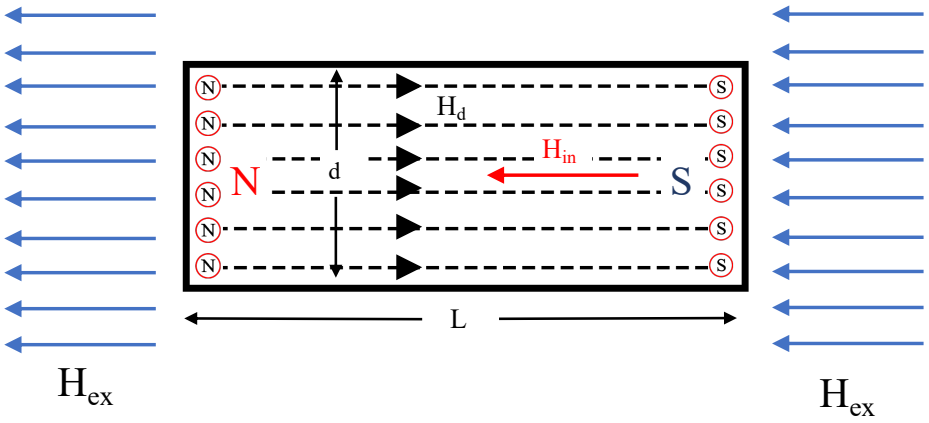

Fig. 2-5 Demagnetization field generated within a magnetic material when exposed to an external magnetic field [68].

The demagnetizing field is determined by two key factors: the magnetization of the material M and the demagnetization factor N_d. While magnetization is an intrinsic material property, the demagnetization factor depends exclusively on the geometry of the magnetic material. Thus the proportional relationship between the demagnetizing field and demagnetization factor can be expressed as [59]:

$$H_d = N_d M \tag{2-15}$$

Consequently, the net magnetic field H_{in} within core must account for this demagnetizing field which yields:

$$H_{in} = H_{ex} - N_d M \tag{2-16}$$

Equation 2-16 demonstrates the influence of geometry on the internal magnetic field H_{in}. For a material with fixed magnetization M, the demagnetization factor can be reduced while minimizing the internal magnetic field attenuation by employing geometric optimization, thereby improving the flux concentration capability of the core. For a cylindrical core, geometric optimization can be achieved by increasing the core length L while reducing its diameter d, thereby minimizing the demagnetization factor [59].

$$N_d \propto \frac{d}{L} \qquad 2\text{-}17$$

This phenomenon can be attributed to two mechanisms: First, the increased core length expand the separation between the magnetic poles formed at each end, thereby weakening the demagnetizing field. Second, decreased core diameter results in reduced pole concentration and consequently reduces demagnetizing field. Therefore, optimizing both the core length and cross-sectional area of the core of the energy harvester is essential for maximizing the power output in free-standing magnetic field energy harvesting systems.

2.3.3 Energy Losses in a Free-Standing MFEH Systems

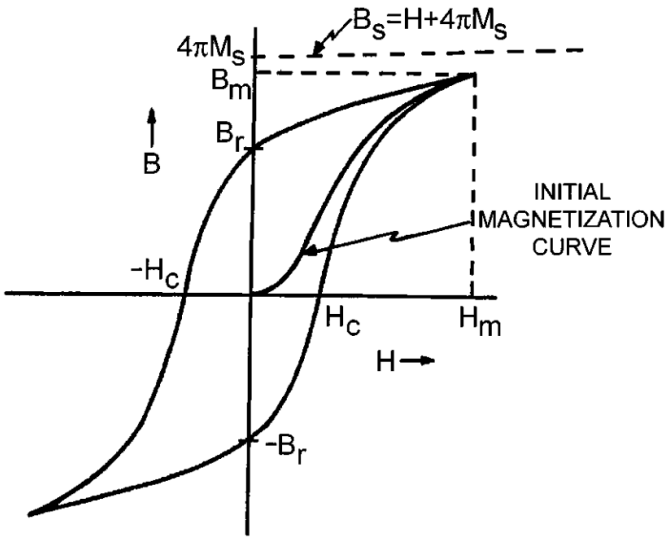

Fig. 2-6 Magnetization curve and hysteresis loop of a typical ferromagnetic material [81]

In free-standing magnetic field energy harvesting systems, ferromagnetic cores are employed to concentrate magnetic flux. Therefore, it is essential to identify inherent energy losses associated with these materials in order to optimize the output of the MFEH. When exposed to an external time-varying magnetic field, ferromagnetic materials dissipate a portion of the energy harvested as heat. These losses are primarily categorized into two types: hysteresis loss and eddy current loss.

Hysteresis loss arises from the irreversible magnetization and demagnetization cycles of the ferromagnetic core under alternating magnetic fields. As shown in Fig. 2-6, the magnetic response of ferromagnetic materials is inherently nonlinear, and the energy dissipated during these cycles manifests as heat. The magnitude of hysteresis loss is dependent on the material and can be quantified by analyzing the area enclosed by the material's hysteresis loop. As illustrated in Fig. 2-7, soft ferromagnetic materials exhibit narrower hysteresis loops (smaller enclosed area) compared to hard ferromagnetic materials, indicating lower hysteresis losses [81,82]. Therefore, soft magnetic materials are preferred for MFEH cores to minimize energy dissipation and maximize efficiency.

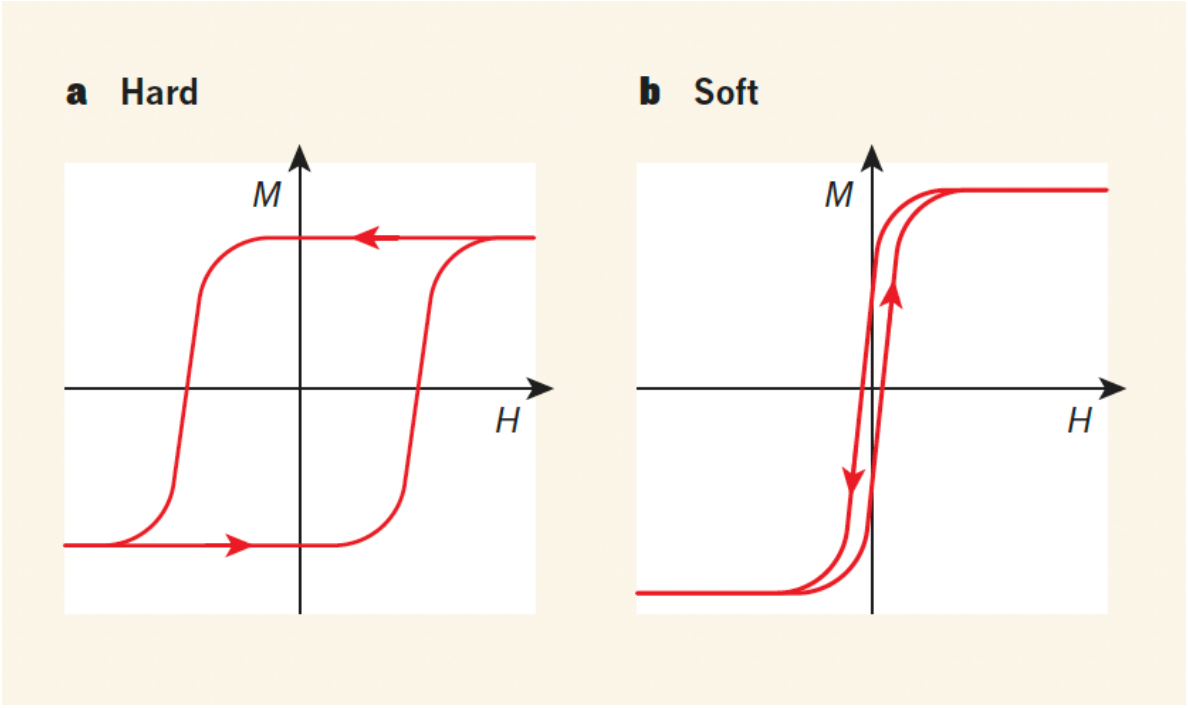

Fig. 2-7 Hysteresis loops of hard and soft ferromagnetic materials [82]

Building on the analysis of hysteresis loss, which arises from the nonlinear magnetic response of ferromagnetic materials, the Steinmetz Equation (SE), introduced in [83] and presented in 2-18, provides an empirical model for calculating core losses per unit volume in magnetic materials which can be referred to assess core losses in free-standing MFEHs [84,85].

$$P_{core,SE} = k_1 f_s^{\alpha} B_m^{\beta} \quad \text{2-18}$$

where f_s is the frequency of the magnetic field and B_m is the peak of the magnetic flux density. The Steinmetz coefficients k_1, α and β are determined by the properties of the magnetic core material. As per the equation it is evident that core losses depend not only on the material's intrinsic properties but also on the frequency and magnetic flux density penetrating the core. Therefore, variations in the rail track current induce changes in the magnetic flux density, thereby altering the core losses in the MFEH.

Eddy current losses in ferromagnetic cores originate from Faraday's law of electromagnetic induction. According to this principle, when a conductive core is exposed to time-varying magnetic flux, it induces circulating currents in the conductive medium. These induced currents, known as eddy currents, flow in closed loops perpendicular to the magnetic flux direction and generate opposing magnetic fields that resist the original flux change [81]. In conductive ferromagnetic materials, these eddy currents dissipate energy as heat through resistive heating.

In conventional transformers, eddy currents are mitigated through laminated core structures, where thin insulated layers are aligned parallel to the flux path. However, this approach proves less effective for free-standing MFEHs, where magnetic flux penetrates the core surfaces rather than following enclosed paths. In order to evaluate the impact of electrical conductivity in free-standing magnetic field energy harvesting, an FEM simulation analysis was performed comparing two high permeability ferromagnetic materials, MnZn Ferrite PC95 (μ_r = 3300 [86]) and Permalloy-80 (μ_r = 75000 [87]). The results illustrated in Fig. 2-8 reveal distinct behaviour between the materials. Despite having a superior relative permeability, a favourable attribute for magnetic field energy harvesting applications, Permalloy demonstrates substantially higher eddy current densities within the core compared to MnZn Ferrite. This discrepancy arises from lower electrical resistivity of Permalloy (58 μΩcm [87]) compared to higher electrical resistivity of MnZn Ferrite which amounts to 6 Ωm [86]. Therefore, these results highlight the necessity of balancing high permeability with adequate electrical resistivity in core material selection to minimize power loss.

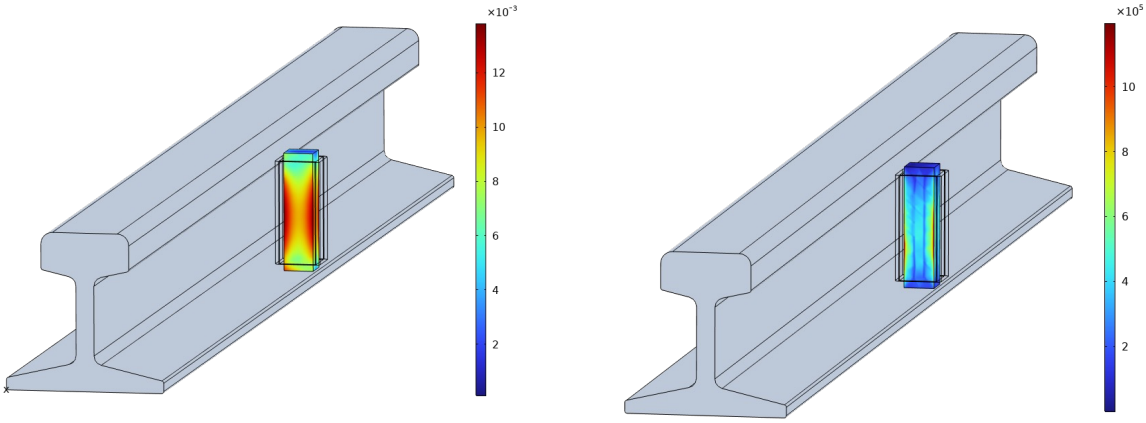

(a) (b)

Fig. 2-8 Eddy current formation in the core of MFEHs (a) MnZn Ferrite (b) Permalloy-80 Units: A/m^2

In addition to the core losses inherent in free-standing MFEHs, another significant secondary loss mechanism critically impacts their performance. When a magnetic core wound with a copper coil is positioned in close proximity to a ferromagnetic rail track, time-varying magnetic flux from the coil current induces eddy currents on the rail track. These eddy currents dissipate energy through joule heating, which results in an increase in the AC resistance of the coil R_{ac}. Simultaneously, the opposing magnetic field created by the eddy currents reduces the apparent coil inductance [78]. The relationship governing the change in coil resistance is detailed in Equation 2-5. Similarly, the apparent coil inductance L_C can be expressed as:

$$L_C = L_0 + L_{ac} \tag{2-19}$$

where L_0 denotes the initial coil inductance and L_{ac} denotes the inductance variation due to eddy currents.

To assess these phenomena, an FEM simulation study was conducted using COMSOL Multiphysics by positioning the MFEH in close proximity to the rail track. In this simulation study, the coil of the MFEH was externally energized with a 100-mA current to emulate the induced current flowing in the circuit during normal operation, and the resultant eddy current formation in the rail track was analyzed. As illustrated in Fig. 2-9, the coil currents generate eddy currents within the rail track, concentrated in regions of highest flux variation beneath the

core's axis. Simultaneously, the coil resistance of the MFEH increased from 285 Ω in free space to 318 Ω as it was positioned closer to the rail track, demonstrating a direct correlation between eddy current formation and increased resistive losses. These findings highlight the critical impacts between proximity effect in free-standing magnetic field energy harvesting. The induced eddy currents not only diminish energy harvesting efficiency through resistive losses but also alter the inductive characteristics of the MFEH.

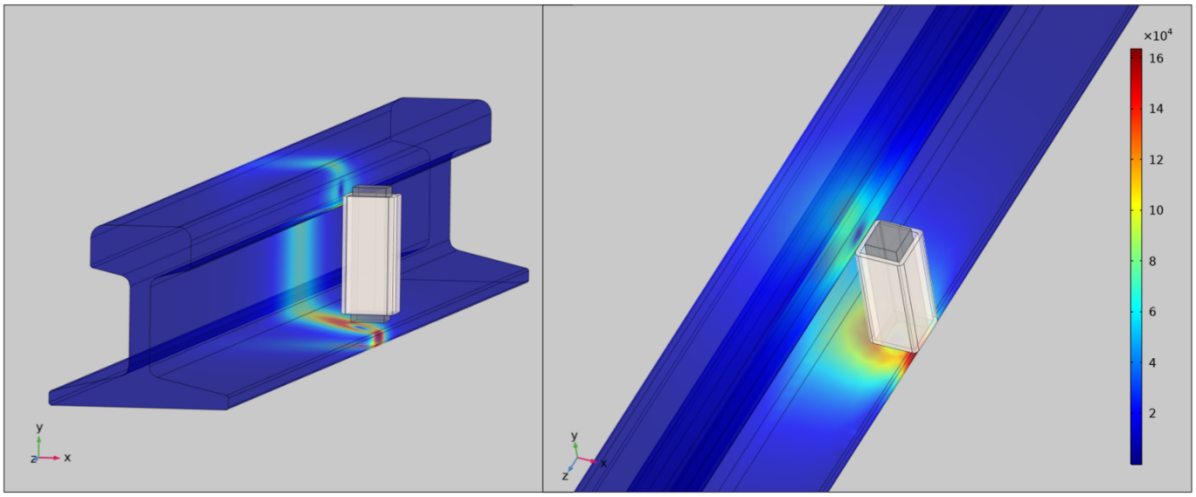

Fig. 2-9 Eddy current density distribution on the rail track generated by the coil current of the MFEH (a) side view (b) top view Units: A/m^2

In this simulation study, the coil inductance also recorded an increment from 2 H to 2.8 H when the MFEH is positioned near the rail track. This phenomenon arises because the ferromagnetic rail track alters the external magnetic flux path of the MFEH, effectively reducing the overall magnetic reluctance similar to the mechanism employed in variable reluctance energy harvesting [88]. By providing a low-reluctance pathway, the rail track concentrates the magnetic flux through the coil, thereby increasing its inductance. It should be noted that the increase in the magnetic flux due to the rail track's influence outweighs the flux reduction caused by eddy currents induced in the rail track.

The visual confirmation of the variation in magnetic flux density resulting from the rail track's proximity is further detailed in Fig. 2-10. Fig. 2-10 (a) illustrates the magnetic flux density distribution of the MFEH in free space, while Fig. 2-10 (b) demonstrates the flux distribution when the MFEH is positioned near the rail track. The latter reveals an explicit concentration of magnetic flux generated by the MFEH, attributable to the rail track's low-reluctance path.

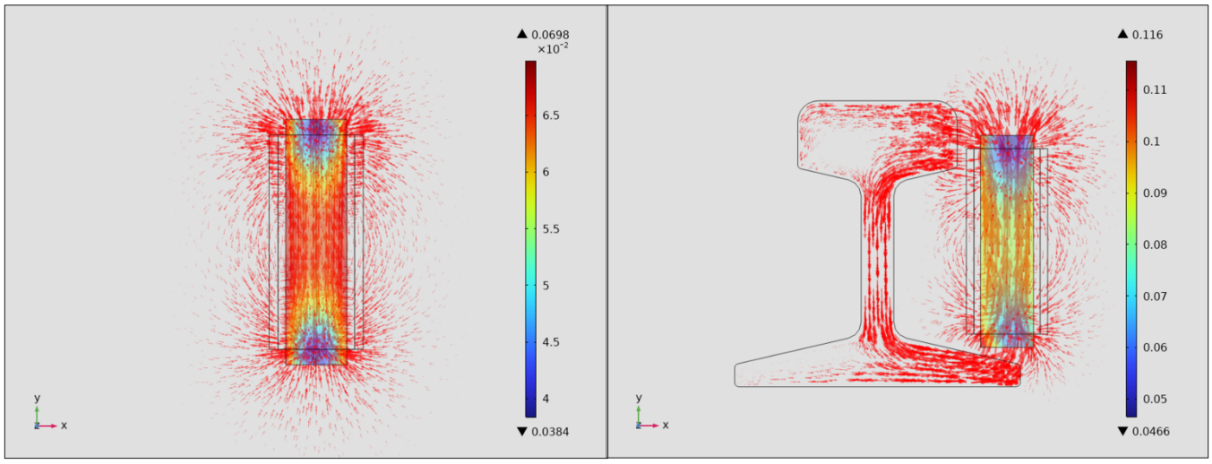

(a) (b)

Fig. 2-10 Magnetic flux density distribution (a) without a rail track present (b) with a rail track present Units: T

The proximity-dependent variation of coil parameters, including both resistance and inductance, highlights the requirement of careful consideration during compensation circuit design. As the coil inductance changes with positioning, the required compensation capacitance must be correspondingly adjusted. Furthermore, as eddy currents induced in the rail track can diminish the system's power output, systematic positioning of the MFEH is critical to optimize energy harvesting efficiency, balancing the trade-off between flux concentration benefits and eddy current losses.

2.3.4 The Proposed System Architecture for the MFEH

This study presents the design and development of a free-standing magnetic field energy harvester to harvest energy from the ambient magnetic fields naturally present in electric railway environments, specifically near current-carrying structures. The harvested energy is intended to power autonomous devices in WSNs. Due to practical constraints, the MFEH is positioned in close proximity to the rail track, which also serves as a conductor in electric railways to return current to the primary supply station. The MFEH consists of a ferromagnetic core wound with a copper coil. When exposed to the time varying magnetic field generated by currents in the rail track, an EMG is induced across the coil of the MFEH. The fundamental system architecture of the proposed energy harvesting system is illustrated in Fig. 2-11.

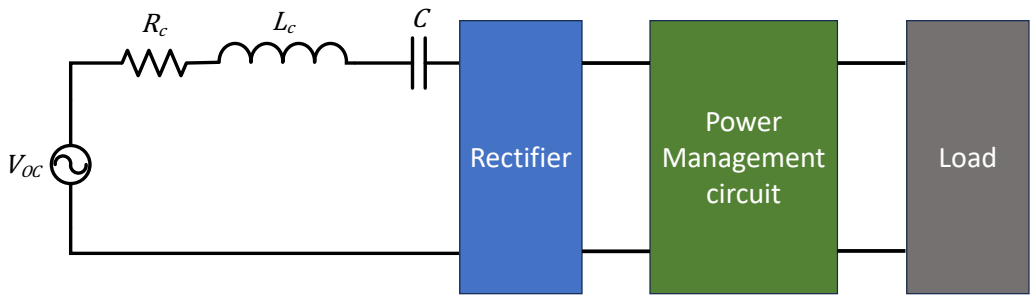

Fig. 2-11 The proposed system architecture of the MFEH

In this energy harvesting system, to extract usable power, the coil inductance of the MFEH must be compensated. This is achieved through compensating capacitors connected in series with the copper coil, that brings the system's net reactance near zero, enabling alternating current to flow when connected to a load. However, since WSN components typically operate on DC power, the harvested AC power must be rectified to DC despite inevitable voltage drops in the conversion process.

While maximum power transfer in the AC domain is achieved through impedance matching, the DC loads require an additional power management circuit to maintain optimal power delivery to the load under varying conditions. To address this, a custom DC-DC converter is integrated into the proposed system to regulate power flow to the DC load. This converter ensures maximum output power is maintained even with fluctuating load demands and fluctuating rail currents, thereby enhancing the system’s efficiency and reliability.

2.4 Summary

In this chapter, a comprehensive system overview of free-standing magnetic field energy harvesting was documented starting from a detailed investigation of magnetic flux density distributions in electric railway environments, for magnetic field energy harvesting applications. It was established that free-standing MFEH techniques are preferred over cable clamped configuration in electric railways, due to physical interference from pantograph operations on overhead lines. Therefore, the magnetic flux density distribution patterns around rail tracks were analyzed using FEM simulations.

The discussion presented the fundamental equivalent circuit and theoretical framework for free-standing MFEH systems in railway applications. Key factors influencing the system's output power were identified and highlighted for optimization during subsequent parametric simulations and experimental analyses. Challenges inherent to free-standing magnetic field energy harvesting systems, including core losses and dynamic variations in coil parameters, were critically examined using FEM analyses. The critical role of core material selection in balancing energy harvesting efficiency with loss mitigation was discussed in the chapter. The chapter concluded by detailing the foundational system architecture developed for this research, providing the basis for the experimental implementation of the study

CHAPTER 3 DESIGN AND FABRICATION OF THE MFEH

3.1 Introduction

The free-standing MFEH, comprising a magnetic core wound with a copper coil is the most critical component of the proposed energy harvesting system as its design significantly impacts the overall power output. As established in the theoretical analysis presented in the previous chapter, performance of the MFEH is governed by multiple interdependent parameters, each affecting the final power output. These parameters exhibit complex interrelationships, whereby modifications to one parameter can alter others. To address these complexities, FEM simulations were employed to systematically optimize the design parameters, ensuring alignment with the overall goal of maximizing power output of the energy harvesting system.

This chapter presents the design and optimization methodologies employed to enhance the output power of the MFEH. The simulation framework established for parametric optimization is first described, including the material properties assigned to various structural components and key assumptions adopted in the simulation model. The chapter consists of detail explanations on diverse simulation studies conducted to evaluate various critical parameters of the MFEH, such as core geometry and coil winding configuration. The results obtained from these parametric investigations are presented graphically and analyzed in detail. Based on these findings, specific recommendations are formulated to optimize the power output of the MFEH. Furthermore, for parameters exhibiting complex interdependencies, where adjustments to one parameter influence others, systematic optimization strategies are introduced to balance trade-offs and maximize overall system performance.

The final section of this chapter outlines the parameter selection process for fabricating the MFEH, based on the results obtained from FEM simulation analysis. Thereafter, a preliminary performance analysis of the MFEH is presented, detailing results from laboratory experiments conducted under controlled conditions. The laboratory experiments were conducted to evaluate the system's response to varying operational parameters. Through these experimental investigations, the optimal positioning of the MFEH is determined to minimize eddy current

losses. Experimental validation is then performed to compare FEM simulation results with experimental data, and discrepancies between the two are analyzed and explained. The output power of the fabricated MFEH is systematically characterized under diverse operating conditions and optimal AC load parameters that maximize power extraction are identified. Finally, the maximum achievable voltage and current levels from the MFEH are recorded to establish design specifications for the rectifier and power management circuitry, ensuring full system compatibility.

3.2 Design and Optimization of the MFEH Using FEM Parametric Simulations

3.2.1 The Simulation Setup

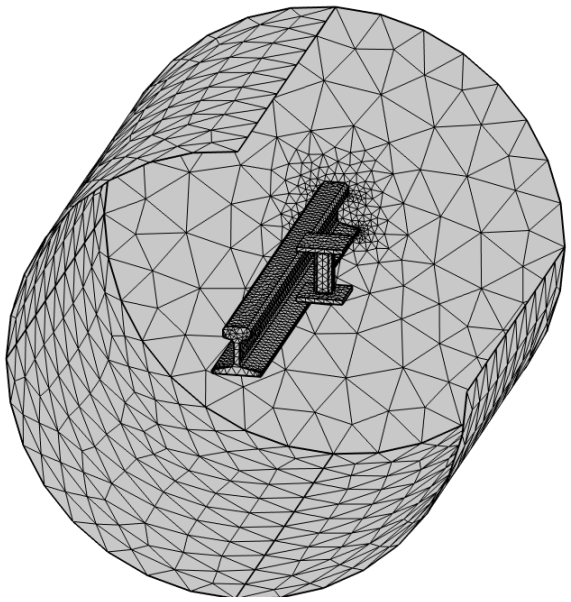

Fig. 3-1 Meshed illustration of the FEM Simulation setup used in COMSOL Multiphysics

The parametric optimization of the geometric design of the MFEH was conducted using COMSOL Multiphysics software. Fig. 3-1 illustrates the FEM simulation setup, which consists of a 1-meter P30 rail track segment positioned at the centre of a cylindrical air domain (1 m diameter × 1 m length). The modelled MFEH design was positioned adjacent to the rail track to maximize flux linkage based on the magnetic flux density distribution analysis presented in the previous chapter. The coil was modelled using COMSOL's built-in rectangular hollow geometry, with its thickness automatically adjusted to accommodate variations in winding count and wire diameter. The core material selection was based on three fundamental criteria derived from theoretical analysis and literature review. As demonstrated by Equations 2-6 and 2-14, high relative permeability is essential to maximize effective permeability and flux concentration. To simultaneously address hysteresis and eddy current losses during cyclic magnetization, a soft magnetic material with low electrical conductivity was identified as optimal. MnZn ferrite was ultimately selected as it satisfies all three requirements, combining a high relative permeability of 3300 with an electrical resistivity of 6 Ωm, making it particularly

suitable for energy harvesting applications. The material properties specified in Table 3-1 were used for the FEM simulations unless otherwise specified.

To maintain computational efficiency, the MnZn ferrite core was modelled with linear magnetic properties, despite its inherent nonlinear B-H characteristics. This simplification is justified by the material's soft magnetic properties and operation well below saturation limits for free-standing magnetic field energy harvesting. Gauge fixing for A-field condition in COMSOL was applied to numerically stabilize the solutions of the simulation study.

Table 3-1 Materials properties assigned in the simulation study

Description	Symbol	Value	Unit
Electrical conductivity of the rail track	σ_S	1.5×10^6	S/m
Relative Permeability of the rail track	μ_S	30	-
Electrical conductivity of the magnetic core	σ_C	1/6	S/m
Relative permeability of the magnetic core	μ_r	3000	-
Electrical conductivity of the copper wire	σ_{cu}	6×10^6	S/m

The parametric optimization process of the MFEH involved systematic evaluation of power output variations in response to changes in key parameters, including core length, cross sectional area of the core, coil length, number of coil turns and wire thickness. Since these parameter modifications sometimes affect either both or one of the coil resistance or the coil inductance, the simulation analysis was performed in two distinct phases: coil parameter analysis and power output analysis.

Phase I - Coil parameter Analysis

In the first phase, the changes in coil resistance and inductance resulting from each parameter variation were characterized. This analysis incorporated the combined effects of both eddy current generation and magnetic reluctance variations on the resulting coil resistance and inductance changes, consistent with the theoretical framework established in the previous chapter. Simulations were conducted with the coil of the MFEH externally energized by a 100 mA current while maintaining the rail track in open-circuit configuration, which allowed precise measurements of impedance parameters under each modified condition.

Phase II – Output Power Analysis

In the second phase the output power of the MFEH was evaluated by implementing a compensated circuit configuration. Based on the inductance values obtained in the first phase, a compensating series capacitor was connected to cancel the coil reactance. Simultaneously, a load resistor matching the measured coil resistance (unless otherwise specified) was connected in series using COMSOL's Electrical Circuit Interface. Power dissipation across the load was then measured while exciting the rail track with a 300 A, 50 Hz current (unless otherwise specified), enabling assessment of each parameter's influence on the power output of the system.

This two-phase approach enabled systematic evaluation of the impact of various parameters on the power output of the magnetic field energy harvester through parametric simulations. Each parameter was varied independently to assess its specific impact. The simulation results, which examine both core and coil parameter optimization, are discussed in detail in the following sections.

3.2.2 Optimization of Core Parameters

The geometric configuration of the core significantly impacts the final output of the MFEH unit. Therefore, optimizing core parameters represents a crucial design step for achieving higher harvesting efficiency and maximum output power. This optimization process involves carefully adjusting the physical dimensions MFEH's core through FEM parametric analysis to maximize power generation while satisfying practical operational constraints.

As specified in Equations 3-1, 3-2 and 3-3, the parametric simulation studies were conducted varying core parameters that impact the output power of the MFEH. Each modification aimed to maximize the harvester's output power, guided by the theoretical framework established in previous chapters. However, due to complex interdependencies between certain parameters, careful trade-offs between competing design parameters are required to achieve optimal performance of the MFEH.

$$P_O = \left(\frac{V_{OC}}{2\sqrt{2}}\right)^2 / R_C = \frac{{V_{OC}}^2}{8R_C} = \frac{(NA_eB_{ex}\omega\mu_{eff})^2}{8R_C} \qquad 3\text{-}1$$

$$\mu_{eff} = \frac{\mu_r}{1 + N_d(\mu_r - 1)} \quad 3\text{-}2$$

$$N_d \propto \frac{D}{L} \quad 3\text{-}3$$

Considering the material availability for fabrication, two preliminary core designs were developed for the MFEH and modelled in COMSOL Multiphysics, as illustrated in Fig. 3-2. Both designs feature a square rod-shaped core with dimensions of 10 mm × 10 mm × 50 mm. The second design incorporates an enhanced configuration with two collector plates (50 mm × 50 mm × 5 mm each) attached to opposite sides of the core to improve magnetic flux penetration through the core. For both configurations, the coil winding consists of 5000 turns of 0.2 mm diameter copper wire, uniformly distributed over a 50 mm length.

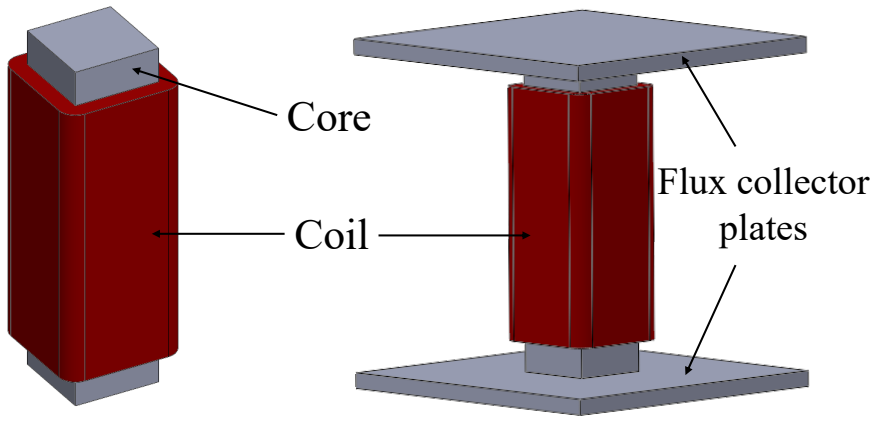

Fig. 3-2 Initial core designs of the MFEH

The comparative performance evaluation of the two MFEH core designs was conducted by measuring both induced open-circuit voltage and output power across a matched load under varying rail track currents, as shown in Fig. 3-3. The results demonstrate that Design 2, incorporating two collector plates, exhibits better performance compared to Design 1 in both measured parameters.

This enhancement primarily arises from two interrelated mechanisms: increased magnetic flux density within the core and improved effective permeability both attributable to the flux

collector configuration [80]. Based on these demonstrated advantages, Design 2 was selected as the preferred configuration for the MFEH and subsequently underwent further optimization in this investigation.

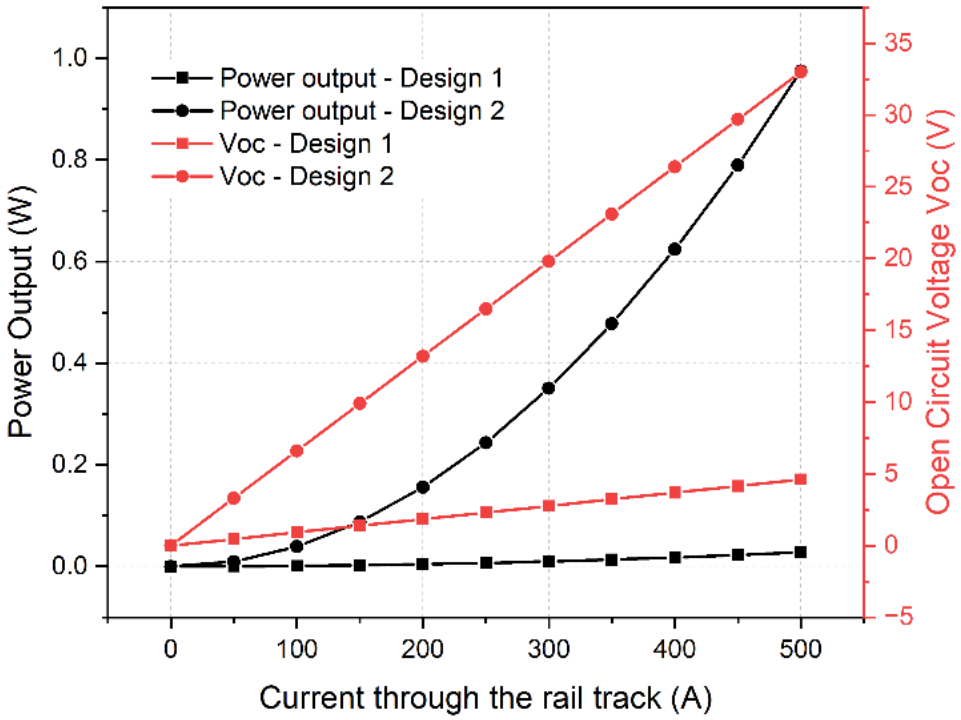

Fig. 3-3 Comparison of power output and open circuit voltage of the two designs against varying rail current

As theoretically established by Equations 2-14 and 2-17 in the preceding chapter, increasing the length of the core enhances the effective permeability of the core, thereby improving the output power of the energy harvester. To validate this relationship, a parametric simulation study was conducted by linearly increasing the core length of the MFEH. The results, illustrated in Fig. 3-4 confirm that both output power and open circuit voltage rise proportionally with core length. Notably, the magnetic flux density through the core remains nearly constant across all tested lengths, as shown in the graph. According to Equation 2-2, the open-circuit voltage depends on two variables under these conditions: magnetic flux density and effective permeability. Since the flux density remains stable, the observed voltage increase can be attributed solely to the enhanced effective permeability of the core. This improvement arises from the reduced demagnetization factor associated with longer core geometry, which aligns with the theoretical framework presented in the previous chapter. Thus, the parametric study conclusively demonstrates that optimizing core length directly amplifies output power by

improved effective permeability of the core. Therefore, a lengthy core for the MFEH is recommended based on the results of the parametric study.

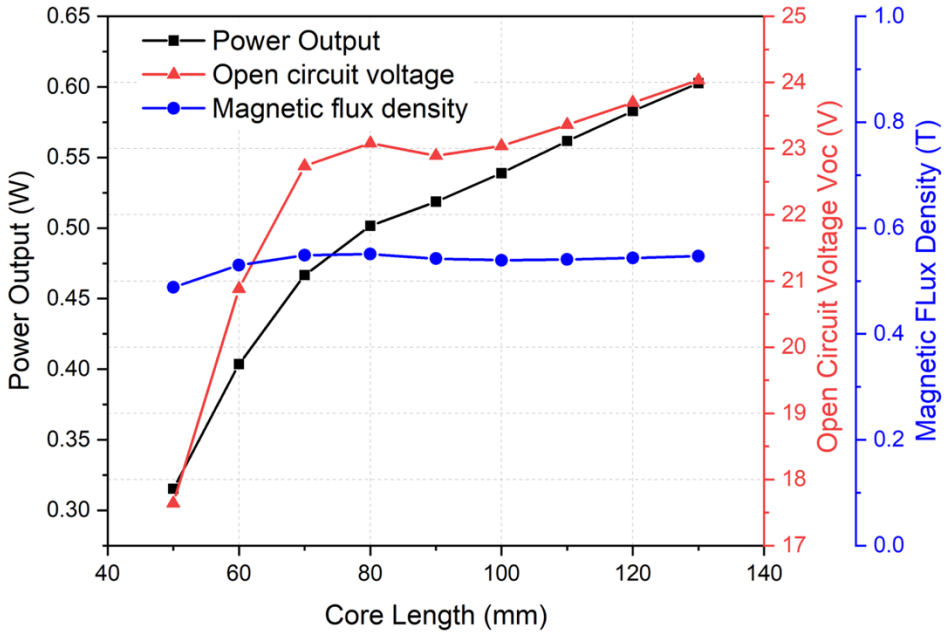

Fig. 3-4 Impact of core length on the power output, open circuit voltage and magnetic flux density

Fig. 3-5 demonstrates the influence of flux collector area on the output power of the MFEH. The results indicate that expanding the collector area enhances magnetic flux density within the core, consequently improving the power output of the MFEH. However, as MnZn Ferrite exhibits a saturation flux density between 0.4-0.5 T, the data reveals that collector areas exceeding 3000 mm^2 would drive the core into saturation, ultimately limiting output power.

This limitation can be mitigated through parameter optimization. Fig. 3-6 illustrates that increasing the cross-sectional area of the core reduces the internal flux density while simultaneously decreasing output power. However, the power reduction from core area adjustment proves negligible compared to the gains achieved through collector plate expansion. This reduction in magnetic flux density results from the increased demagnetization factor associated with larger cross-sections. As established by Equation 2-17, the demagnetization factor exhibits a direct proportionality with diameter in cylindrical geometries. This relationship remains applicable to square rod configurations through appropriate geometric adaptation. Therefore, to ensure optimal performance, the core design of the MFEH should

maintain a minimum cross-section of 300 mm², corresponding to an 18 mm side length for the square rod configuration employed in this study.

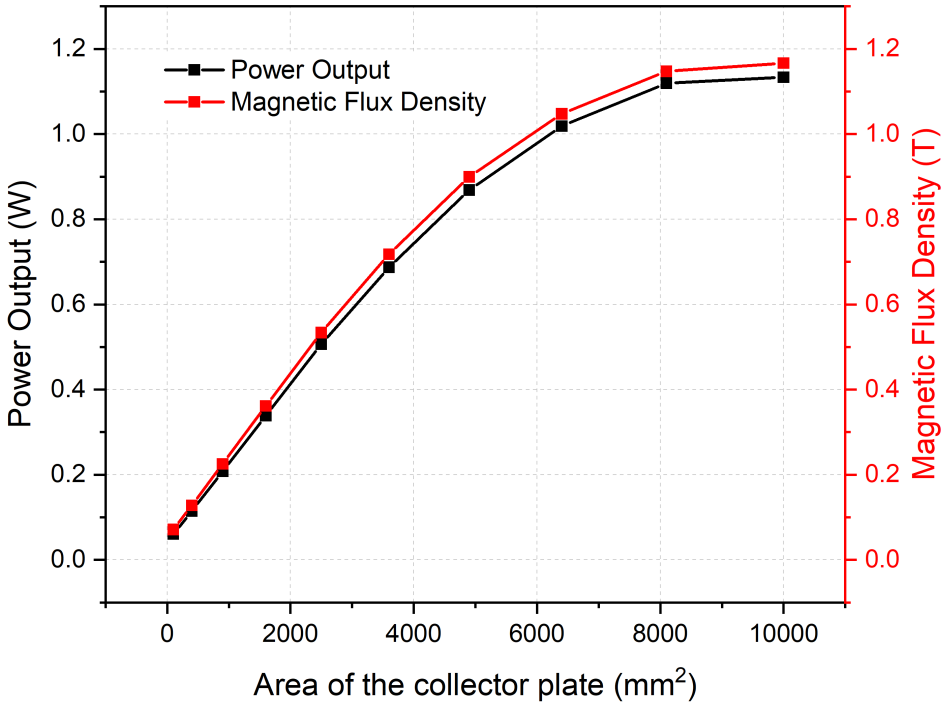

Fig. 3-5 Impact of flux collector area on power output of the MFEH

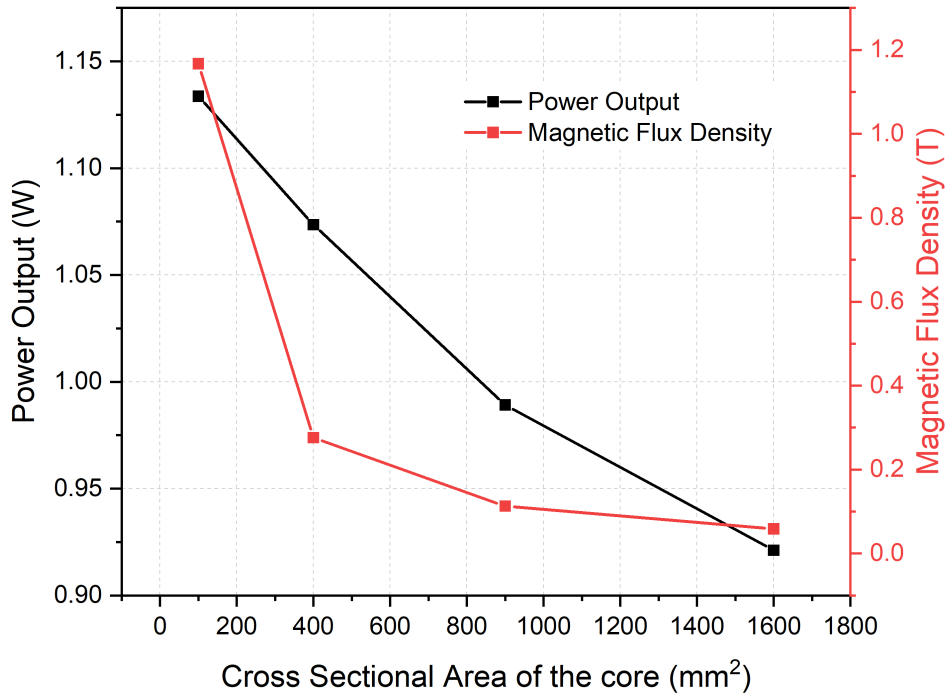

Fig. 3-6 Impact of cross sectional area of the core on output power

3.2.3 Optimization of Coil Parameters

The optimization of coil parameters represents a critical aspect of enhancing the power output of the energy harvesting system. Three key coil parameters, the number of coil windings N, wire diameter D_w and windings length l_c exert significant impact on the overall energy harvesting system performance. These parameters collectively influence four critical performance metrics: coil resistance, induced voltage, magnetic flux density within the core, and coil inductance. Given the strong interdependencies among these parameters and their combined effects on power output, a systematic FEM-based parametric simulation analysis was conducted. A tightly wound coil configuration was assumed during the simulation analysis to regulate the computational burden. To isolate the effect of each coil parameter, other variables were held constant by adjusting the coil thickness t specified in Equation 3-4.

$$t = \frac{N \times {D_w}^2}{l_c} \tag{3-4}$$

The results of the parametric simulations investigating the effect of coil winding length l_c variation on performance of the MFEH is illustrated in Fig. 3-7. The results demonstrate a significant improvement in output power with increasing coil length, while the open-circuit voltage remains relatively constant. This improvement in output power is attributed to a reduction in coil resistance, which decreases as l_c increases. The coil resistance reduction arises from two factors. When windings are distributed along the core, shorter effective wire length due to decreased coil thickness as quantified by Equation 3-4 results in reduced wire resistance R_W. Due to the distributed coil configuration diminished eddy current formation results in reduced AC resistance R_{ac} thus, lowering the total coil resistance R_C.

Although output power of the MFEH vary significantly with the increased coil length, the induced open-circuit voltage remains stable due to the constant winding number, with only minor variations attributable to reduced magnetic flux density caused by the expanded winding distribution. Based on these observations, increasing the coil winding length was recognized as an effective strategy for enhancing power output of the MFEH while maintaining voltage characteristics.

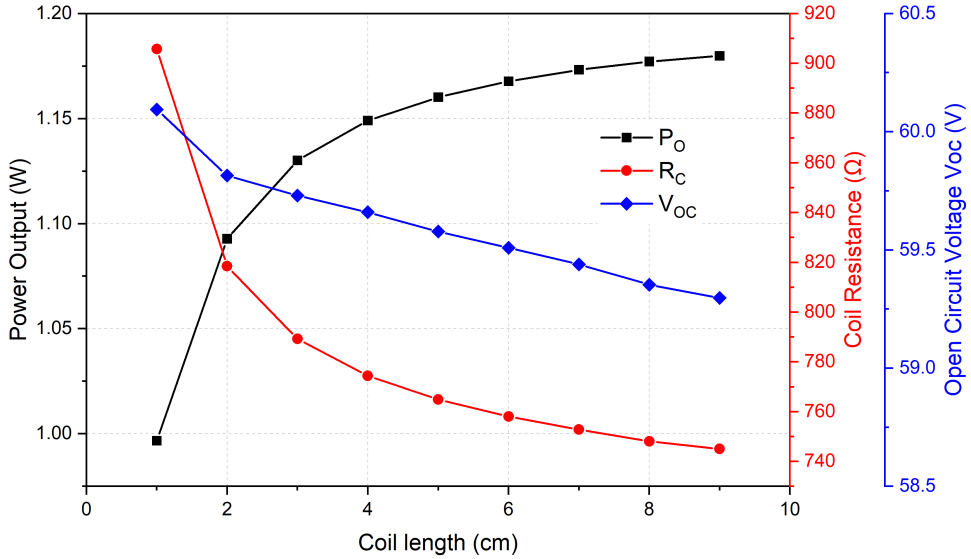

Fig. 3-7 Impact of Coil length on power output, coil resistance and open circuit voltage

The remaining two coil parameters, number of coil windings N and wire diameter D_w critically influence overall performance of the energy harvesting system by modulating coil resistance, open-circuit voltage, and magnetic flux density within the core. These interdependent effects collectively determine the output power of the MFEH. However, varying these parameters also significantly alters the total copper volume in the winding assembly, which requires careful optimization. To systematically evaluate these relationships, comprehensive parametric simulations were conducted examining all feasible combinations of N and D_w within a specified range.

Fig. 3-8 (a) illustrates the output power heat map for these parameter combinations. The results demonstrate that increasing either N or D_w enhances output power of the MFEH. The figure further reveals that different parameter combinations can yield equivalent performance. For instance, a configuration using 0.6 mm diameter copper wire with 1,000 windings produces similar output power to one using 0.3 mm wire with 4,000 windings. This equivalence is further supported by the corresponding magnetic flux density heat map illustrated in illustrated in Fig. 3-8 (b) which exhibits nearly identical response patterns to parameter variations. Therefore, these findings collectively establish that the output power of the MFEH depends fundamentally on the total copper volume in the winding assembly rather than on the individual parameters of winding count or wire diameter.

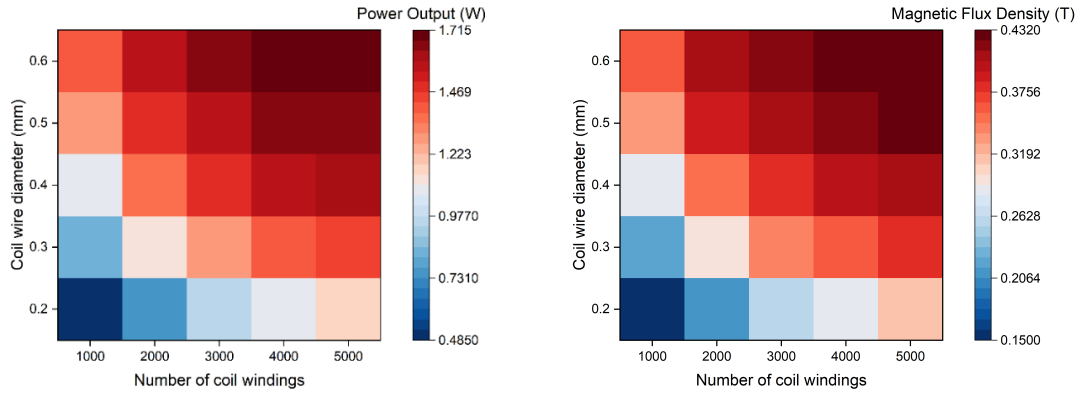

(a) (b)

Fig. 3-8 Impact of coil wire diameter and number of coil windings on (a) overall power output of the MFEH (b) magnetic flux density within the core

However, as shown in Fig. 3-9 (a), the open-circuit voltage exhibits a linear increase with the number of coil turns irrespective of variations in wire diameter. A similar trend is observed in the load voltage profile demonstrated in Fig. 3-9 (b) where higher winding counts amplify voltage levels. However, these elevated voltage levels may introduce significant design challenges, as the resulting voltage stress could adversely affect both the rectifier and power management circuitry. To mitigate these issues while maintaining optimal output power, the analysis suggests selecting a configuration employing thicker wire with fewer winding turns. This design approach achieves two critical objectives of maintaining voltage levels within practical operational limits for downstream electronics, and preserving the system's power generation capability.

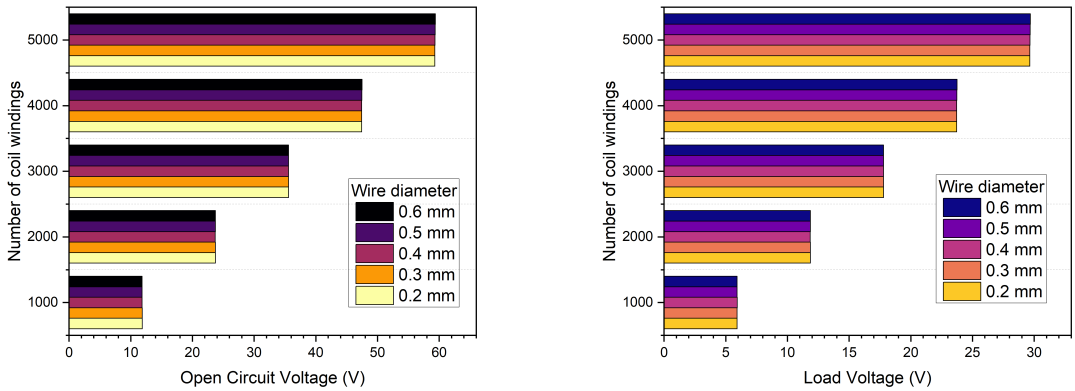

(a) (b)

Fig. 3-9 Impact of coil wire diameter and number of coil windings on (a) open circuit voltage (a) load voltage

Furthermore, Fig. 3-10 reveals an inverse relationship between winding count and load current, demonstrating a significant load current reduction as the number of turns increases. While configurations with higher winding numbers achieve greater voltage and output power, this comes at the expense of diminished current delivery capability, a critical limitation for WSN applications where sufficient current is required to power their autonomous electronic devices. Therefore, it is important to select a good combination of coil parameters for N and D_w that delivers both a feasible voltage and sufficient current to drive the loads while securing a maximum power output from the MFEH.

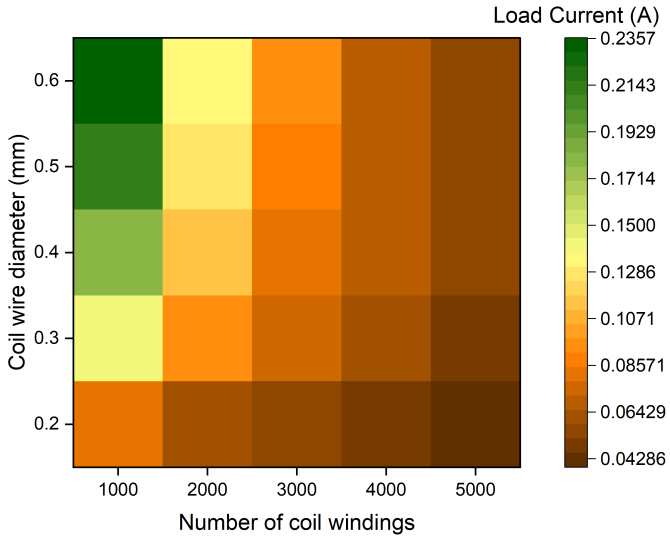

Fig. 3-10 Impact of coil wire diameter and number of coil windings on the load current.

3.3 Fabrication and Preliminary Performance Analysis of MFEH

The parametric simulation studies performed systematically investigated the complex interdependencies between critical design parameters influencing output power of the MFEH. These analyses yielded optimized configuration parameters, which guided the fabrication of the MFEH prototype depicted in Fig. 3-11. The recommendations derived from the simulation studies were incorporated for final design implementation to maximize energy harvesting performance.

The core of the MFEH was constructed using MnZn Ferrite PC95 material, selected for its high relative permeability of 3300 (± 25%) and low electrical conductivity of 0.167 S/m. The material exhibits a saturation flux density ranging from 410 to 520 mT, which depends on operating temperature. The core dimensions were determined based on the recommendations noted through FEM simulation analyses while also considering commercial material availability. Therefore, the final design was fabricated using a square-shaped ferrite rod (25 mm × 25 mm × 102 mm) with two attached collector plates (100 mm × 100 mm × 10 mm) bonded using an adhesive. For the coil assembly, a 3D-printed square bobbin (29 mm outer side length) was fixed around the central ferrite rod. A 0.5 mm diameter enamelled copper wire was manually wound to create 2065 coil turns distributed over a 95 mm winding length. Fabricated MFEH prototype, featuring a square-shaped rod ferrite core with dual collector plates and a 2065-turn copper winding

Table 3-2 presents a comparison of the measured coil resistance and inductance obtained in a ferromagnetic-free environment versus simulated results obtained in a cylindrical air domain. The close alignment between simulated and experimental values underscores the validity of the design methodology while the minor discrepancies in coil parameters revealed during experimental measurements can be primarily attributed to geometric irregularities introduced by the manual winding process.

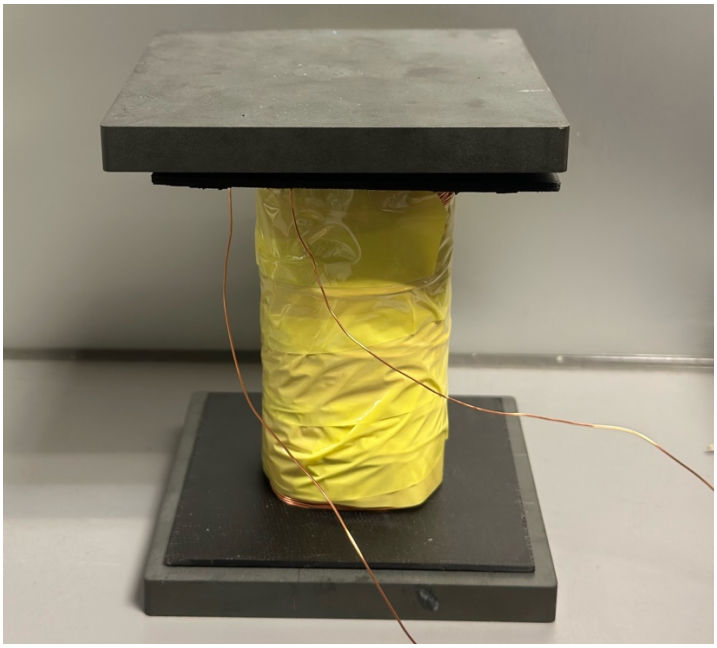

Fig. 3-11 Fabricated MFEH prototype, featuring a square-shaped rod ferrite core with dual collector plates and a 2065-turn copper winding

Table 3-2 Comparison of simulated and experimentally measured coil parameters

Coil resistance		Coil inductance	
FEM (Ω)	Experiment (Ω)	FEM (H)	Experiment (H)
23.76	23.9	1.89	1.75

3.3.1 Experimental Setup

The fabricated MFEH was evaluated in a laboratory environment through AC power analysis, which involved measuring the power dissipated across a load directly connected to the coil through compensation capacitors connected in series. The initial phase of the analysis focused on identifying the optimal positioning of the MFEH to maximize output power accounting to the variations in both coil resistance and inductance due to proximity to the rail track. Once this position was established, the induced open-circuit voltage range and the maximum achievable load current generated by the harvester were systematically recorded. The rectifier and power management circuitry were subsequently designed and fabricated based on the obtained experimental results, to ensure optimal compatibility with the MFEH's operational parameters.

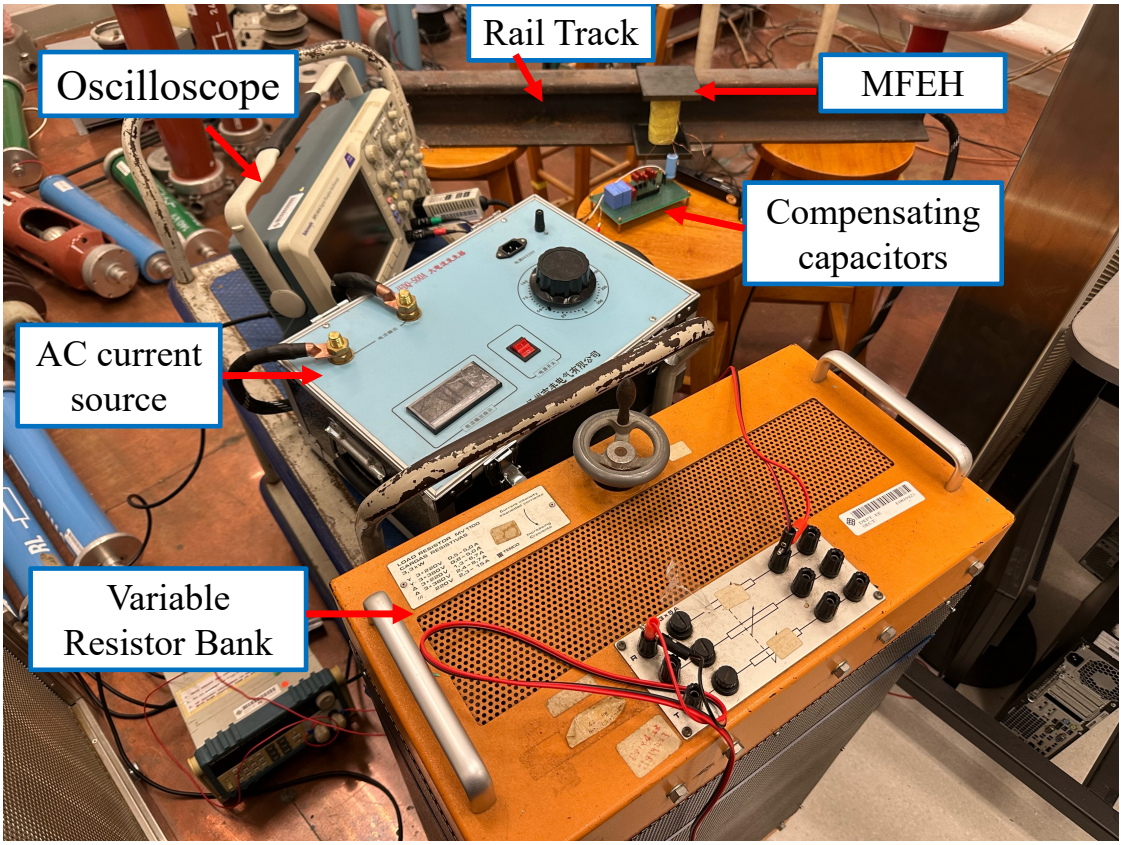

Fig. 3-12 Experimental setup for performance analysis of MFEH

The experimental setup for MFEH performance analysis is shown in Fig. 3-12. A 1-meter long P30-type rail track fabricated from Q235 steel was employed to replicate real-world operating conditions in an electric railway. The MFEH was positioned adjacent to the rail track using a rigid 3D-printed platform securely fixed to the rail surface. The variations in the coil resistance and inductance of the MFEH caused by proximity to the ferromagnetic rail track, were systematically measured at each adjusted position using an NF ZM2371 LCR meter operating at 50 Hz. These measurements captured the resultant changes in coil resistance influenced by eddy currents formation in the rail track and changes in coil inductance due to magnetic reluctance variations, phenomena which were theoretically detailed in prior sections of this study. Following the measurements of coil parameters, the coil inductance was compensated by adding a combination of ceramic capacitors in series with the coil while monitoring the combined reactance until it approached zero. A variable resistor bank was then connected in series with the compensated coil to complete the circuit. For performance evaluation, the rail track was energized with a 50 Hz AC current source (0–500 A range), while current flow was monitored via a UNI-T UT202 clamp meter. The voltage across the load resistor was measured to quantify instantaneous AC power output of the MFEH.

3.3.2 Optimal Positioning Analysis for the MFEH

The positioning of the MFEH relative to the rail track critically influences the power output of the energy harvesting system. This dependence arises primarily from variations in captured magnetic flux density, which diminishes with increasing distance from the current-carrying rail as explained by Equation 2-1. Although close proximity enhances magnetic flux density penetration through the core of MFEH, it simultaneously promotes eddy current formation on the rail track that can degrade performance due to increased coil resistance. Consequently, an optimal positioning strategy must balance these competing effects to maximize power output of the energy harvester. This section presents a systematic methodology to determine the optimal position for the MFEH to extract maximum output power while accounting for proximity effects on coil impedance.

A systematic analysis was performed to determine the optimal positioning of the MFEH by evaluating its output power at varying distances from the rail track. The horizontal distance between the base of the rail track and the edge of the bottom collector plate of the MFEH was adjusted, with each change recorded using a predefined sign convention, as illustrated in Fig. 3-13. At each position, the coil resistance and inductance were first measured using the LCR meter. Following these measurements, compensation capacitors were integrated in series with the coil to minimize coil reactance ensuring optimal power transfer from the MFEH. Thereafter, the output power of the MFEH at each position was quantified by measuring the voltage across a matched load resistor connected in series with the rail track energized by a 300 A current at 50 Hz using the AC current source. This systematic approach ensured consistency in the laboratory experiments which accounted the variations in coil parameters prompted due to proximity of the MFEH to the rail track. The comprehensive results of this investigation are presented and discussed in forthcoming sections.

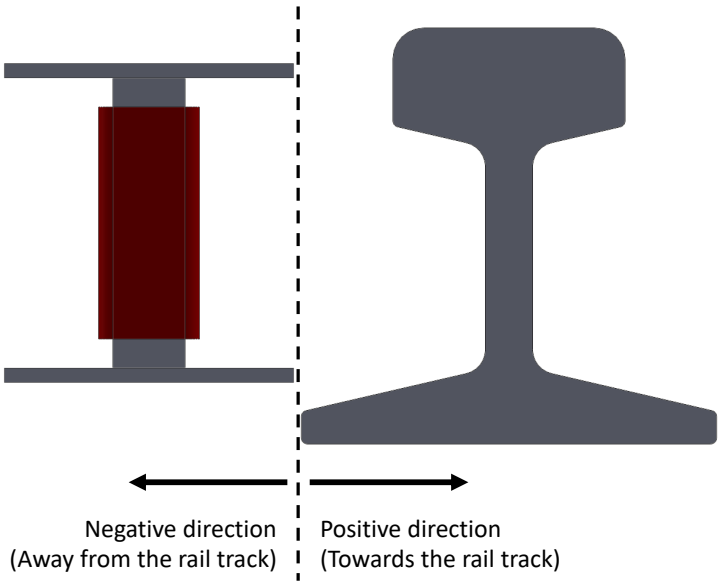

Fig. 3-13 Sign convention adopted to record positional variations of the MFEH

The variations in coil resistance and inductance as the MFEH is moved from a distant position towards the rail track from is illustrated in Fig. 3-14. The data demonstrate a progressive increase in both coil resistance and inductance as the MFEH is brought closer to the rail. The elevated coil resistance is attributed to enhanced in eddy current losses due to proximity to the rail. Increased coil inductance is resulted from reduced magnetic reluctance as the ferromagnetic rail track concentrates the magnetic flux.

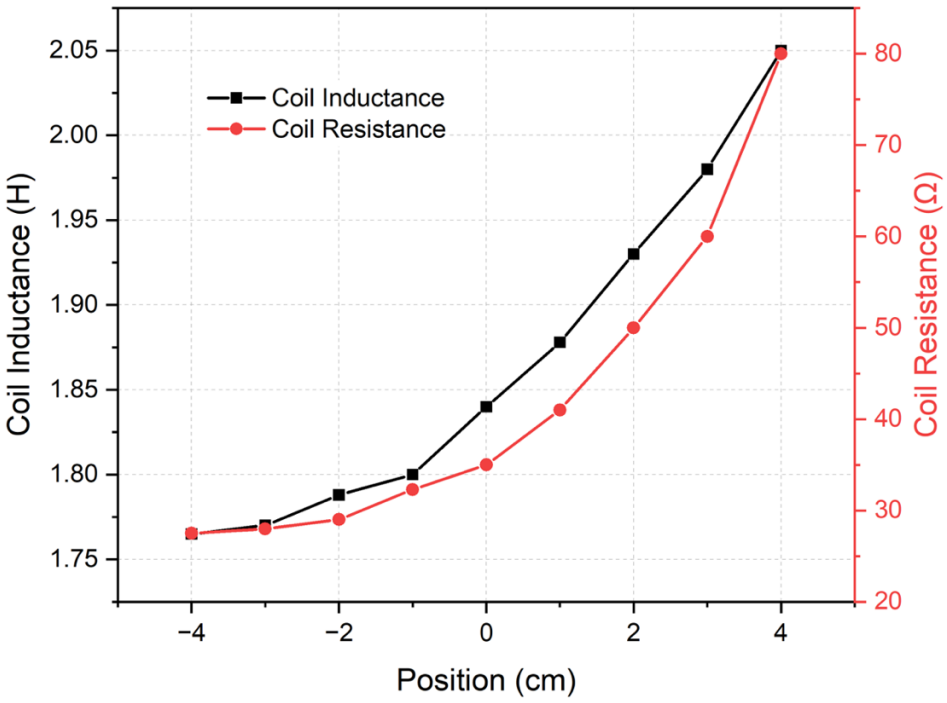

Fig. 3-14 Effect of the position of MFEH on coil inductance and resistance

Fig. 3-15 demonstrates the increasing induced open-circuit voltage as the MFEH approaches the current carrying rail track, a phenomenon which can be attributed to enhanced magnetic flux density closer to the rail track as explained by Equation 2-1. However, the output power exhibits a distinct behaviour compared to monotonic increase observed in open-circuit voltage. Experimental data reveal that the maximum output power of 2.06 W occurs when the MFEH is positioned at the 2 cm while it decreases beyond that point. This discrepancy arises from the combined effects of enhanced magnetic flux density and eddy current losses. While enhanced magnetic flux close to rail track improves the induced voltage, it simultaneously elevates eddy currents losses within the conductive rail structure which results in increased coil resistance close to the rail track. These losses, which escalate beyond the 2 cm mark, impede the gains from higher induced voltage, ultimately diminishing net power output. Experimental measurements recorded a 2.06 W maximum output power at the 2 cm position under 300 A rail current, establishing this as the optimal operational configuration. The results clearly demonstrate that higher induced voltages do not necessarily yield greater power output due to the influence of eddy current losses.

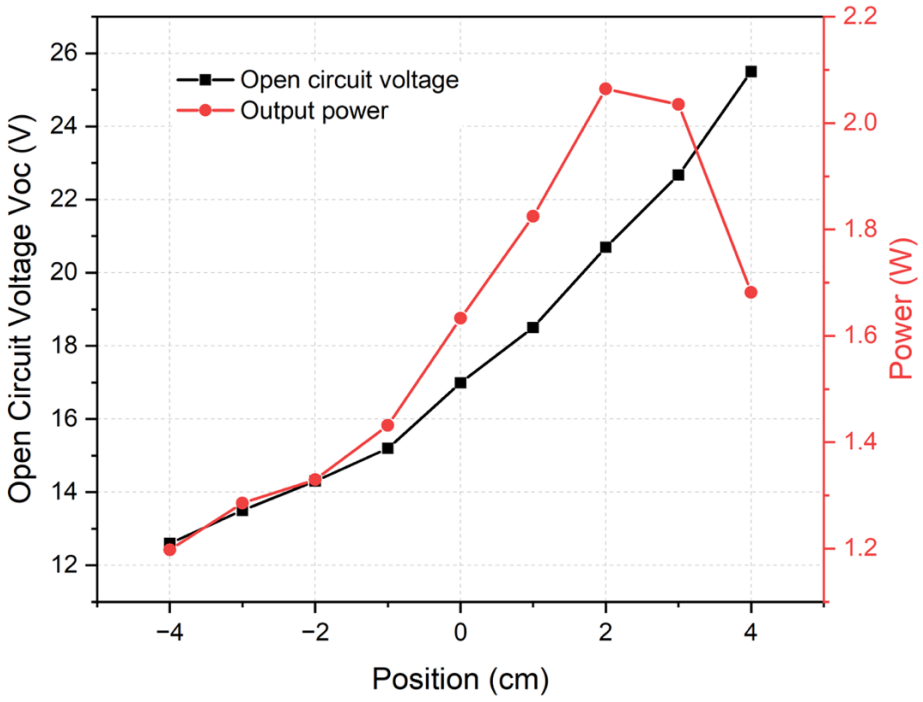

Fig. 3-15 Effects of the position MFEH on its induced open-circuit voltage and power output

However, the optimal position (2 cm) identified is specific to the MFEH design employed in this study, as the relationship between eddy current formation and power output of the MFEH varies with its core geometry. While the experimental methodology employed remains

applicable to alternative designs, the particular optimal positioning will differ depending on the geometric characteristics of the MFEH. In addition, the optimal position identified in this study is located in close proximity to the rail track, at a distance of 2 cm. At this position, the energy harvester is susceptible to damage from moving train components and may be affected by rail vibrations. Although the optimal position determined is maintained in the study, a practical placement option for the proposed energy harvester must be considered. A position on the sleepers is suggested as a suitable alternative to meet this requirement.

3.3.3 Experimental Validation of the Fabricated MFEH

To validate the fabricated MFEH against its FEM simulation design, the induced open-circuit voltage was characterized after experimentally determining the optimal positioning. As illustrated in Fig. 3-16, induced open-circuit measurements were conducted across a current range of 0–500 A applied through the rail track specimen. The results demonstrate a linear dependence of open-circuit voltage on rail current amplitude, with close agreement between experimental and simulated values. This proportionality arises from the direct relationship between rail current and magnetic flux density, as theoretically described by Equations 2-1 and 2-2. The fabricated MFEH achieved a maximum open-circuit voltage of 34.3 V at 500 A rail current. The maximum open-circuit voltage recorded during the experiments marked a critical design parameter to configure the power management circuitry.

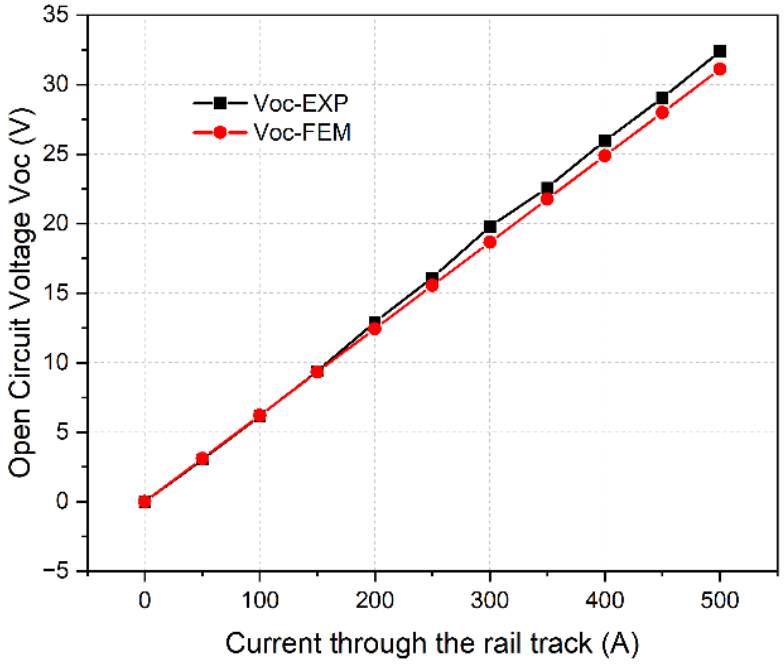

Fig. 3-16 Measured and simulated Induced open-circuit voltage against rail current amplitude

3.3.4 Power Rating Characterization of Fabricated MFEH

This section presents the experimental characterization of the power rating for the fabricated MFEH. The power output of the MFEH unit was determined by measuring the voltage across a variable load resistor connected in series with the compensated coil of the MFEH. To evaluate the device's maximum power delivery capacity, the load resistance R_L was varied from 0 to 100 Ω while maintaining a constant rail current of 300 A. The results illustrated in Fig. 3-17 reveal that the maximum power output of 2.2 W occurs at a load resistance of 60 Ω, despite the measured coil resistance R_C at the optimal 2 cm position, being 48 Ω. These findings highlight the importance of considering parasitic losses when designing free-standing MFEHs, as purely theoretical impedance matching may not yield optimal performance under practical operating conditions.

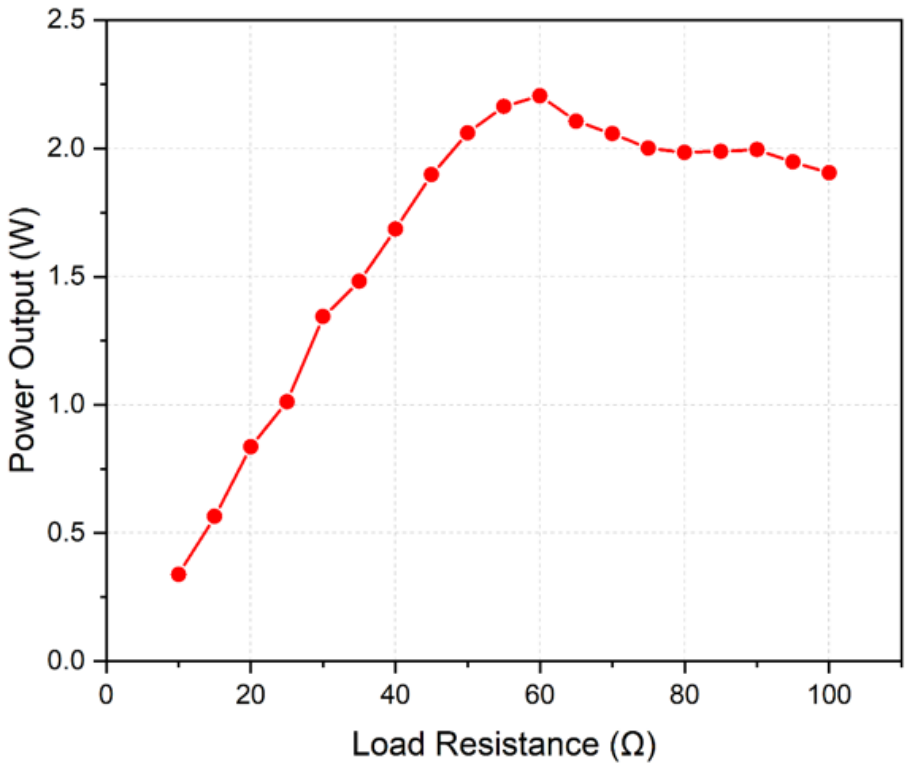

Fig. 3-17 Variation of power output against load resistance

The experimental investigation of the response of MFEH under increasing rail currents is shown in Fig. 3-18. A comparison of power output across both matched and optimal load conditions previously determined at 300 A rail current is illustrated in the figure. The results demonstrate nearly identical rapid growth in power output for both load configurations as the

rail current increases to 300 A. This behaviour is attributed to the proportionally enhanced magnetic flux density within the core, driven by the rising current in the rail track. Beyond the 300 A threshold, however, the power output exhibits only marginal increases, irrespective of load configuration. This saturation effect arises when the magnetic flux density inside the core exceeds the saturation flux density limit of the MnZn ferrite material (410–520 mT, as previously specified), leading to nonlinear magnetization and diminished flux variations within the core. The load voltage trends showing a linear relationship with rail current up to 300 A, followed by marginal voltage gains at higher currents confirm this phenomenon. These results emphasize the impact of magnetic saturation on the energy conversion efficiency of the MFEH. Despite these limitations, the MFEH achieved a maximum power output of 2.8 W under optimal load conditions and a power output of 2.36 W under matched load conditions at a rail current of 500 A.

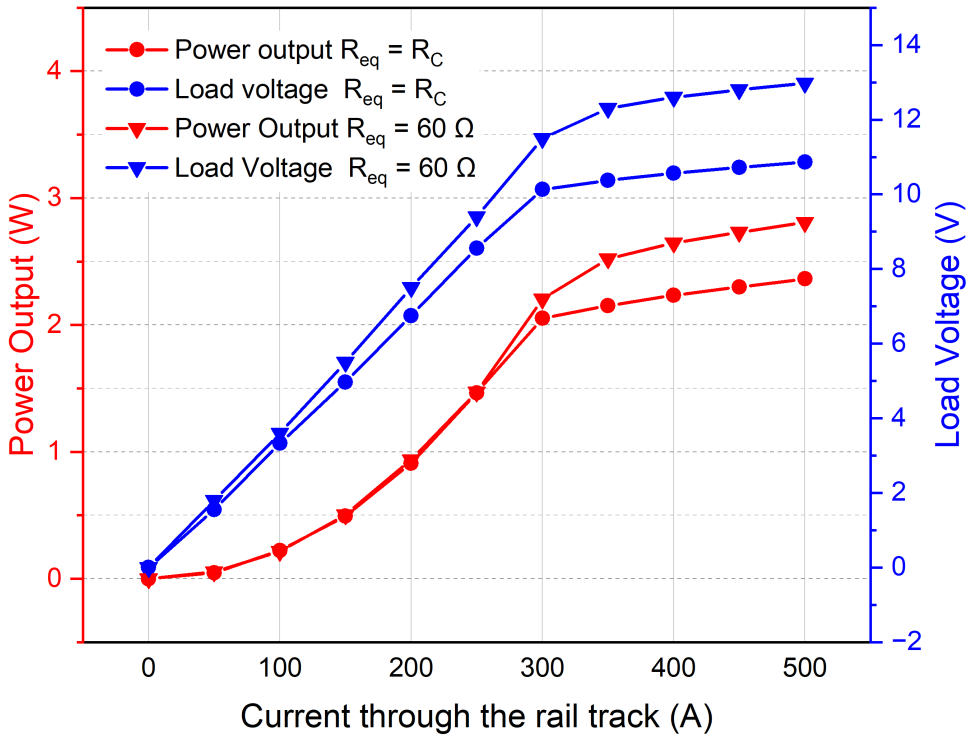

Fig. 3-18 Performance of the fabricated MFEH under matched load (48 Ω) and optimal load (60 Ω) conditions

In the subsequent phase of the experiment, the current through the rail track was maintained at constant levels of 350 A, 400 A, and 450 A, while the load resistance was varied from 0 to 120 Ω to investigate changes in the optimal resistance. As depicted in Fig. 3-19, the results demonstrate that the optimal load resistance of the MFEH varies with increasing rail current.

At each rail current level, the output power initially increases with load resistance, reaches a maximum at an optimal resistance, and subsequently decreases as the load resistance continues to rise. Specifically, for rail current levels of 350 A, 400 A, and 450 A, the optimal load resistances were determined to be 70 Ω, 80 Ω, and 100 Ω, respectively. The increase in optimal load resistance at higher current levels can be partly attributed to elevated magnetic core losses associated with increased current intensities. Additionally, an increase in load resistance reduces the magnetic flux density induced within the core by the coil current [73,89]. This reduction in magnetic flux density subsequently decreases core losses, as described by the Steinmetz equation [85]. Consequently, the optimal load resistance exceeds the coil resistance under these conditions. However, beyond this optimal resistance, further increases in coil resistance lead to a reduction in the output power of the MFEH. Ultimately, with an optimal load resistance of 100 Ω, the MFEH achieved a maximum power output of 4 W when the rail current was set to 450 A.

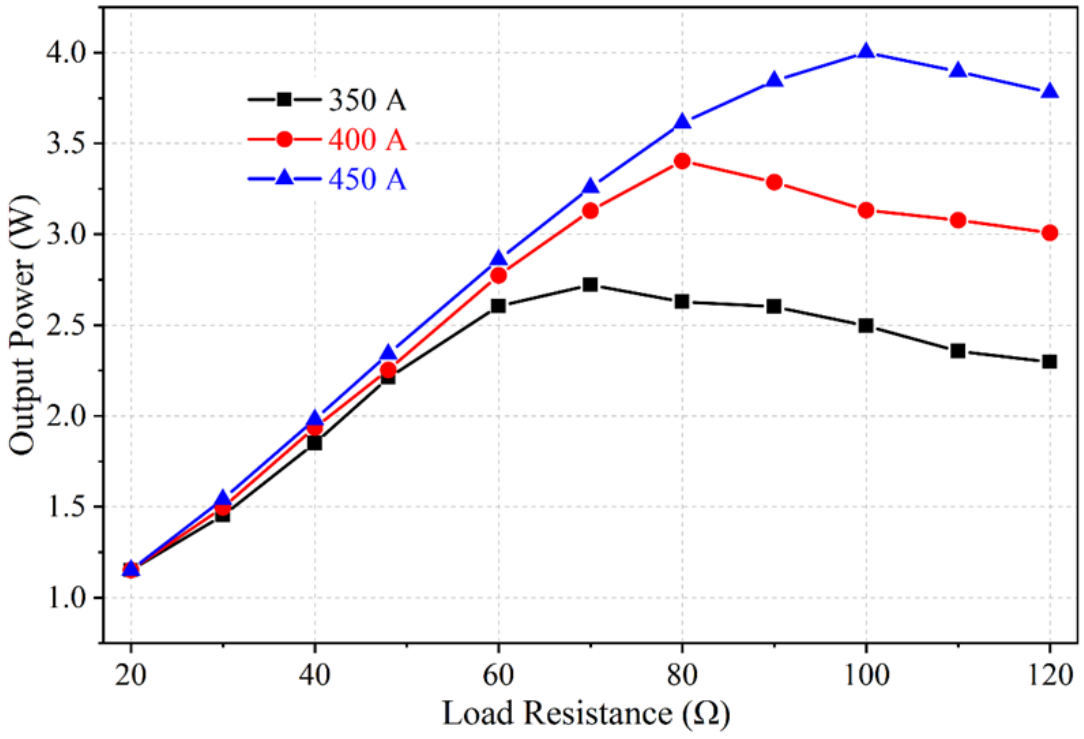

Fig. 3-19 Change of optimal load of the MFEH at different rail current levels

3.3.5 Requirement of a Power Management Circuit

The experimental characterization of the fabricated MFEH unit in previous sections demonstrated AC power output of the energy harvester when connected directly to an external resistive load with series capacitor compensation for coil inductance. However, as most components in WSNs require DC power input, power conversion and conditioning circuitry are required to enable practical implementation. Furthermore, while maximum power transfer occurs when the load resistance reaches the optimal resistance, which changes at different rail current conditions, autonomous devices employed in WSN applications also present dynamic load requirements that vary significantly across different components and their operational modes. In order to address these operational variations in both source and load, an adaptive power management system capable of simultaneously performing efficient AC-DC conversion and dynamic impedance matching is required to ensure stable and efficient power delivery to connected loads. This demands careful design consideration of rectifier topology selection, control circuitry reimplementation and control strategy development to balance energy harvesting efficiency and load compatibility.

3.4 Summary

This chapter presented a systematic investigation of the design, optimization, and fabrication of a free-standing MFEH for railway applications. The chapter begins by demonstrating the FEM simulation framework employed for parametric analysis of the MFEH design. Critical material properties, particularly the importance of relative magnetic permeability and electrical conductivity for core material selection, are discussed in the chapter. The comprehensive parametric simulation processes that employed multiple simulation analyses to evaluate design variations, yielding specific recommendations for performance enhancement for both core geometry and coil parameter optimization, are documented in the chapter. Results obtained via parametric simulations demonstrated the significant influence of core geometry and coil parameters on harvesting efficiency, with graphical representations illustrating optimization outcomes and their impact on power generation.

The MFEH fabrication phase implemented the parameter optimization recommendations, with justification provided for all design choices. Experimental validation confirms close agreement between measured coil resistance and inductance characteristics and FEM simulation predictions. Performance evaluation of the MFEH first determined the optimal positioning through a predefined sign convention, followed by a comparative analysis of open-circuit voltage that validated the simulation model. Key operational parameters, including maximum induced open-circuit voltage and power ratings, were established during the performance analysis to aid in the design of the power management system. The chapter concludes by discussing the essential requirements for downstream power conversion and management circuitry to address the challenge of interfacing the AC power output of the MFEH with DC-powered devices in WSNs while ensuring maximum power delivery.

CHAPTER 4 DESIGN AND IMPLEMENTATION OF THE POWER CONVERSION AND MANAGEMENT UNIT

4.1 Introduction

The free-standing magnetic field energy harvester (MFEH) developed in this study addresses the critical need for sustainable energy solutions for autonomous devices and sensors in WSNs deployed throughout electric railway environments. Conventional electrochemical batteries currently used in these applications present limitations due to their finite energy capacity and requirement for periodic replacements. The proposed free-standing MFEH units, offers a sustainable energy supply alternative that can expand the number of wireless sensors deployed, thereby enhancing condition monitoring capabilities that can improve system reliability and ensure passenger safety in the electric railway systems.

Among various ambient energy sources available in railway environments, including solar, wind, and vibrational energy, magnetic field energy harvesting emerges as the most viable solution. As thoroughly discussed in Sections 1.2.1 and related earlier sections, this approach demonstrates distinct advantages by eliminating weather dependencies, avoiding the need for structural modifications to railway infrastructure and reducing periodic maintenance burden that characterize alternative harvesting methods.

The theoretical foundation and system overview of the developed MFEH were established in CHAPTER 3. The comprehensive design optimization process, fabrication methodology, and experimental validation of the MFEH, including verification of its operational parameters were presented in CHAPTER 3. To effectively utilize the AC output of the MFEH for powering DC-based WSN components, this chapter presents the complete design and implementation of an integrated power management system. The system architecture incorporates a full-bridge rectifier stage for efficient AC-DC conversion, followed by a DC-DC converter stage specifically designed to ensure optimal power delivery across varying load conditions.

The chapter proceeds with a detailed examination of rectifier circuit requirements, beginning with an analysis of existing approaches in comparable studies and justifying the selected design configuration. In the following sections the theoretical framework for the power management system is developed explaining its working principles. Theoretical justification for component selection in the design process of the power management circuit is discussed later followed by presentation and analysis of laboratory validation results, demonstrating the performance characteristics of the developed MFEH. In the next section, measures implemented enhance the energy harvesting system's efficiency are discussed, followed by a comprehensive analysis of losses within the system. In the final section, the necessity of an advanced control strategy for the proposed magnetic field energy harvester is elaborated, with a comparison made to control techniques documented in the literature.

4.2 Rectifier Design

Magnetic field energy harvesting operates fundamentally based on Faraday's law of induction, where an alternative EMF is induced across a coil exposed to a time-varying magnetic field. However, this presents an implementation challenge, as most electronic circuits in WSNs require DC power for operation. Therefore, efficient conversion of the AC voltage generated from the developed MFEH to a stable DC voltage represents a critical design requirement of the energy harvesting system. While free-standing MFEH remains an emerging research area where voltage conversion has not been explored in most of the reported studies, examining energy harvesting systems that generate AC power, such as vibrational and triboelectric approaches, provides valuable insights into rectifier circuit design.

4.2.1 Passive Rectifier Topologies

Existing literature reports two primary rectifier topologies as active and passive configurations. Unlike active rectifiers that require additional components such as gate drivers and auxiliary power supplies, passive designs offer greater simplicity and lower power consumption maximizing net energy output in harvesting systems. Diode-based rectifier circuits typically employ several fundamental topologies, including single-series (half-wave), single-shunt, voltage multiplier, and bridge-type configurations. Fig. 4-1 (a) illustrates the basic single-series diode rectifier, commonly referred to as a half-wave rectifier due to its characteristic output waveform containing only the positive half cycle of the input voltage. Despite its simplicity, the rectifier topology exhibits a lower efficiency due to power dissipation during the blocked negative half-cycles [90]. The full-wave rectifier topology, shown in Fig. 4-1 (b), addresses this limitation. During negative half-cycles, diode D1 becomes forward-biased, charging capacitor C1 to the peak input voltage V_{peak}. In the successive positive half-cycles, D1 is reverse-biased while D2 becomes forward-biased, enabling charge transfer from C1 to C2 and effectively doubling the output voltage. This voltage doubling technique has led to adoption of cascaded voltage multiplier configurations, such as Cockcroft-Walton circuits, in low voltage energy harvesting applications [90–92].

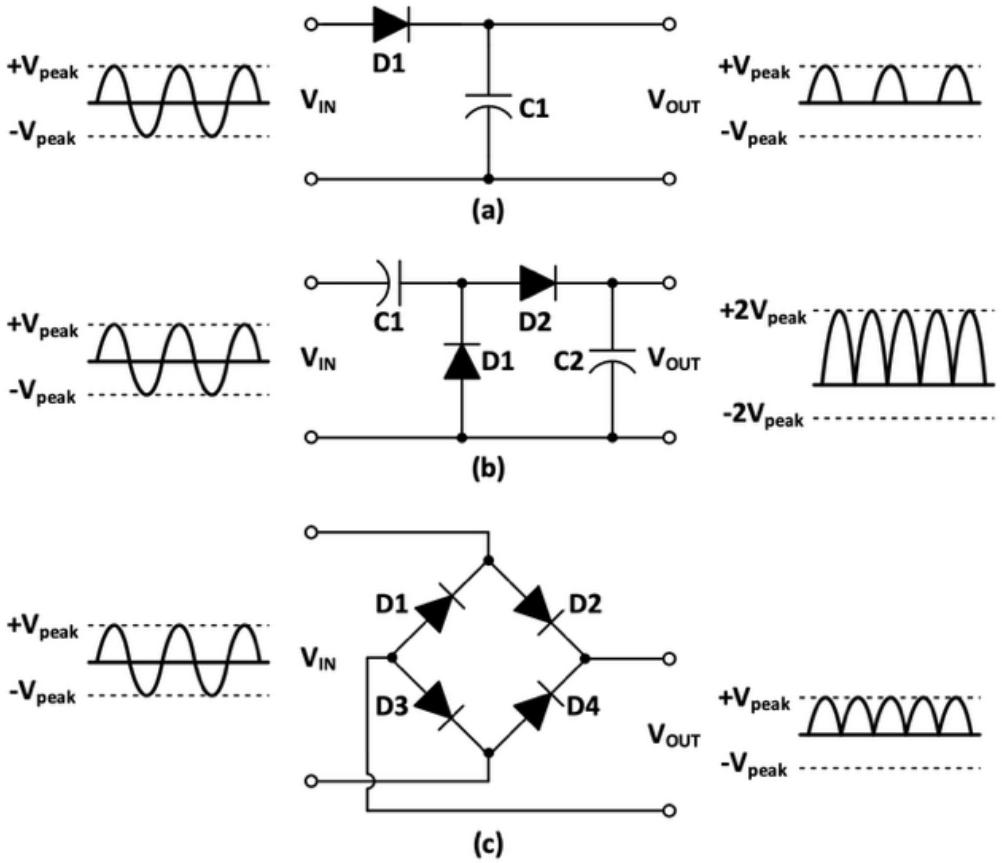

Fig. 4-1 (a) Half-wave rectifier (b) Full-wave rectifier (c) Full-bridge diode rectifier

In energy harvesting systems that typically output low power, the forward voltage drops incurred by diodes significantly affect their efficiency. To improve system efficiency, the use of MOSFETs in a diode-tied configuration instead of diodes has been reported in the literature. A conventional two-way rectifier with MOSFETs connected as diodes is shown in Fig. 4-2 (a). In this configuration, the forward voltage drop amounts to twice the threshold voltage of the MOSFETs used. Another topology, shown in Fig. 4-2 (b), utilizes four CMOS transistors: two NMOS and two PMOS types [93]. The minimum operating voltage of this rectifier configuration depends on the transistors' threshold voltage, and it outputs nearly the entire input voltage. Although these configurations are forms of passive rectifiers, their efficiency is hindered by their threshold voltage dependence. Furthermore, their performance deteriorates due to leakage currents, limiting their effectiveness [94].

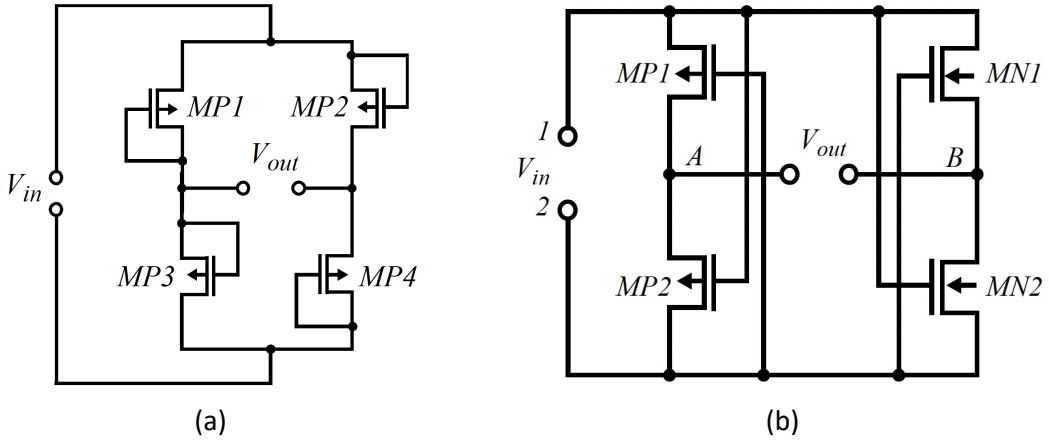

Fig. 4-2 Passive rectifier bridges using diode-tied configuration of MOSFETs [93].

4.2.2 Active Rectifier Topologies

To further enhance the efficiency of energy harvesters, active rectifier topologies have been adopted in several studies. An active rectifier typically consists of controllable switches instead of the diodes found in passive bridge rectifiers. A major benefit of active bridge rectifiers is their lack of a significant forward voltage drop, which reduces conduction loss. This characteristic is critically important for energy harvesting applications, where low power output means that conversion losses significantly impact overall efficiency. This is particularly essential in magnetic field energy harvesting for electric railways, where the intermittent energy generated only when a train passes must be captured with minimal loss.

The literature on energy harvesting techniques describes numerous active AC-DC rectifier configurations, which are designed to minimize losses, enhance efficiency, and regulate power flow from the harvester to the load. Numerous research studies have documented active AC-DC boost converter topologies for low voltage energy harvesting applications. For instance, Dwari *et al.* [95] introduced two dual boost converter topologies that utilize a single inductor and operate in discontinuous conduction mode (DCM) to reduce switching losses while aiming to improve the secondary voltage. The first topology, depicted in Fig. 4-3 (a), employs four switches and requires input voltage polarity sensing, while in the second topology, shown in Fig. 4-3 (b), the secondary switches are replaced with two split capacitors. The authors reported a conversion efficiency of 60% for both designs. Later, Chen *et al.* [96] enhanced the power

conversion efficiency of the dual boost split capacitor AC-DC converter by implementing GaN transistors and an impedance matching control strategy. Their results indicate that the proposed converter achieved an efficiency of 72.3% under closed-loop control.

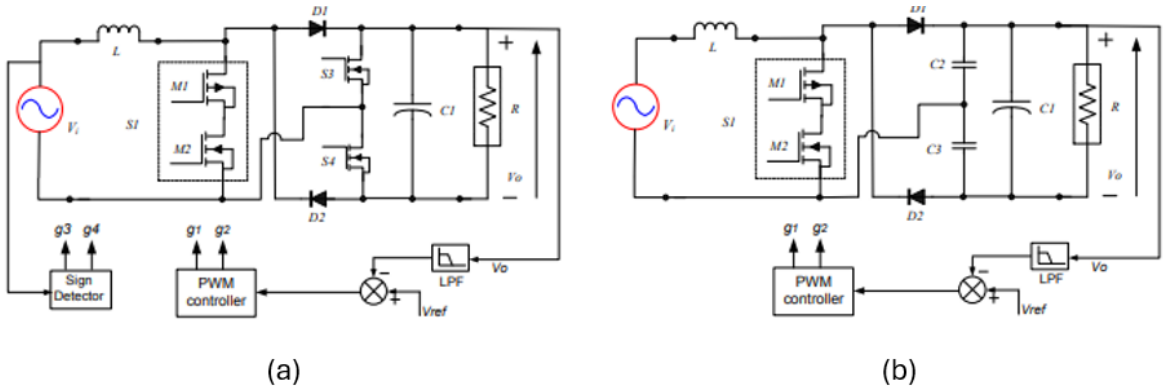

Fig. 4-3 Dual boost converter topologies proposed in [95]

Researchers have also employed active full-bridge rectifiers that utilize switching transistors to achieve further improvements in power conversion efficiency. For instance, Liu *et al.* [97] implemented an inverter-type active converter which incorporated a large inductor, as illustrated in Fig. 4-4 (a), to mitigate instantaneous voltage transients. This design was reported to yield a five-fold improvement in performance. Nevertheless, the external control circuit used for this converter consumed additional power, and the inductor itself contributed to dissipative losses. To overcome these limitations, Edla *et al.* [98] proposed an H-bridge converter topology, shown in Fig. 4-4 (b), which eliminates the need for an inductor. A significant advantage of this design is that it operates without external control circuitry to drive its MOSFETs, thereby substantially reducing its power consumption. The authors reported a power conversion efficiency of 63% for this inductor-less H-bridge converter.

In another study, Noohi *et al.* [99] utilized an H-bridge active rectifier topology comprising two N-type and two P-type MOSFETs, as depicted in Fig. 4-5. The authors employed three control loops for impedance matching, voltage regulation and maximum power point tracking while only using low power comparators and basic digital gates for control circuitry to reduce power losses and minimize energy usage for control circuitry. This approach yielded a notably high-power conversion efficiency of 92% for the proposed topology.

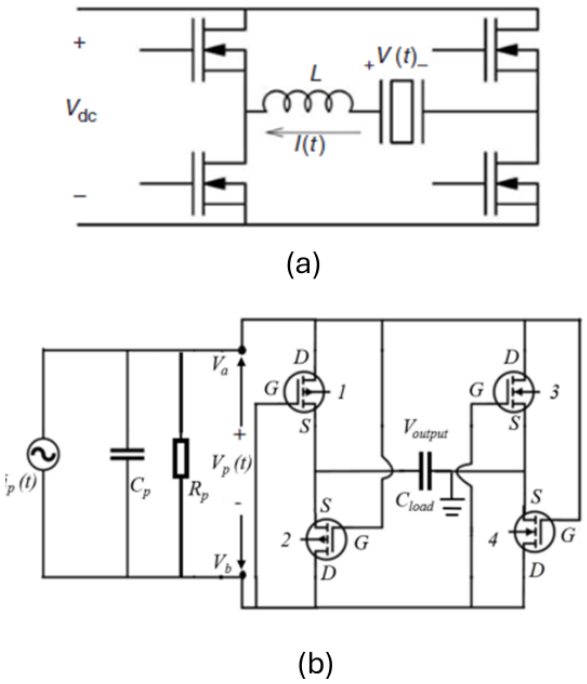

Fig. 4-4 Active AC-DC rectifier topologies derived from the full-bridge rectifier [97]

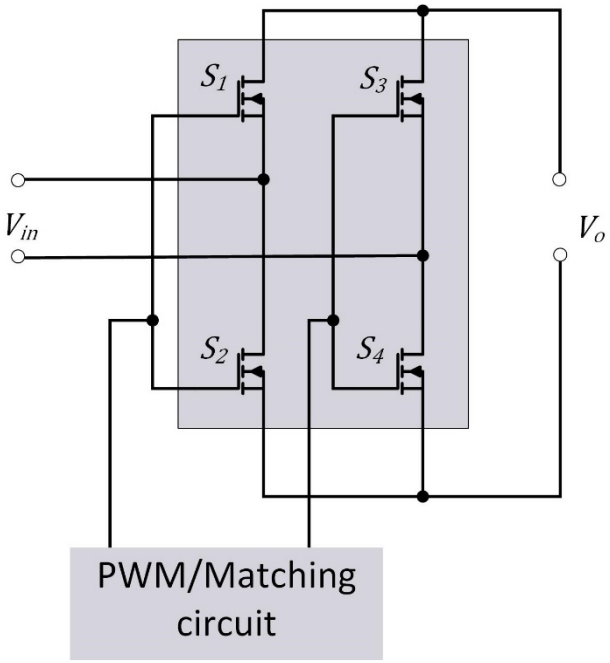

Fig. 4-5 H-Bridge type active AC-DC rectifier topology

The literature reveals many different active AC-DC converter topologies introduced to improve the performance of energy harvesting systems. Many combine MOSFET switches and diodes, and a general trend shows that efficiency improves when conventional diodes are replaced with

MOSFETs. More prominent efficiency gains are observed when advanced control strategies are utilized with full-bridge rectifier topologies. It is also noted that the voltage output of most reported energy harvesting devices is comparatively low, and most converter topologies aim to improve the load voltage.

However, the magnetic field energy harvesting system developed in this study generates a comparatively higher output voltage, as reported in previous chapters. Therefore, the conventional full-bridge rectifier configuration shown in Fig. 4-1 (c) was selected for implementation. A simple conversion stage was required at this stage to observe the proposed MFEH's performance. The selected passive rectifier topology provides complete waveform rectification while maintaining stable output voltage characteristics. This design choice is supported by prior research demonstrating the successful implementation of full-bridge rectifiers in freestanding magnetic field energy harvesting systems.

The full-bridge rectifier plays a critical role in ensuring a stable output voltage regardless of the input voltage polarity from the MFEH, which is essential for the subsequent power management circuit. However, the two diodes in the current path create a cumulative voltage drop equivalent to twice the forward voltage of a single diode. To minimize this power loss, a bridge rectifier with a low forward voltage drop was prioritized during component selection. A rectifier chip with a voltage rating exceeding the MFEH's maximum recorded open-circuit voltage was also selected. Based on these criteria, the MDD DB101S bridge rectifier chip was chosen, offering a maximum forward voltage drop of 1.1 V. Furthermore, a 2200 μF, 50 V capacitor was integrated parallel to the rectifier’s output terminals to suppress voltage ripple and enhance the stability of the rectified output.

4.3 Power Management Circuit

4.3.1 Introduction

Modern railway networks increasingly rely on condition monitoring systems supported by WSNs to improve operational reliability, efficiency, and passenger safety. However, a critical challenge in deploying WSNs lies in securing a sustainable power supply for their autonomous devices such as sensors and communication modules. To address this limitation, this study introduces a free-standing MFEH designed to scavenge energy from the ambient magnetic fields generated by railway infrastructure.

As demonstrated experimentally in previous chapter, the developed MFEH effectively harvests magnetic field energy and delivers AC electrical power to an external load. The MFEH achieves maximum power output is when the load resistance matches the internal coil resistance. However, to practically implement the energy harvester in WSNs, DC power output is required to operate diverse electronic components, each with distinct load requirements. Furthermore, the fluctuating rail track currents during the passage of rolling stock causes variations in the available magnetic field energy. These factors underscore the need for an adaptive power management system capable of maximizing power extraction from the energy harvester under variable source conditions while accommodating fluctuating load demands.

The power management circuit developed in this study prioritizes maximum power extraction across fluctuating load and source parameters. To achieve this objective, a four-switch buck-boost (FSBB) DC-DC converter is proposed. This topology enables power flow regulation by dynamically controlling semiconductor switching operations. By adjusting duty cycles, the FSBB converter ensures efficient power delivery to diverse range of load demands. This approach not only enhances the harvester's compatibility with diverse WSN components but also ensures reliable operation under transient energy conditions. The integration of this converter represents a critical advancement in enabling self-sustaining WSNs for modern rail systems.

4.3.2 Theoretical Analysis

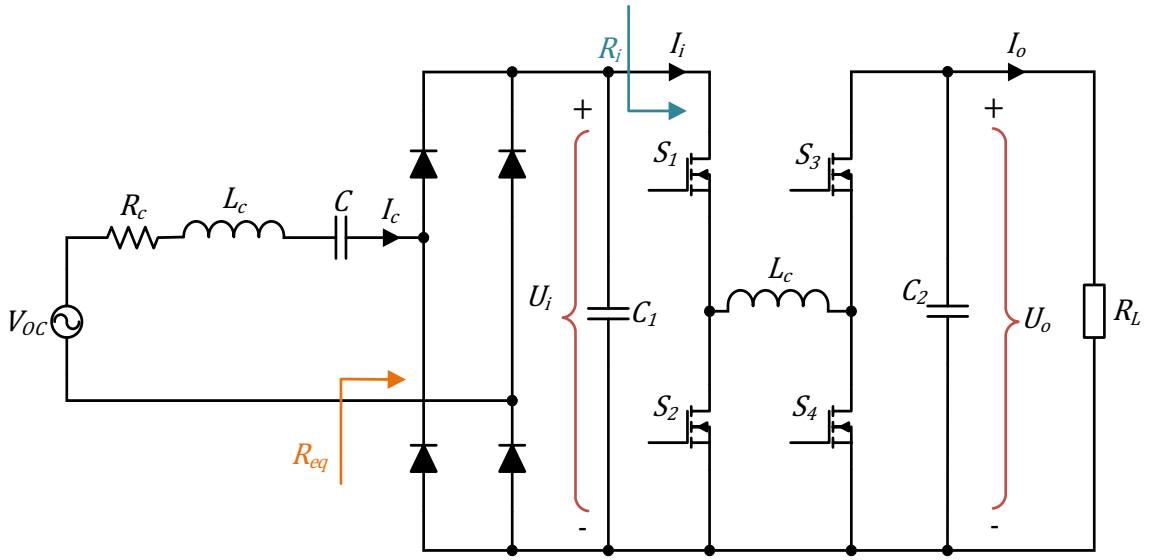

Fig. 4-6 : Schematic diagram of the magnetic field energy harvesting system

The schematic diagram of the proposed magnetic field energy harvesting system is illustrated in Fig. 4-6. The parameters of the MFEH is represented in the schematic by its induced open circuit voltage V_{OC}, coil resistance R_C and coil inductance L_C with a compensating capacitor C connected in series. The subsequent stage consists of a full-bridge diode rectifier comprising four diodes. This is followed by the proposed FSBB converter which is composed of four MOSFET switches (S_1, S_2, S_3, S_4) and an inductor L_1. C_1 and C_2 are the input and output capacitors of the FSBB converter.

The equivalent circuit resistance of the composite full-bridge rectifier and FSBB circuit from rectifier input perspective is denoted as R_{eq}. The input resistance of the FSBB converter is denoted as R_i and the DC load resistance is denoted as R_L as shown in the schematic diagram.

Preliminary performance analysis of the MFEH revealed that its output voltage remains at practical levels, allowing the FSBB converter to operate predominantly in buck mode for output voltage regulation. In this mode S_3 remains continuously switched on while S_4 remains off. S_1 and S_2 operate in a complementary manner with a duty cycle D. The working principle of the FSBB converter is further detailed in Fig. 4-7. Based on this configuration, the timing

diagrams in Fig. 4-8 were derived, illustrating the inductor voltage V_L, inductor current i_L and switching period T_S.

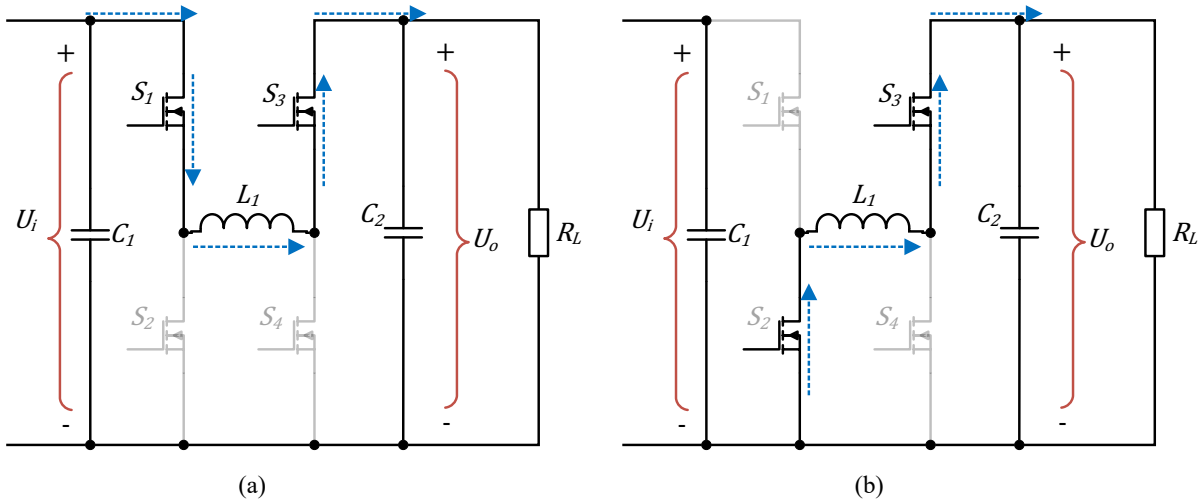

Fig. 4-7 The working principle of the FSBB converter

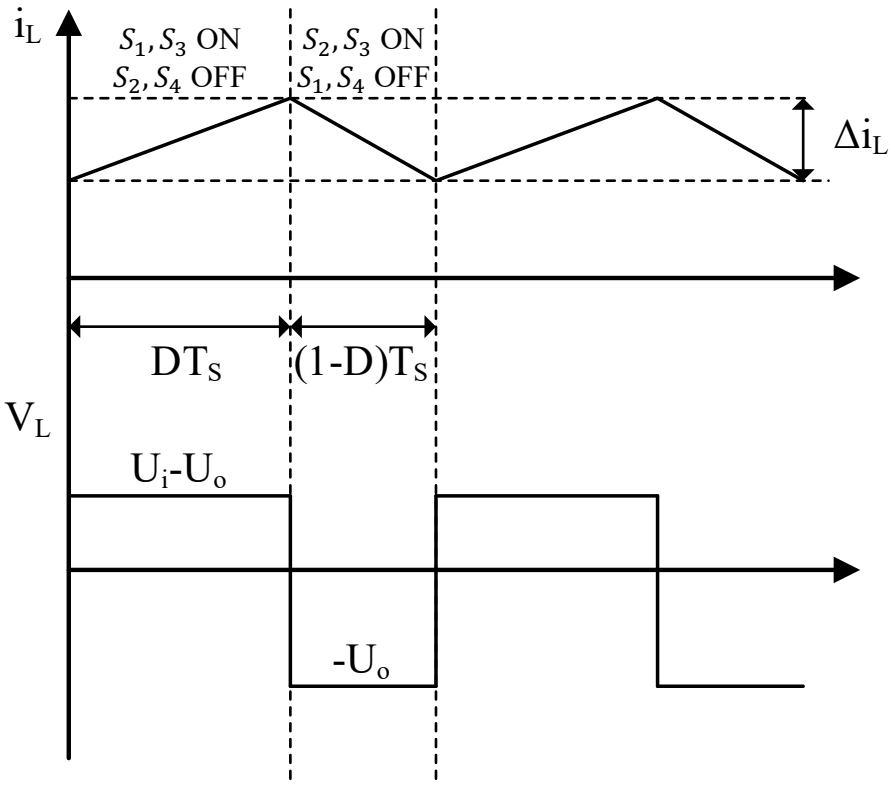

Fig. 4-8 Current and voltage waveform of the inductor in the FSBB converter

Based on the timing diagrams, following relationship can be derived considering the volt-second balance of the inductor.

$$D = \frac{U_o}{U_i} = \frac{I_i}{I_o} \tag{4-1}$$

Therefore, the input resistance of the FSBB converter can be written as:

$$R_i = \frac{U_i}{I_i} = \frac{U_o}{D^2 I_o} = \frac{R_L}{D^2} \tag{4-2}$$

However, according to resonant converter circuit analysis, the relationship between the equivalent circuit resistance R_{eq} and FSBB input resistance R_i can be expressed as [100]:

$$R_{eq} = \frac{8}{\pi^2} R_i \tag{4-3}$$

Therefore, the relationship of equivalent circuit resistance and load resistance can be deduced by Equations 4-2 and 4-3 as:

$$R_{eq} = \frac{8}{\pi^2 D^2} R_L \tag{4-4}$$

Equation 4-4 defines the relationship between the AC load resistance and DC load resistance.

However, as derived in a previous chapter, the MFEH unit achieves maximum power output with an AC load when the load resistance matches the source resistance R_C denoted as:

$$P_O = \left(\frac{V_{OC}}{2\sqrt{2}}\right)^2 / R_L = \frac{{V_{OC}}^2}{8R_C} = \frac{(NA_e B_{ex} \omega \mu_{eff})^2}{8R_C} \tag{4-5}$$

Therefore, by substituting Equation 4-4 into 4-5, the governing equation for power output of the energy harvesting system can be expressed as:

$$P_O = \frac{(\pi DNA_e B_{ex} \omega \mu_{eff})^2}{64 R_L} \quad 4\text{-}6$$

Therefore, based on the relationship between R_{eq} and R_L established in Equation 4-4, impedance matching can be achieved through appropriate adjustment of the duty cycle D in the FSBB converter. This duty cycle control enables direct regulation of the power output of the energy harvesting system. The proposed configuration thus demonstrates the capability to maintain maximum power transfer capacity across varying load resistance conditions.

4.3.3 Design and Fabrication of FSBB Converter

It is important to design the DC-DC converter with careful consideration to ensure reliable operation under varying voltage stresses and current levels accounting for expected fluctuations in both energy source and load conditions. The design process of the FSBB converter involves in selecting appropriate components including MOSFETs, inductors, input/output capacitors, gate driver chips and gate resistors based on theoretical analyses conducted within the operational parameters observed during preliminary performance testing of the MFEH.

As the first step, MOSFET selection was conducted considering its drain to source voltage rating, ensuring it exceeded the maximum voltage recorded during MFEH characterization. MOSFETs with a low threshold voltage (V_{TH}) and minimal turn on resistance ($R_{DS(on)}$) were prioritized to reduce conduction losses and associated thermal effects. Following MOSFET selection, gate resistance values were determined according to the total gate charge requirement of the MOSFET specified in the device datasheet.

Afterwards, gate driver selection process was undertaken. Gate drivers serve the essential function of amplifying low-power control signals from microcontroller units to effectively drive power MOSFETs. In this design implementation, a dedicated gate driver IC configured for half-bridge operation was selected to control the MOSFET pairs in each converter leg. Specifically, a dual-input half-bridge gate driver was selected over a single-input configuration, as this approach provides independent signal control for each MOSFET.

In this study, the switching frequency for the FSBB converter was established at 200 kHz, a comparatively higher frequency specifically selected to reduce inductor ripple current Δi_L as described in Equation 4-7. Furthermore, selection of higher switching frequencies permits the use of smaller passive components used in the circuitry [101]. However, as excessive frequencies lead to diminished efficiency through increased switching losses, a balance between component size reduction and switching loss management was considered.

$$\Delta i_L = \frac{(U_i - U_o) \times U_o}{f_{SW} \times L_1 \times U_i} \tag{4-7}$$

Component specifications were derived from the operational parameters recorded during performance analysis of the MFEH, where load currents remained below 300 mA. To accommodate potential current variations, the design incorporated a 400-mA maximum current rating. Inductor selection criteria included limiting the ripple current to 40% of the rated output current, while capacitor selection focused on maintaining voltage ripple below 100 mV at the input and 50 mV at the output. Additional parallel ceramic capacitors were incorporated to mitigate high-frequency noise at both converter terminals. The implemented FSBB converter design utilizes four N-channel MOSFETs from Infineon Technologies, controlled by a Texas Instruments TMS320F28379D digital signal processor (DSP). The specifications of the main components utilized in the FSBB converter are detailed in Table 4-1. The printed circuit board was designed using EasyEDA Pro software, with the fabricated converter shown in Fig. 4-9.

Table 4-1 Component specifications

Component	Specification
MOSFETs ($\boldsymbol{S_1, S_2, S_3, S_4}$)	IRF8736PbF
Gate driver	UCC27282
Inductor	$L_1 =$ 100 μH
Capacitors	$C_1 =$ 4.7 μF $C_2 =$ 47 μF
Frequency	$f = 200kHz$
Full bridge rectifier	DB101S (V_f = 1.1 V)

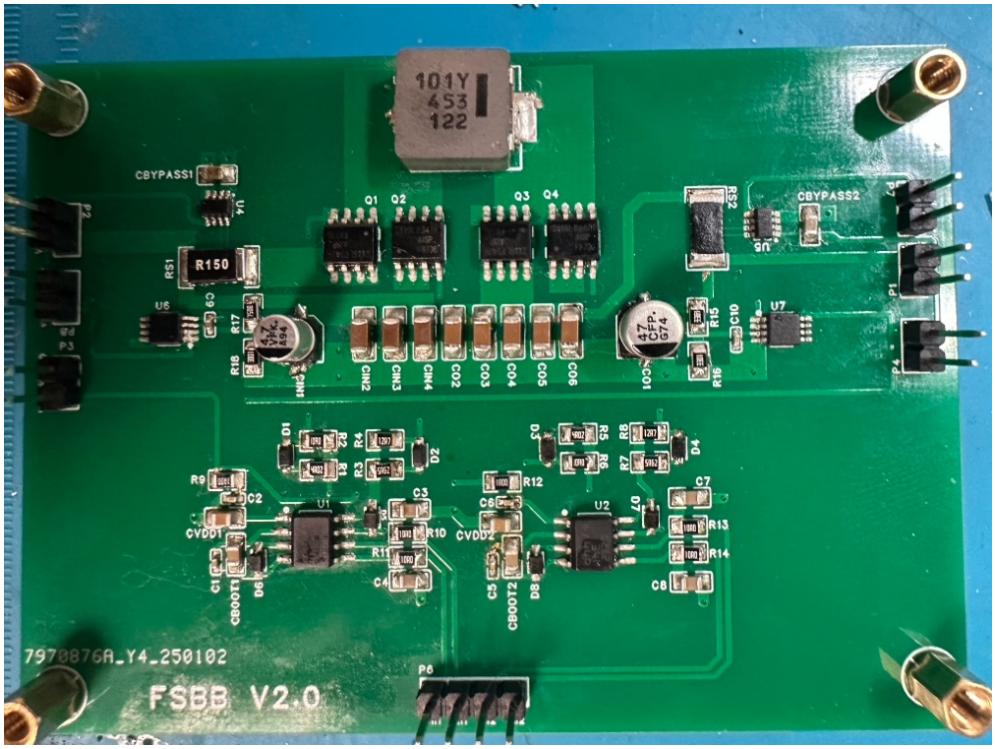

Fig. 4-9 Fabricated FSBB circuit

4.4 Experimental Validation and Result Analysis

4.4.1 Experimental Setup

To evaluate the performance of the integrated energy harvesting system comprising the MFEH, compensation circuit, full-bridge rectifier and FSBB converter, a comprehensive series of laboratory experiments were conducted. Fig. 4-10 illustrates the experimental setup employed for these investigations.

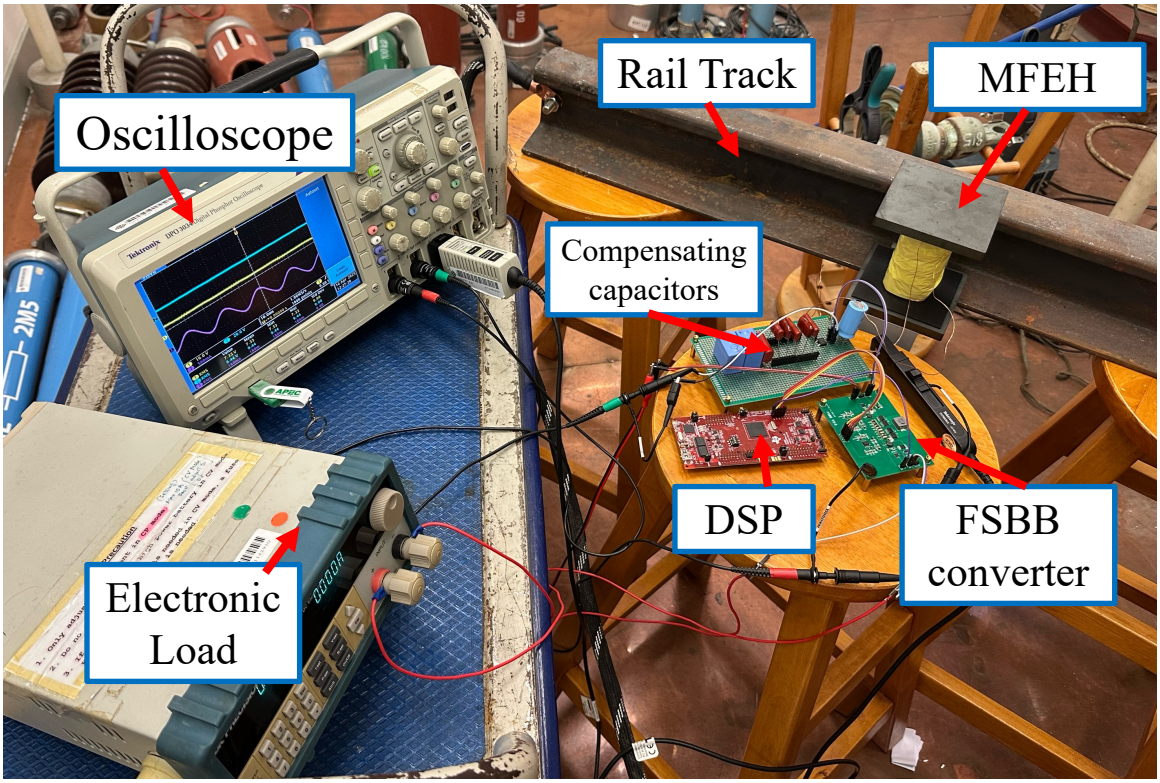

Fig. 4-10 Experimental setup for MFEH characterization

The MFEH unit was positioned in close proximity to the rail track at the predetermined optimal location (2 cm mark). Following placement, the coil inductance was carefully measured using an LCR meter and appropriate combination of compensation capacitors ware connected to minimize the system's net reactance. This compensation process involved iterative adjustment of the capacitor values while monitoring the resultant reactance until it approached zero.

The system configuration was completed by connecting the MFEH output to the FSBB converter through a full-bridge rectifier. A programmable electronic load was attached to the

converter output to simulate various operating conditions, with the load voltage being continuously monitored throughout the experiments. The resulting operational waveforms, including the rectifier output voltage, FSBB converter output voltage, and rectifier input current, are presented in Fig. 4-11.

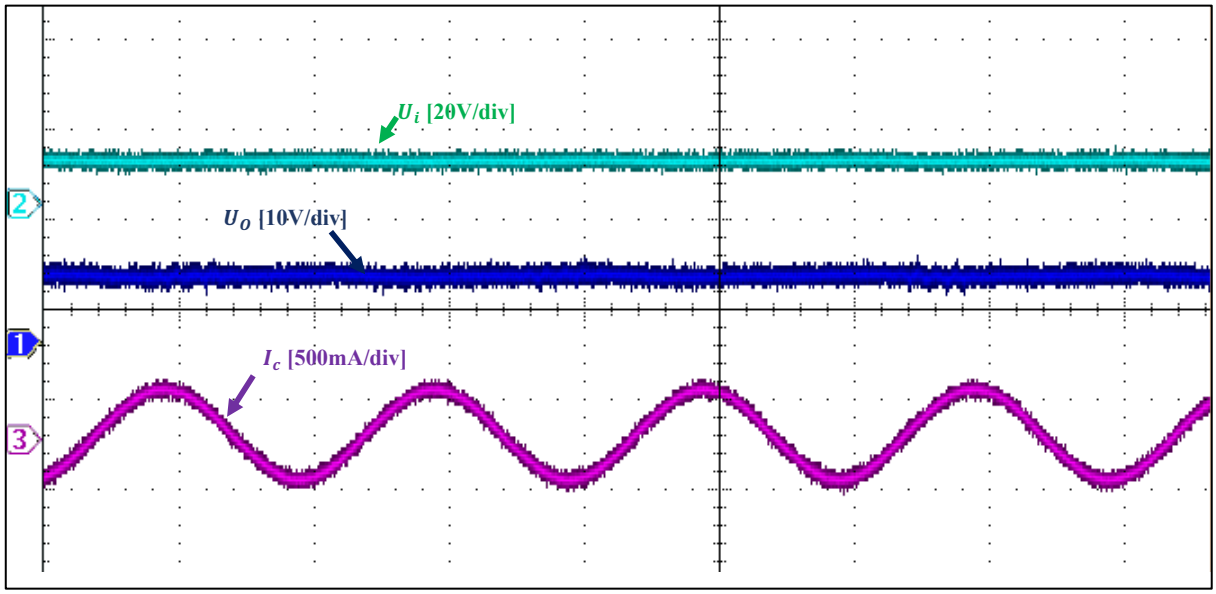

Fig. 4-11 Experimental waveforms of rectifier output voltage U_i, FSBB output voltage U_O and rectifier input current I_c

4.4.2 Results Analysis

The previous performance analysis of the MFEH system demonstrated that peak power output occurs when the load resistance approximates the coil resistance, though perfect matching was not achieved due to inherent system losses. Based on these findings, this experimental investigation aimed to validate whether maximum power extraction could be maintained across varying operating conditions through appropriate duty cycle adjustment of the FSBB converter.

The first experimental process involved evaluating system performance under different load resistances while maintaining a constant rail current of 300 A. For each discrete load resistance value, the duty cycle was incrementally varied from 0.1 to 0.9, with simultaneous measurement of the resultant power delivered to the load. The collected data, presented in Fig. 4-12, illustrates the relationship between power output and duty cycle across the tested load conditions.

The experimental results, as illustrated in the figure, demonstrate the system's performance across seven distinct load resistance values. Notably, five of the seven load conditions (R_L = 10 Ω, 20 Ω, 30 Ω, 40 Ω, and 50 Ω) exhibit well-defined local maxima in power output at specific duty cycle settings. For instance, at R_L = 30 Ω, the system achieves peak power output of 1.49 W with the FSBB converter operating at a duty cycle of 0.71. This operating point corresponds to an equivalent AC resistance of 48.2 Ω, as calculated using Equation 4-4. The remaining load conditions similarly demonstrate distinct maxima at their respective optimal duty cycles, each corresponding to their characteristic equivalent AC load resistances. These experimental findings validate the theoretical analysis, confirming that the FSBB converter can effectively maintain maximum power transfer conditions through appropriate duty cycle adjustment, even under varying load resistance.

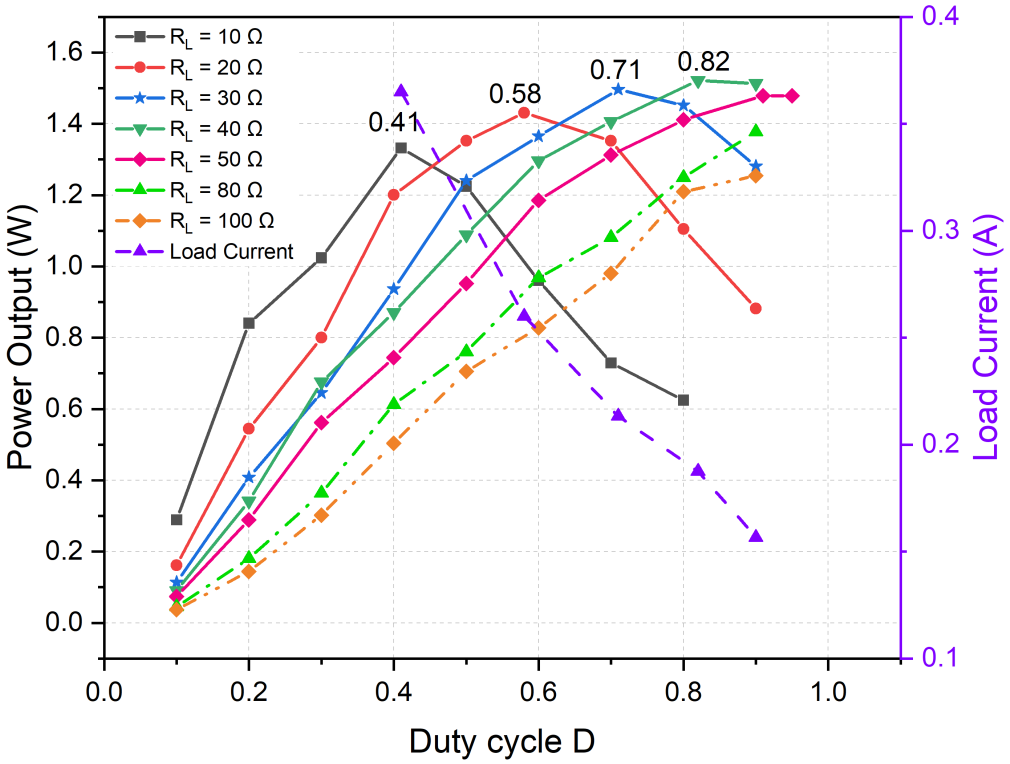

Fig. 4-12 Power output versus duty cycle characteristics for varying load resistances at 300 A rail current

However, experimental results reveal that the maximum power output recorded at each load level gradually increases with the load resistance. For instance, the system delivers a maximum output power of 1.33 W at R_L= 10 Ω, while it rises to 1.51 W at R_L= 40 Ω. This behaviour can be attributed to the improved efficiency of the FSBB converter at higher duty cycles. As the FSBB converter is primarily operated in buck conversion mode, its efficiency is adversely

affected at lower duty cycles, similar to synchronous buck converters [102]. Further examination of the experimental results reveals that the corresponding load current decreases as the load resistance increases. (The load current at maximum power output of each load level is presented in the figure.) This reduction in load current leads to lower conduction losses, thereby enhancing the converter's efficiency. Thus, the maximum power output of the MFEH increases at higher duty cycle values.

The experimental results reveal distinct behaviour for the two highest load resistances (80 Ω and 100 Ω), which deviate from the pattern observed at lower resistances. This deviation occurs because these load values exceed the theoretically optimal resistance range for the system at 300 A rail current. As derived from Equation 4-4, the maximum achievable ratio between equivalent circuit resistance R_{eq} and load resistance R_L is 1.113 when operating at the maximum duty cycle of 0.95. According to the experimentally determined coil resistance of 48.2 Ω, this ratio establishes an upper limit of 53.6 Ω for effective load matching. Consequently, when the load resistance exceeds this threshold value, as in the 80 Ω and 100 Ω cases shown in the figure, the system cannot achieve impedance matching even at maximum duty cycle operation. This limitation explains why these higher resistance conditions fail to reach the power output levels attained by loads within the optimal resistance range.

As in the preliminary performance analysis, the next experimental analysis examined the relationship between rail current and system power output when the load and duty cycle were kept constant. For this investigation, three distinct load resistance values were selected, with the duty cycle maintained at its predetermined optimal value for each respective load condition. The rail current was systematically varied from 0 to 500 A, with the resultant obtained illustrated in Fig. 4-13.

The experimental data reveal behaviour consistent with the preliminary performance analysis. As rail current increases, both power output and load voltage demonstrate a linear response up to approximately 350 A, beyond which they approach saturation. As discussed in previous experimental analyses, this phenomenon occurs because the magnetic flux density in the PC95 core material reaches its saturation flux density threshold at this current level, thus limiting the performance of the MFEH. Under these conditions, the system achieves a maximum power output of 1.98 W with a 40 Ω load resistance and 0.82 duty cycle, corresponding to a rail current beyond 350 A.

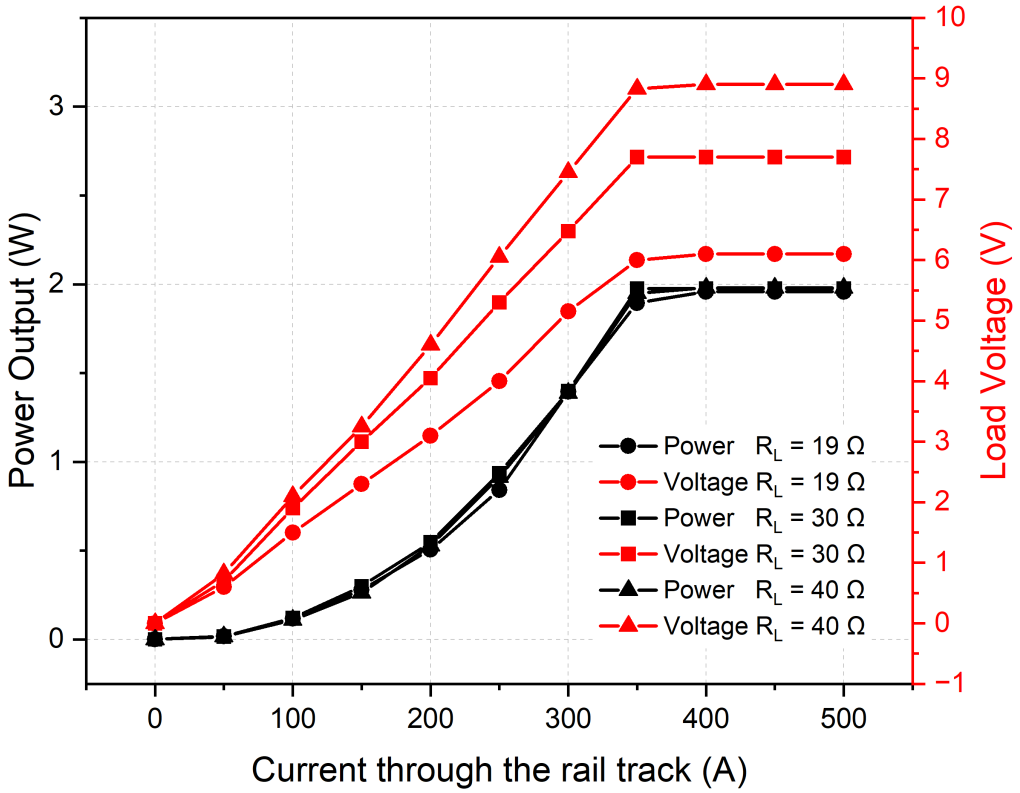

Fig. 4-13 Output power of the MFEH against increasing rail current while maintaining duty cycles value constant at each load condition

Consistent with the preliminary performance analysis, the variation in the optimal resistance of the MFEH at higher rail currents was further investigated. The rail current was maintained at constant levels of 350 A, 400 A, and 450 A, while the DC load was held constant, and the duty cycle of the FSBB converter was varied to observe the MFEH's output power. Fig. 4-14 illustrates the output power variation of the MFEH at a rail current of 350 A under five different load conditions, with the duty cycle adjusted. Two load conditions (R_L = 20 Ω and 40 Ω) exhibit local maxima when the equivalent circuit resistance (R_{eq}) approaches the optimal load resistance of 70 Ω, as derived from Equation 4-4. For the remaining load conditions, the highest output power is achieved when R_{eq} is adjusted closer to the optimal resistance by increasing the duty cycle.

Similarly, the output power of the MFEH was evaluated at rail currents of 400 A and 450 A by varying the duty cycle of the FSBB converter under five different load conditions. The results are presented in Fig. 4-15 and Fig. 4-16. As shown in Fig. 4-15, at 400 A, the MFEH achieves maximum output power when R_{eq} for each load condition is adjusted to approach the optimal resistance of 80 Ω. For instance, with a load resistance of R_L = 60 Ω, the MFEH reaches a

maximum output power of 2.5 W when R_{eq} is tuned to 76 Ω, which is close to the optimal resistance of 80 Ω determined during the preliminary performance analysis for a 400 A rail current. Similarly, at a rail current of 450 A, as depicted in Fig. 4-16, four of the five load conditions exhibit local maxima when R_{eq} is adjusted by modifying the duty cycle of the FSBB converter. Notably, the MFEH, integrated with the power management unit, achieves a maximum output power of 3.27 W at R_L = 60 Ω by setting the duty cycle to 0.7, resulting in an R_{eq} of 99 Ω, which closely aligns with the previously determined optimal resistance of 100 Ω for a 450 A rail current.

These findings align with the results from the preliminary analysis, confirming that the optimal resistance of the MFEH increases at higher rail currents. Nevertheless, the results demonstrate that the FSBB converter can effectively maximize power extraction from the MFEH by adjusting the duty cycle regardless of variations in rail current and load resistance.

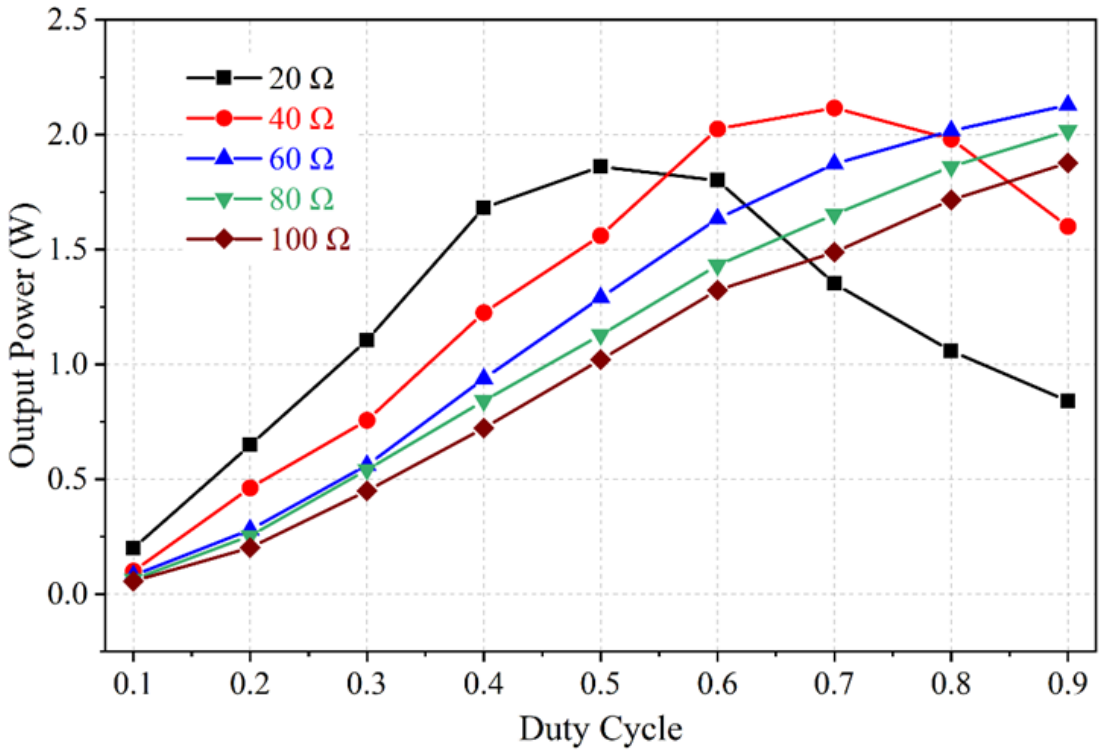

Fig. 4-14 Output power variation of the MFEH with duty cycle adjustments to match the optimal load resistance of 70 Ω at a constant rail current of 350 A

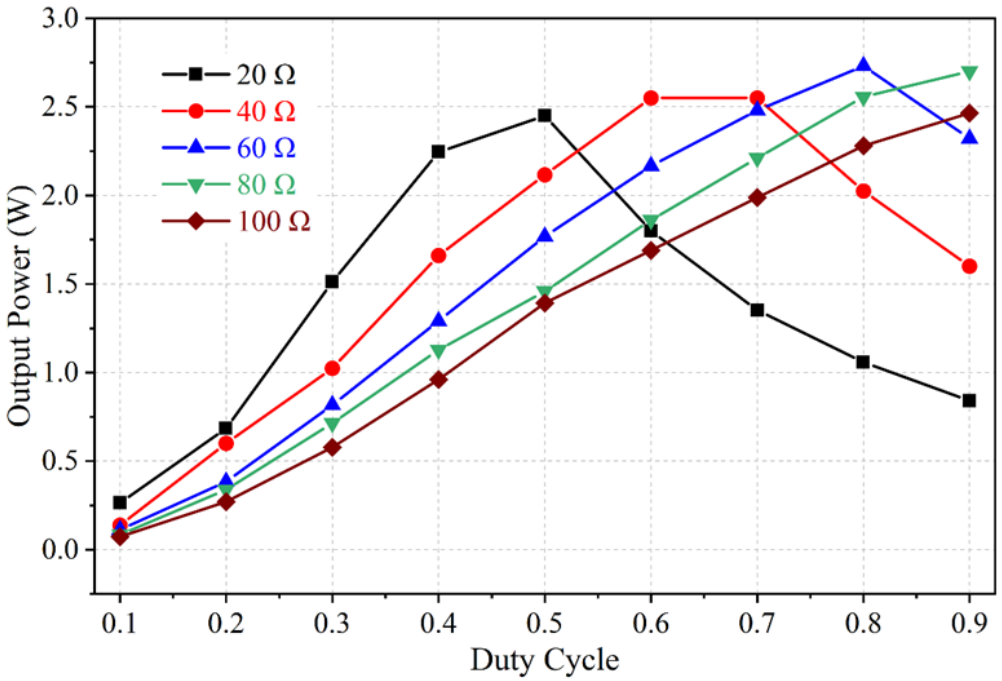

Fig. 4-15 Output power variation of the MFEH with duty cycle adjustments to match the optimal load resistance of 80 Ω at a constant rail current of 400 A

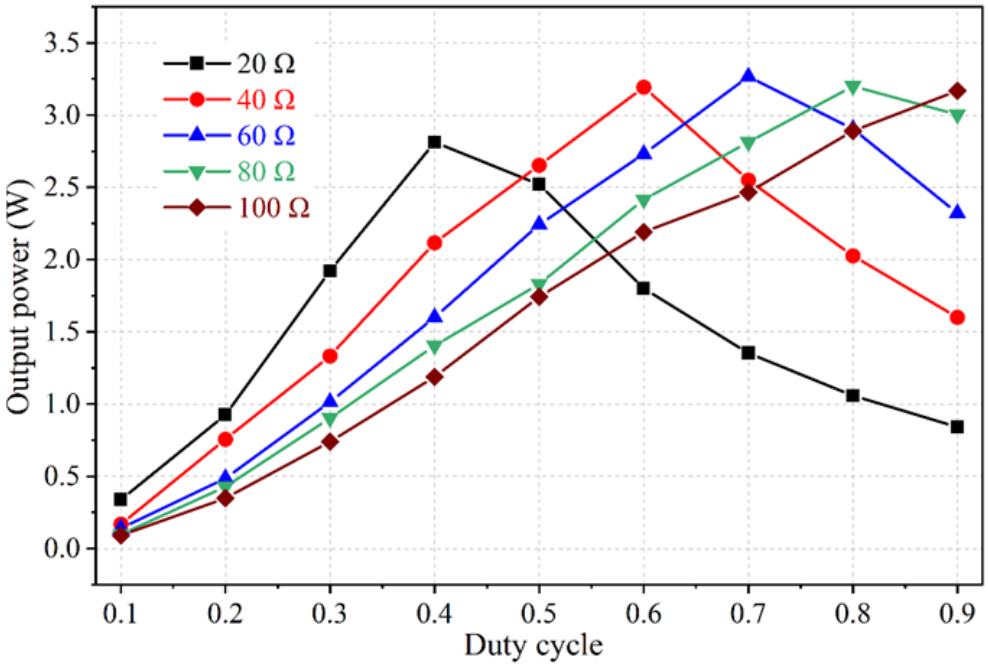

Fig. 4-16 Output power variation of the MFEH with duty cycle adjustments to match the optimal load resistance of 100 Ω at a constant rail current of 450 A

4.4.3 Efficiency and Loss Analysis

In free-standing MFEHs, the energy harvester is not directly coupled to the magnetic field source. To enhance efficiency, it is essential to increase magnetic flux density penetration through the core by optimizing the MFEH design, while simultaneously minimizing core losses and maximizing power transfer to the connected load. Efficiency in this context refers to improving output power and power density while reducing losses in both the magnetic core and the power management unit. Given the dynamic operating conditions of MFEHs in electric railway applications, the system must efficiently deliver power to the load under varying magnetic field strengths and load requirements.

As discussed in Section 3.2, optimizing the core geometry of a MFEH enhances magnetic flux density penetration, thereby improving its performance and efficiency. Incorporating collector plates into the core design increases magnetic flux concentration and elevates the effective permeability of the core, resulting in higher output power. In this study, the use of MnZn ferrite as the core material further augmented the MFEH's output power due to its favourable magnetic properties. However, the adhesive used to attach the collector plates may slightly impair the magnetic flux concentration capability of the core, an aspect that warrants further investigation to enhance MFEH efficiency. Additional optimizations, as outlined in Section 3.2, contributed to improved output power and power density in the reported MFEH design.

Reducing core losses is critical for maximizing MFEH's efficiency. Core losses were minimized by selecting MnZn ferrite PC95, which has a high electrical resistivity of 6 Ωm, effectively reducing eddy current losses. As detailed in Section 2.3.3, the Steinmetz equation describes core losses per unit volume, indicating that losses are directly proportional to the frequency of the magnetic field and the magnetic flux density penetrating the core. According to [73] and [89], the magnetic field generated by the coil current dominates and superimposes over the external magnetic field produced by the rail current within the core. Furthermore, the magnetic flux density generated from the coil current is dependent on the load resistance. Preliminary performance analysis revealed that the optimal load resistance of the MFEH increased with higher rail currents, driven by elevated core losses due to enhanced magnetic fields, as explained by the Steinmetz equation. By increasing the load resistance to the optimal value, surpassing the coil resistance value, the output power was significantly improved. For

instance, the MFEH positioned at a 2 cm distance from the rail track, with a coil resistance of 48 Ω, achieved a maximum output power of 2.3 W at a rail current of 450 A when the load resistance matched the coil resistance. By increasing the load resistance to 100 Ω, closer to the optimal resistance at higher magnetic flux densities, resulted in an output power of 4 W, a 74% increase. These results show that at higher flux densities, system losses can be reduced by increasing the load resistance. The specific resistance that maximizes power output is therefore the optimal load resistance for the MFEH at a given rail current level.

The integration of a power management unit significantly enhanced the energy harvester's performance by dynamically adjusting the equivalent circuit resistance (R_{eq}) closer to the optimal resistance. This was achieved by tuning the duty cycle of the FSBB converter in response to varying rail currents and load conditions. For instance, with a 40 Ω load and a 500 A rail current, setting the duty cycle to 0.82 adjusted the R_{eq} to 48 Ω, matching the coil resistance which yielded an output power of 1.958 W. Conversely, at 450 A, reducing the duty cycle to 0.6 increased the R_{eq} to 90 Ω. This closely approximated the previously determined optimal resistance of 100 Ω, resulting in a 63% improvement to 3.2 W of output power. This impedance matching technique, facilitated by the power management unit, substantially improved the MFEH's efficiency under dynamic operating conditions.

As discussed in Section 2.3.1 and experimentally validated in Section 3.3.2, the placement of the MFEH relative to the rail track also influences efficiency. Positioning the MFEH closer to the rail track increases coil resistance and induced voltage, but there exists an optimal position where output power peaks. Moving the MFEH closer beyond this point increases eddy current losses, reducing output power, as confirmed through experimental validation.

The efficiency of the power management circuitry is crucial, particularly for magnetic field energy harvesting from electric railways, where the energy source is intermittent. The power management system in this study employed a full-bridge passive rectifier followed by a FSBB converter, with capacitors to mitigate current fluctuations, reduce noise, and smooth the output at different stages. Comparative analysis indicated an 18% reduction (730 mW) in maximum output power compared to the preliminary MFEH performance of 4 W, with the integrated system achieving 3.27 W. This performance degradation stems from multiple loss mechanisms. The full-bridge diode rectifier introduced a forward voltage drop of 1.1 V, resulting in approximately 200 mW of power loss. The FSBB converter incurred additional losses,

including switching losses in the MOSFETs, which are limited to two MOSFETs in the current configuration. As higher switching frequencies exacerbate these losses, careful selection of an appropriate frequency is necessary. Conduction losses in the MOSFETs, determined by their on-resistance, can be minimized by selecting MOSFETs with low on-resistance. Losses related to the inductor the FSBB converter, include copper losses and core losses that are dependent on switching frequency, can significantly affect the efficiency of the MFEH [103]. Therefore, careful inductor selection, considering both DC and AC resistance of inductors, is essential. Additionally, losses arise from the equivalent series resistance (ESR) of capacitors and general thermal dissipation in the power conversion circuitry. These cumulative losses account for the observed reduction in the efficiency of the energy harvesting system.

4.4.4 Advanced Control Strategies for Power Management Circuit

Theoretical analysis in a previous section demonstrated that the proposed MFEH achieves maximum output power when the load resistance matches the source resistance, a phenomenon explained by the maximum power transfer theorem and widely recognized as impedance matching. Numerous studies in the literature have explored impedance matching in energy harvesting applications. This study showed that the proposed MFEH maximizes output power through an impedance matching mechanism. Preliminary performance analysis revealed that the optimal resistance of the energy harvesting unit deviates from the coil resistance at elevated rail current levels. Maximum output power was achieved when the load resistance was increased beyond the coil resistance to an optimal value. This adjustment was necessary because higher rail current levels caused additional core losses, effectively increasing the optimal resistance. The Steinmetz equation indicated that core losses increase with higher magnetic flux density in the core, which is predominantly generated by the induced coil current. Increasing the load resistance reduced this magnetic flux density, thereby enhancing output power.

Subsequent analysis utilized an FSBB converter to regulate power flow and maximize power extraction from the energy harvester. Theoretical analysis confirmed that by adjusting the duty cycle of the FSBB converter, the equivalent circuit resistance of the energy harvesting unit can be modified. Experimental results validated that the FSBB converter achieved impedance

matching and extracted maximum output power, even with varying load resistance, by altering the equivalent circuit resistance through duty cycle adjustments. The FSBB converter effectively adjusted the equivalent circuit resistance close to the optimal value at higher rail current levels, despite variations in load resistance and rail track current. However, the study employed an open-loop control technique for impedance matching and maximum power point tracking, without regulating load voltage. Voltage regulation is essential in energy harvesting applications, as the harvested energy typically powers a component in a WSN or an energy storage unit requiring stable voltage for reliable operation. Therefore, advanced control strategies integrating impedance matching, maximum power point tracking, and voltage regulation are necessary to enhance the proposed energy harvesting system.

Li *et al*. [104] proposed a simple impedance matching technique by modifying a full-bridge diode rectifier, replacing one diode with a MOSFET to switch between full-bridge and half-bridge configurations, thereby maximizing the output power of a free-standing magnetic field energy harvester. Their schematic, illustrated in Fig. 4-17, measures load resistance and compares it with a predetermined coil resistance. However, their controller cannot adapt when the optimal resistance changes.

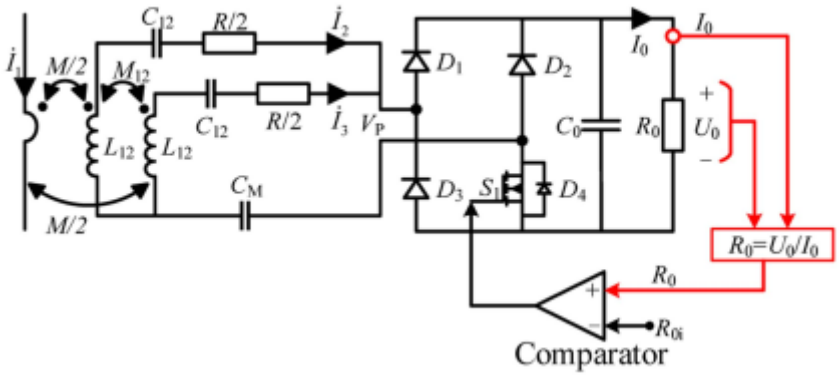

Fig. 4-17 The controlled strategy proposed in [104] with full bridge rectifier consisting of a MOSFET

Proynov *et al*. [105] introduced a resistive matching approach to maximize power transfer in an electromagnetic energy harvester designed for vibration energy harvesting. They utilized a non-synchronous boost rectifier topology, shown in Fig. 4-18, to rectify and step up the output voltage of the energy harvester. The input current and voltage of the converter are measured, and a feedforward control dynamically adjusts the rectifier's duty cycle to maintain a constant

proportionality between input current and voltage. While this technique optimizes output power, it does not regulate output voltage.

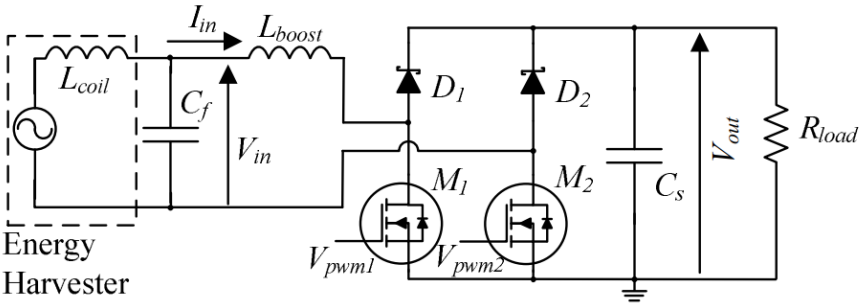

Fig. 4-18 The non-synchronous boost AC-DC converter topology used for resistive matching control strategy [105].

The control strategy proposed in [106] employs a full-bridge rectifier circuit, similar to the one previously described, equipped with two MOSFET switches to enhance the output power of a cable-clamped MFEH. The control technique monitors the input current to the rectifier and load resistance to determine the initial operating point of the active rectifier circuit. This approach adjusts the input impedance of the rectifier circuitry to maximize output power. The authors emphasize that this technique achieves maximum power tracking despite changes in source impedance and load conditions. The authors also report that the proposed control technique is only applicable to MFEHs that reach saturation.

Noohi *et al.* [99] proposed a direct AC-DC converter topology based on an H-bridge type rectifier topology to maximize the output power of a free-standing MFEH designed to harvest energy from a transmission line over a long distance. Their control technique, illustrated in Fig. 4-19, performs maximum power point tracking using impedance matching while also regulating the output voltage. The H-bridge MOSFET configuration is used to transfer harvested energy to a capacitor, followed by a Schmitt trigger-based voltage regulator. The controller monitors the voltage output of the regulator and employs a feedback loop to maintain the system at the optimal operating point through impedance matching. However, this design assumes that coil inductance is negligible, which is a critical oversight in magnetic field energy harvesting, as uncompensated coil inductance reduces system efficiency. In contrast, Tse *et al.* [107] proposed a maximum power point tracking technique for electromagnetic energy harvesters with non-negligible internal reactance by using a direct AC-DC conversion approach, as shown in Fig. 4-20. While most studies measure the internal inductance of the

energy harvester and compensate it externally using composite capacitors, their method compensates for coil inductance without prior knowledge of the coil impedance. Their control strategy employs a perturb-and-observe approach to measure and compensate for coil inductance while simultaneously maximizing output power through resistive matching. The primary drawback of this technique is its slow response time.

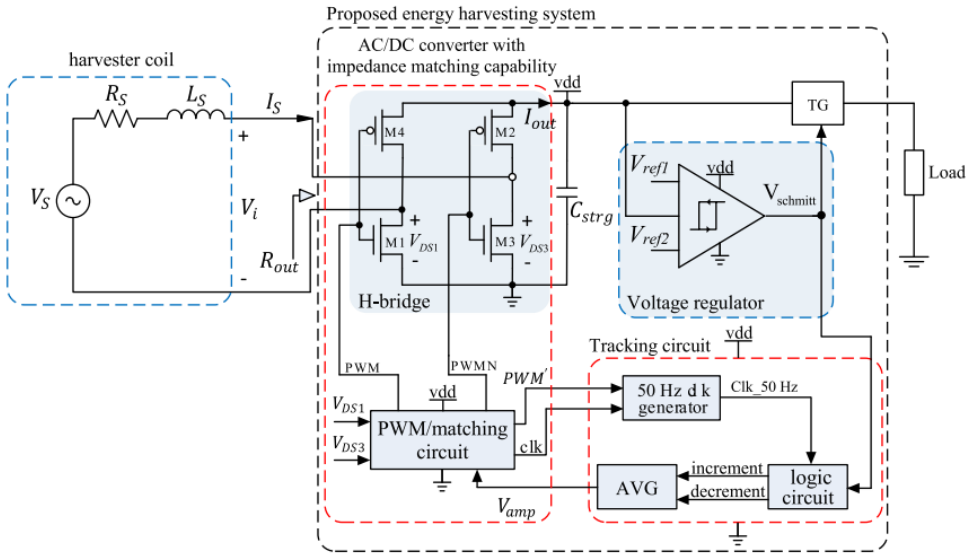

Fig. 4-19 The control technique introduced for impedance matching while voltage regulating using an H-Bridge type AC-DC converter topology [99]

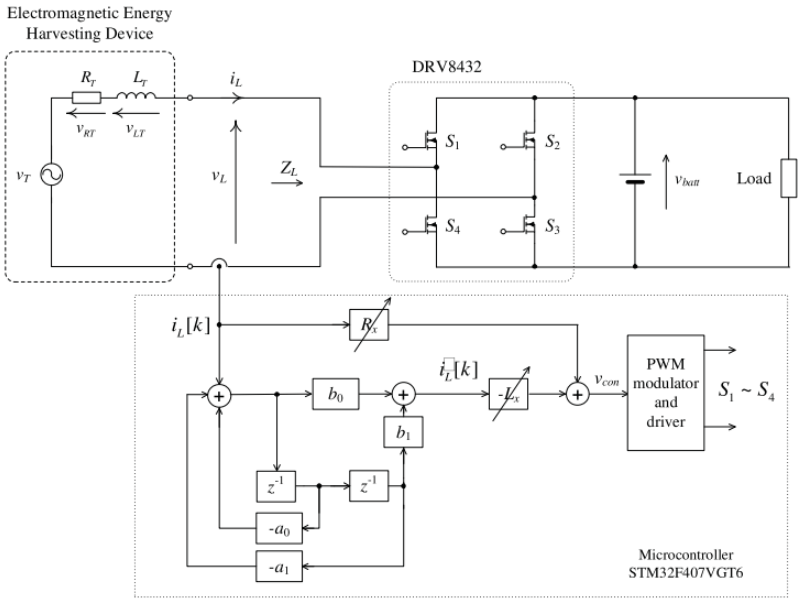

Fig. 4-20 Maximum power point tracking control technique for electromagnetic energy harvesters with non-negligible internal reactance

In literature, various control techniques that are suitable for advanced control of the proposed magnetic field energy harvesting system can be found. However, the control strategy depends on the circuitry used. Some studies employ direct AC-DC conversion for power control, while others use initial rectifiers followed by DC-DC converter topologies to manage power flow [108,109]. Theoretical analysis in this study indicates that an impedance matching control technique is suitable for maximizing power transfer from the energy harvester to the converter. However, preliminary performance analysis revealed that optimal resistance changes due to losses in higher rail current levels. Therefore, a control technique such as perturb-and-observe, which monitors output power, is necessary. This approach enables the converter to adjust the equivalent resistance until it reaches the optimal resistance point, maximizing output power. Additionally, in order to address the intermittent nature of magnetic field energy near rail tracks in electric railways, an energy storage unit is required for reliable operation. Thus, voltage regulation is essential to maintain a stable input voltage for the energy storage unit.

Furthermore, the proposed energy harvesting system requires energy management algorithms to optimize the performance of the energy harvesting unit. Most control units demand additional power to operate, and given the intermittent nature of the energy source, implementing energy management protocols is crucial for efficient operation of the energy harvester. Some studies in the literature have addressed this challenge by employing low-power control circuitry that does not require ancillary power. For example, [99] utilized low-power comparators and basic digital gates to mitigate this issue. However, low-power energy harvesting systems with intermittent energy supplies often encounter startup challenges, with cold start being a significant problem. Several research studies have incorporated cold-start circuits to initialize the power management circuit, including transformer-based, LC oscillator-based, and micro-electro-mechanical systems (MEMS)-based approaches [110]. Additionally, some studies have employed separate supercapacitors or battery storage units as startup mechanisms [111,112]. Task scheduling techniques with predetermined schedules also present a potential solution to address startup issues in energy harvesters. Further investigation is required to optimize the performance of the proposed MFEH through these techniques.

4.5 Summary

This chapter documented the development of the power management unit for the magnetic field energy harvesting system. The discussion began with a thorough analysis of rectifier requirements and evaluated suitable topologies for the proposed energy harvesting system. A full-bridge diode rectifier configuration was selected based on its stable output. In the next section the critical need for power management unit in the energy harvesting system was addressed, proposing an FSBB converter as the optimal solution. The theoretical framework for the FSBB converter was carefully developed through detailed derivations while emphasizing on establishing impedance matching under varying load conditions by adjusting duty cycle of the FSBB converter.

The implementation process of the FSBB circuit was described, beginning with the component selection process and followed by comprehensive experimental validation. The results from extensive testing conclusively demonstrated the converter's ability to maintain maximum output power across a wide range of load conditions through precise duty cycle modulation. Furthermore, the study extensively detailed how the output power of the MFEH was maximized under different rail currents. This was achieved by adjusting the duty cycle to modulate the equivalent circuit resistance. The experimental results quantitatively characterized the system's performance, with a maximum output power of 3.27 W recorded. This peak was achieved under a 450 A rail current by setting the duty cycle to 0.6 and connecting a 60 Ω load. The chapter concluded with an extensive discussion on methods to improve MFEH efficiency. This discussion first addressed improvements in energy harvesting capability and the reduction of losses within the MFEH itself. The discussion further assessed the power losses associated with the integrated power management circuit and methods to mitigate the losses in integrated circuitry. In the last section, a detailed description of several advanced control strategies documented in the literature was provided. The necessity of a robust control technique for the proposed energy harvesting unit was further elaborated, and the suitability of the reported control strategies for this study was compared.

CHAPTER 5 DISCUSSION AND CONCLUSION

This study presents the development and validation of an efficient free-standing magnetic field energy harvesting system designed to power autonomous devices in WSNs employed in railway applications. The implemented MFEH demonstrates the capability to generate sufficient electrical power when positioned in proximity to current-carrying rail tracks, offering a sustainable energy solution for railway monitoring systems. The research study makes significant advancements beyond existing literature on free-standing MFEH through its novel power management circuit design. The developed energy harvesting system's key innovation lies in its ability to maintain maximum power extraction under variable load conditions, addressing a critical limitation in reported literature.

This chapter provides a comprehensive comparison between the research outcomes of this study and prior work in free-standing magnetic energy harvesting. Following this comparative analysis, the thesis presents a structured summary, draws conclusions based on experimental results and proposes specific directions for future research to enhance the performance and applicability of free-standing MFEHs. The conclusions drawn from this study are supported by extensive experimental validation and comparative analysis with existing literature, establishing a solid foundation for future advancements in free-standing MFEHs in electric railway environments.

5.1 Comparison and Discussion

In railway transportation systems it is essential to conduct periodic maintenance and identify faults and degradations to ensure reliability of service and guarantee passenger safety. While traditional maintenance methods remain prevalent, recent technological advancements have introduced condition monitoring techniques as a more efficient alternative. These techniques analyze vast amounts of sensor data to detect faults, degradations, and potential failures before they escalate. Given the demanding operational environment of railway network which are prone to frequent breakdowns, such monitoring systems have gained significant attraction.

WSNs are particularly well-suited for this application, as they typically employ numerous sensors deployed across diverse terrains, including remote and inaccessible locations, while

facilitating real-time data transmission. However, conventional power solutions, such as electrochemical batteries, present challenges due to their limited lifespan and finite energy capacity. Therefore, energy harvesting offers a sustainable alternative by scavenging ambient energy to power WSN components, thereby eliminating dependency on battery replacements.

Among various energy harvesting techniques explored for powering autonomous devices in railway applications, magnetic field energy harvesting stands out as a viable solution for electric railway environments. Although other studies have investigated alternative energy sources such as solar, vibration, and thermal energy, this study demonstrates that MFEH holds distinct advantages for powering WSNs in electric railways. To substantiate this claim, Table 5-1 presents a comparative analysis between existing energy harvesting methods and the outcomes of this research, highlighting the superior feasibility of the proposed MFEH in electric railway environments.

Table 5-1 Comparison of energy harvesters proposed for railway systems

	Solar [25]	Wind [27]	Vibration [37]	Thermoelectric [44]	This Work
Maximum Power output	10.934 W	0.8 W	1.365 W	316.8 mW	3.27 W
Dimensions **(cm^3)**	146×220×0.2	45×45×8.4	-	5.44×5.44×3.4	12×10×10
Cost	High	High	High	High	Low
Installation	Hard	Hard	Hard	Hard	Easy
Reliability	Medium	Low	Medium	Low	High
Power Management	-	-	-	LTC3105 TPS63070	FSBB

As demonstrated in Table 5-1, various energy harvesting methods have been explored for powering autonomous devices in railway environments, each with distinct advantages and limitations. Among these, the solar energy harvester reported in [25] achieves the highest power output due to its large-scale design comprising four solar panels. However, widespread deployment of such systems across railway networks would be expensive and logistically challenging. Furthermore, solar energy harvesting exhibits inherent reliability issues due to dependence on weather conditions and cannot be implemented in underground sections of railway networks, significantly limiting its applicability.

Although wind energy harvesting is typically weather dependent, innovative wind energy harvesters such a reported in [27], utilize airflow from passing trains to generate power. While this approach demonstrates creative engineering, its practical implementation is constrained by relatively low energy yields and the maintenance requirements associated with mechanical turbine components. Similarly, vibration-based energy harvesters though capable of generating substantial power, often involve complex mechanical transduction mechanisms, as exemplified by the study in [37]. Fabrication processes of these systems are typically costly and require physical connection to rail infrastructure for operation, presenting significant barriers to large-scale adoption.

In contrast, the free-standing magnetic field energy harvester proposed in this study offers several compelling advantages for electric railway applications. It employs a non-invasive mechanism that does not interfere with existing rail infrastructure or its operation. In addition, the developed MFEH achieves competitive power output levels while maintaining consistent performance independent of environmental conditions and its harvested energy can be directly utilized by in WSNs, to power varying DC loads while ensuring maximum power delivery.

Table 5-2: Comparison of previous studies on free-standing MFEH and this study

	[71]	[73]	[113]	[114]	This Work
Core material	Ferroxcube 4B1	MnZn Ferrite (PC40)	Ferrite	Permalloy 1J85	MnZn Ferrite (PC95)
Core Dimensions (cm^3)	17×5×5	24.2×10×10	15×6×6	4×3×3	12×10×10
Number of windings	80000	2798	3000	4000	2065
Wire diameter	0.1 mm	0.5 mm	0.4 mm	0.15 mm	0.5 mm
The maximum Output power	40.5 mW	5.05 W	182 mW	13.25 mW	3.27 W
Current and frequency	200 A 50 Hz	520 A 50 Hz	300 A 50 Hz	100 A 50 Hz	350 A 50 Hz
Power Management	No	No	TPS54202	No	FSBB

A comparison of free-standing magnetic field energy harvesting devices, including this study, is presented in Table 5-2. While research on free-standing magnetic field energy harvesting systems for railway environments remains limited, several notable studies have explored this

technology with varying approaches. The studies in [71,73,113] investigated magnetic field energy harvesting near current-carrying rail tracks, similar to this work. In contrast, [113] presented a free-standing MFEH for installation on freight trains, while [114] focused on energy harvesting near electric bus bars. Among the studies compared in the table, only [113] incorporated a power management circuit, though its functionality was limited to voltage regulation which limits the ability to maximize the power output of the energy harvester.

In comparison to MFEHs reported in [71,113,114], the MFEH presented in this study generates a higher power output. However, the device presented in [73] achieves the highest power output among all compared studies. The increased power output of their device is attributed to its design characteristics: an extended core structure, increased coil windings, and operation under high rail currents (520 A). However, this configuration presents practical limitations as its placement directly beneath the rail track, is impractical for real-world implementation although it maximize flux linkage. Furthermore, the absence of a power conversion and management unit in their design restricts their applicability for direct DC power delivery to autonomous devices.

The proposed design achieves comparatively high output power while reducing bulkiness. Unlike other studies, this design uses fewer coil windings, though the volume of copper consumed cannot be directly compared due to limited available data. However, the winding coil is distributed across the core’s length, which reduces the bulkiness of the design. Furthermore, the core design itself has been optimized for compactness. While the core's effective permeability depends on its structure, the proposed design achieves a smaller footprint without sacrificing output power.

This study advances the field through several key innovations. The implementation of an optimized power management system enables maximum power extraction under varying operating conditions including changes in both source current and load resistance, while maintaining practical positioning adjacent to rail tracks. Experimental results demonstrate robust performance across a wide rail current range (0-500 A) and confirm direct DC power delivery compatibility for WSN components. These combined advantages address both performance and implementation challenges present in alternative designs. Thus, promoting the developed MFEH as a particularly viable solution for providing a sustainable power supply for autonomous devices in WSNs deployed in electric railway applications.

5.2 Conclusion

This thesis proposed an efficient free-standing MFEH designed to scavenge energy from the magnetic fields generated by time-varying currents in electric railway networks. The research includes comprehensive theoretical analyses, FEM simulations, optimization through parametric simulation studies, material selection criteria, design and fabrication of the power management unit, and laboratory testing of the developed system.

The simulation analyses conducted provided critical insights into the intercorrelated parameters of the MFEH. It was found that a longer core with a smaller cross-sectional area enhances power output by improving the core's effective permeability. The inclusion of flux collectors increased the magnetic flux density within the core, at times exceeding the saturation flux density of the core material. To mitigate core saturation, the cross-sectional area was carefully optimized using parametric simulations. Additionally, a detailed coil parameter study, supported by graphical illustrations, revealed that power output is primarily dependent on the volume of copper wound around the core. While increasing the number of coil windings improved both power output and voltage, a trade-off between wire diameter and winding count was implemented to maintain voltage at a suitable level without laying excessive stress on the power management circuit components.

Based on the findings of the simulation analyses, an MFEH prototype was fabricated and subjected to preliminary performance testing. Under a 450 A current applied through the rail track, the harvester generated a maximum AC power output of 4 W with load resistance tuned to optimal resistance of 100 Ω at that rail current level. These results informed the design specifications for the power management circuit, which was developed and tested in a laboratory environment.

The power management unit incorporated a full-bridge rectifier followed by a four-switch buck-boost converter. The integrated system demonstrated effective operation, in a laboratory setting delivering a maximum power output of 3.27 W when a 60 Ω load was connected while the FSBB operated at a 0.7 duty cycle with a 450 A current applied on through the rail track. The power management circuit showcased the capacity to extract maximum power output by adjusting the duty cycle of the FSBB converter under varying operating condition including variations in both rail current and load resistance. This approach addressed a key limitation in

existing research by ensuring maximum power delivery under fluctuating operating conditions. Furthermore, the variation in the optimal resistance of the energy harvester at different rail current levels was highlighted in the study. Despite this variation, the equivalent resistance was successfully adjusted to approach the optimal resistance through duty cycle modifications by the integrated FSBB circuit, thereby enhancing the power output of the energy harvesting system. In conclusion, the proposed MFEH system proves capable of reliably supplying power to wireless sensors and devices in WSNs deployed in electric railway environments. The combination of optimized harvester design and adaptive power management ensures efficient energy extraction and improved performance, making it a viable solution for real-world applications.

5.3 Future work

This thesis establishes a comprehensive theoretical foundation for the design of an efficient free-standing magnetic field energy harvester, supported by simulations and experimental validation through prototype fabrication and testing. While the proposed system demonstrates practical feasibility and suitability for powering WSNs in electric railway environments, several areas for further improvement have been identified based on the findings of the study.

One key limitation of the current MFEH design is its tendency to reach magnetic saturation prematurely. Future research should focus on optimizing the geometry of the MFEH to capture greater magnetic flux, thereby increasing power output. Additionally, the ferrite core material used in this study, while effective, is both fragile and heavy. Investigating alternative materials with superior mechanical robustness and magnetic properties should be prioritized in future work. Since rail currents are intermittent, occurring only when a train passes, an energy storage unit is essential to ensure continuous power delivery. Supercapacitors present an ideal solution due to their high power density and rapid charge-discharge capabilities. However, further research is needed to develop efficient supercapacitor charging and discharging algorithms, potentially through advanced control of the existing FSBB converter for enhanced energy management.

To enhance system efficiency and controllability, the FSBB converter should incorporate an advanced control technique capable of tracking the maximum power point of the energy harvester by impedance monitoring while dynamically managing energy flow between the harvester, storage unit, and load. Once an energy storage system is integrated, intelligent control algorithms implemented via a DSP in conjunction with the FSBB converter could further improve energy management of the energy harvesting system. In addition, the control circuitry of the energy harvesting unit should be equipped with cold start circuits to address the intermittent availability of magnetic field energy in railway environments.

Finally, while core saturation remains a challenge, future studies could explore techniques for maximizing power extraction even under saturated conditions. Research on cable-clamped magnetic energy harvesters, which face similar saturation issues, may provide insights adoptable for free-standing MFEH systems. Extending these investigations could yield innovative solutions for maintaining high efficiency across varying magnetic field strengths.

By addressing these areas, future work can significantly enhance the performance, reliability, and practicality of free-standing magnetic field energy harvesters for railway applications.

APPENDIX

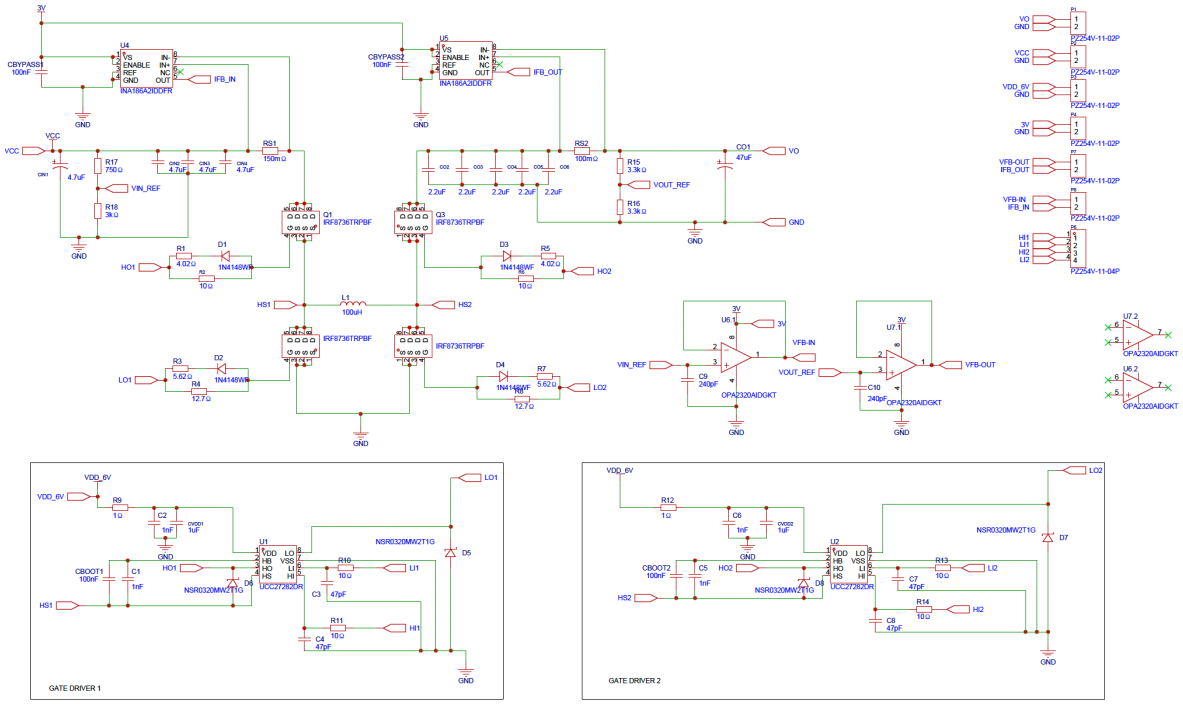

Fig. A-0-1 Schematic diagram of the FSBB converter

REFERENCES

[1] Selmic RR, Phoha V V, Serwadda A. Wireless Sensor Networks. Springer; 2016.

[2] Li X, Hu G, Guo Z, Wang J, Yang Y, Liang J. Frequency Up-Conversion for Vibration Energy Harvesting: A Review. Symmetry (Basel) 2022;14:631. https://doi.org/https://doi.org/10.3390/sym14030631.

[3] Sanad MF, Shalan AE, Abdellatif SO, Serea ESA, Adly MS, Ahsan MdA. Thermoelectric Energy Harvesters: A Review of Recent Developments in Materials and Devices for Different Potential Applications. Top Curr Chem 2020;378:48. https://doi.org/10.1007/s41061-020-00310-w.

[4] Safaei B, Sertan E, Mohammad KK, and Arman S. State-of-the-art review of energy harvesting applications by using thermoelectric generators. Mechanics of Advanced Materials and Structures 2024;31:5605–37. https://doi.org/10.1080/15376494.2023.2217660.

[5] Xu C, Wang W, Su W, Duan M, Hu M. Sensitivity Analysis of Free-Standing Columnar Magnetic Field Energy Harvester for Powering Wireless Monitoring Sensors. IEEE Transactions on Circuits and Systems I: Regular Papers 2023;70:4650–9. https://doi.org/10.1109/TCSI.2023.3306983.

[6] Li W, Sun A, Wang X, Chen Y, Wang C, Li Y, et al. Isolated Orthogonal Magnetic Energy Harvesting System Around High Voltage Transmission Lines. Journal of Electrical Engineering & Technology 2024;19:4239–52. https://doi.org/10.1007/s42835-024-01839-2.

[7] Barnard M. Most Rail Is Already Electric And All Will Be Even In North America. Forbes 2023.

[8] Ngamkhanong C, Kaewunruen S, Afonso Costa BJ. State-of-the-Art Review of Railway Track Resilience Monitoring n.d. https://doi.org/10.3390/infrastructures3010003.

[9] Mosleh A, Ribeiro D, Malekjafarian A, Martínez-Rodrigo MD. Advances in Condition Monitoring of Railway Infrastructure. Sensors 2024;24. https://doi.org/10.3390/s24030830.

[10] Davari N, Veloso B, de Assis Costa G, Pereira PM, Ribeiro RP, Gama J. A Survey on Data-Driven Predictive Maintenance for the Railway Industry. Sensors 2021;21:5739. https://doi.org/https://doi.org/10.3390/s21175739.

[11] Rolek P, Bruni S, Carboni M. Condition monitoring of railway axles based on low frequency vibrations. Int J Fatigue 2016;86:88–97. https://doi.org/https://doi.org/10.1016/j.ijfatigue.2015.07.004.

[12] Kostrzewski M, Melnik R. Condition Monitoring of Rail Transport Systems: A Bibliometric Performance Analysis and Systematic Literature Review. Sensors 2021;21. https://doi.org/10.3390/s21144710.

[13] Bianchi Giovanni, Fanelli Chiara, Freddi Francesco, Giuliani Felice, La Placa Aldo. Systematic review railway infrastructure monitoring: From classic techniques to predictive maintenance. Advances in Mechanical Engineering 2025;17:16878132241285632. https://doi.org/10.1177/16878132241285631.

[14] Hodge VJ, O'Keefe S, Weeks M, Moulds A. Wireless Sensor Networks for Condition Monitoring in the Railway Industry: A Survey. IEEE Transactions on Intelligent Transportation Systems 2015;16:1088–106. https://doi.org/10.1109/TITS.2014.2366512.

[15] Chan ICF. 2022/10/17 - 2022/10/18 - Facilitation and Promotion of I&T For Enhancement of Railway Safety – Hong Kong Experience - International Railway Safety Council 2022. 2022.

[16] Takikawa M. Innovation in Railway Maintenance utilizing Information and Communication Technology (Smart Maintenance Initiative). n.d.

[17] Dziadak B, Kucharek M, Starzyński J. Powering the WSN Node for Monitoring Rail Car Parameters, Using a Piezoelectric Energy Harvester. Energies (Basel) 2022;15. https://doi.org/10.3390/en15051641.

[18] Bin S, Sun G. Optimal Energy Resources Allocation Method of Wireless Sensor Networks for Intelligent Railway Systems. Sensors 2020;20. https://doi.org/10.3390/s20020482.

[19] Prauzek M, Konecny J, Borova M, Janosova K, Hlavica J, Musilek P. Energy Harvesting Sources, Storage Devices and System Topologies for Environmental Wireless Sensor Networks: A Review. Sensors 2018;18:2446. https://doi.org/https://doi.org/10.3390/s18082446.

[20] Qi N, Dai K, Yi F, Wang X, You Z, Zhao J. An Adaptive Energy Management Strategy to Extend Battery Lifetime of Solar Powered Wireless Sensor Nodes. IEEE Access 2019;7:88289–300. https://doi.org/10.1109/ACCESS.2019.2919986.

[21] Hosseinkhani A, Younesian D, Eghbali P, Moayedizadeh A, Fassih A. Sound and vibration energy harvesting for railway applications: A review on linear and nonlinear techniques. Energy Reports 2021;7:852–74. https://doi.org/https://doi.org/10.1016/j.egyr.2021.01.087.

[22] Hodge VJ, O'Keefe S, Weeks M, Moulds A. Wireless Sensor Networks for Condition Monitoring in the Railway Industry: A Survey. IEEE Transactions on Intelligent Transportation Systems 2015;16:1088–106. https://doi.org/10.1109/TITS.2014.2366512.

[23] Bosso N, Magelli M, Zampieri N. Application of low-power energy harvesting solutions in the railway field: a review. Vehicle System Dynamics 2021;59:841–71. https://doi.org/10.1080/00423114.2020.1726973.

[24] Cii S, Tomasini G, Bacci ML, Tarsitano D. Solar Wireless Sensor Nodes for Condition Monitoring of Freight Trains. IEEE Transactions on Intelligent Transportation Systems 2022;23:3995–4007. https://doi.org/10.1109/TITS.2020.3038319.

[25] Hao D, Zhang T, Guo L, Feng Y, Zhang Z, Yuan Y. A High-Efficiency, Portable Solar Energy-Harvesting System Based on a Foldable-Wings Mechanism for Self-Powered Applications in Railways. Energy Technology 2021;9:2000794. https://doi.org/10.1002/ente.202000794.

[26] Pan H, Li H, Zhang T, Laghari AA, Zhang Z, Yuan Y, et al. A portable renewable wind energy harvesting system integrated S-rotor and H-rotor for self-powered applications in high-speed railway tunnels. Energy Convers Manag 2019;196:56–68. https://doi.org/https://doi.org/10.1016/j.enconman.2019.05.115.

[27] Hongye pan, Jia C, Li H, Zhou X, Fang Z, Wu X, et al. A renewable energy harvesting wind barrier based on coaxial contrarotation for self-powered applications on railways. Energy 2022;258:124842. https://doi.org/https://doi.org/10.1016/j.energy.2022.124842.

[28] Tairab AM, Wang X, Zhang Z, Hao D, Abdelrahman M, Salman W, et al. The Nexus of IoT technology: A renewable multi-module energy harvester for self-powered on railway. Sustainable Materials and Technologies 2023;38:e00752. https://doi.org/https://doi.org/10.1016/j.susmat.2023.e00752.

[29] Zhang T, Kong L, Zhu Z, Wu X, Li H, Zhang Z, et al. An electromagnetic vibration energy harvesting system based on series coupling input mechanism for freight railroads. Appl Energy 2024;353:122047. https://doi.org/https://doi.org/10.1016/j.apenergy.2023.122047.

[30] Wang Y, Li S, Wang P, Gao M, Ouyang H, He Q, et al. A multifunctional electromagnetic device for vibration energy harvesting and rail corrugation sensing. Smart Mater Struct 2021;30:125012. https://doi.org/10.1088/1361-665X/ac31c5.

[31] Pan Y, Zuo L, Ahmadian M. A half-wave electromagnetic energy-harvesting tie towards safe and intelligent rail transportation. Appl Energy 2022;313:118844. https://doi.org/https://doi.org/10.1016/j.apenergy.2022.118844.

[32] Wang P, Yang F, Gao M, Wang Y. Study on an elastic lever system for electromagnetic energy harvesting from rail vibration. Journal of Vibroengineering 2019;21:384–95. https://doi.org/10.21595/jve.2018.19715.

[33] Wang P, Yang F, Gao M, Wang Y. Study on an elastic lever system for electromagnetic energy harvesting from rail vibration. Journal of Vibroengineering 2019;21:384–95. https://doi.org/10.21595/jve.2018.19715.

[34] Zhang X, Zhang Z, Pan H, Salman W, Yuan Y, Liu Y. A portable high-efficiency electromagnetic energy harvesting system using supercapacitors for renewable energy applications in railroads. Energy Convers Manag 2016;118:287–94. https://doi.org/https://doi.org/10.1016/j.enconman.2016.04.012.

[35] Wang W, Huang R-J, Huang C-J, Li L-F. Energy harvester array using piezoelectric circular diaphragm for rail vibration. Acta Mechanica Sinica/Lixue Xuebao 2014;30:884–8. https://doi.org/10.1007/s10409-014-0115-9.

[36] Cao Yalei, Zong Rui, Wang Jianjun, Xiang Hongjun, Tang Lihua. Design and performance evaluation of piezoelectric tube stack energy harvesters in railway systems. J Intell Mater Syst Struct 2022;33:2305–20. https://doi.org/10.1177/1045389X221085654.

[37] Shan G, Wang D, Zhu M. Piezo stack energy harvesters with protection components for railway applications. Sens Actuators A Phys 2024;373:115454. https://doi.org/https://doi.org/10.1016/j.sna.2024.115454.

[38] Yang F, Gao M, Wang P, Zuo J, Dai J, Cong J. Efficient piezoelectric harvester for random broadband vibration of rail. Energy 2021;218. https://doi.org/10.1016/j.energy.2020.119559.

[39] Wang J, Shi Z, Xiang H, Song G. Modeling on energy harvesting from a railway system using piezoelectric transducers. Smart Mater Struct 2015;24:105017. https://doi.org/10.1088/0964-1726/24/10/105017.

[40] Qi L, Pan H, Pan Y, Luo D, Yan J, Zhang Z. A review of vibration energy harvesting in rail transportation field. IScience 2022;25:103849. https://doi.org/https://doi.org/10.1016/j.isci.2022.103849.

[41] Guo W, Long Y, Bai Z, Wang X, Liu H, Guo Z, et al. Variable stiffness triboelectric nano-generator to harvest high-speed railway bridge's vibration energy. Energy Convers Manag 2022;268:115969. https://doi.org/https://doi.org/10.1016/j.enconman.2022.115969.

[42] He Z, Xinjie S, Liwei Q, Jiqing J, Beibei D, Gang W. Sponge-Supported Triboelectric Nanogenerator for Energy Harvesting from Rail Vibration. Journal of Energy Engineering 2021;147:04021006. https://doi.org/10.1061/(ASCE)EY.1943-7897.0000751.

[43] Kim W-G, Kim D-W, Tcho I-W, Kim J-K, Kim M-S, Choi Y-K. Triboelectric Nanogenerator: Structure, Mechanism, and Applications. ACS Nano 2021;15:258–87. https://doi.org/10.1021/acsnano.0c09803.

[44] Gao M, Su C, Cong J, Yang F, Wang Y, Wang P. Harvesting thermoelectric energy from railway track. Energy 2019;180:315–29. https://doi.org/https://doi.org/10.1016/j.energy.2019.05.087.

[45] Foltz H, Constantine T, Martin A, Sebastian T, and Capitanachi Avila D. Thermoelectric energy harvesting for wireless onboard rail condition monitoring. International Journal of Rail Transportation 2024;12:514–31. https://doi.org/10.1080/23248378.2023.2201247.

[46] Amaro M, Tarawneh C, Foltz H, Toro RA, Peña C. PERFORMANCE OF A THERMOELECTRIC-BASED ENERGY HARVESTING DEVICE ON A REALISTIC RAILROAD ROUTE. 2022.

[47] Wang H, Shi G, Han C. A Free-Standing Electromagnetic Energy Harvester for Condition Monitoring in Smart Grid. Wireless Power Transfer 2021;2021. https://doi.org/10.1155/2021/6685308.

[48] 2019 IEEE 5th World Forum on Internet of Things (WF-IoT). IEEE; 2019.

[49] Gupta V, Kandhalu A, Rajkumar R. Energy harvesting from electromagnetic energy radiating from AC power lines. Proceedings of the 6th Workshop on Hot Topics in Embedded Networked Sensors, HotEmNets 2010, 2010. https://doi.org/10.1145/1978642.1978664.

[50] Yang H, Li Y, Liu Z, Luo H, Yan Y, He Z. An Accurate Power Model and High Power Density Design Method of Free-Standing Magnetic Field Energy Harvesters With H-Shaped Core. IEEE Transactions on Industrial Electronics 2023;70:7965–75. https://doi.org/10.1109/TIE.2022.3225854.

[51] Roscoe NM, Judd MD. Harvesting Energy From Magnetic Fields to Power Condition Monitoring Sensors. IEEE Sens J 2013;13:2263–70. https://doi.org/10.1109/JSEN.2013.2251625.

[52] Schmid F, Goodman CJ, Watson C. Overview of electric railway systems. 7th IET Professional Development Course on Railway Electrification Infrastructure and Systems (REIS 2015), 2015, p. 1–15. https://doi.org/10.1049/ic.2015.0320.

[53] Steimel A. Power-electronic grid supply of AC railway systems. 2012 13th International Conference on Optimization of Electrical and Electronic Equipment (OPTIM), 2012, p. 16–25. https://doi.org/10.1109/OPTIM.2012.6231844.

[54] Panda NK, Poikilidis M, Nguyen PH. Cost-effective upgrade of the Dutch traction power network: Moving to Bi-directional and controllable 3 kV DC substations for improved performance. IET Electrical Systems in Transportation 2023;13:e12084. https://doi.org/https://doi.org/10.1049/els2.12084.

[55] Elbelkasi M, Badran E, Abdel-Rahman M. Overview of DC and AC Electric Railway Systems Considering Energy Efficiency Enhancement Methods. Port-Said Engineering Research Journal 2019;0:0–0. https://doi.org/10.21608/pserj.2019.18206.1012.

[56] Allen John G, Aurelius John P, Black Joseph. Electric Power Supply for Commuter Rail: Are Railroads Keeping Up? Transp Res Rec 2011;2219:88–96. https://doi.org/10.3141/2219-11.

[57] Kolář V, Hrbáč R, Mlčák T. Measurement and simulation of stray currents caused by AC railway traction. 2015 16th International Scientific Conference on Electric Power Engineering (EPE), 2015, p. 764–8. https://doi.org/10.1109/EPE.2015.7161203.

[58] Park B, Huh S, Kim J, Kim H, Shin Y, Woo S, et al. The Magnetic Energy Harvester With Improved Power Density Using Saturable Magnetizing Inductance Model for Maintenance Applications Near High Voltage Power Line. IEEE Access 2021;9:82661–74. https://doi.org/10.1109/ACCESS.2021.3085989.

[59] Jiles D. Introduction to Magnetism and Magnetic Materials; Third Edition. n.d. https://doi.org/10.4324/9780429160097.

[60] Du L, Wang C, Li X, Yang L, Mi Y, Sun C. A Novel Power Supply of Online Monitoring Systems for Power Transmission Lines. IEEE Transactions on Industrial Electronics 2010;57:2889–95. https://doi.org/10.1109/TIE.2009.2037104.

[61] Zhuang Y, Xu C, Song C, Chen A, Lee W, Huang Y, et al. Improving Current Transformer-Based Energy Extraction From AC Power Lines by Manipulating Magnetic Field. IEEE Transactions on Industrial Electronics 2020;67:9471–9. https://doi.org/10.1109/TIE.2019.2952795.

[62] Paul S, Chang J. Design of novel electromagnetic energy harvester to power a deicing robot and monitoring sensors for transmission lines. Energy Convers Manag 2019;197:111868. https://doi.org/https://doi.org/10.1016/j.enconman.2019.111868.

[63] Najafi SAA, Ali AA, Sozer Y, Abreu-Garcia A De. Energy Harvesting from Overhead Transmission Line Magnetic fields. 2018 IEEE Energy Conversion Congress and Exposition (ECCE), 2018, p. 7075–82. https://doi.org/10.1109/ECCE.2018.8558356.

[64] Monagle D, Ponce E, Leeb SB. Generalized Analysis Method for Magnetic Energy Harvesters. IEEE Trans Power Electron 2022;37:15764–73. https://doi.org/10.1109/TPEL.2022.3195149.

[65] Gupta V, Kandhalu A, Rajkumar R. Energy harvesting from electromagnetic energy radiating from AC power lines. Proceedings of the 6th Workshop on Hot Topics in Embedded Networked Sensors, HotEmNets 2010, 2010. https://doi.org/10.1145/1978642.1978664.

[66] Moghe R, Yang Y, Lambert F, Divan D. A scoping study of electric and magnetic field energy harvesting for wireless sensor networks in power system applications. 2009 IEEE Energy Conversion Congress and Exposition, 2009, p. 3550–7. https://doi.org/10.1109/ECCE.2009.5316052.

[67] Yuan S, Huang Y, Zhou J, Xu Q, Song C, Thompson P. Magnetic Field Energy Harvesting Under Overhead Power Lines. IEEE Trans Power Electron 2015;30:6191–202. https://doi.org/10.1109/TPEL.2015.2436702.

[68] Yuan S, Huang Y, Zhou J, Xu Q, Song C, Yuan G. A high-efficiency helical core for magnetic field energy harvesting. IEEE Trans Power Electron 2017;32:5365–76. https://doi.org/10.1109/TPEL.2016.2610323.

[69] Wang H, Shi G, Han C. A Free-Standing Electromagnetic Energy Harvester for Condition Monitoring in Smart Grid. Wireless Power Transfer 2021;2021. https://doi.org/10.1155/2021/6685308.

[70] Espe AE, Mathisen G. Towards Magnetic Field Energy Harvesting near Electrified Railway Tracks. 2020 9th Mediterranean Conference on Embedded Computing (MECO), 2020, p. 1–4. https://doi.org/10.1109/MECO49872.2020.9134113.

[71] Espe AE, Haugan TS, Mathisen G. Magnetic Field Energy Harvesting in Railway. IEEE Trans Power Electron 2022;37:8659–68. https://doi.org/10.1109/TPEL.2022.3141437.

[72] Zhang J, Xu L, Shen T, Luo J. Energy harvesting approach for trackside health monitoring devices in railroads. IET Electr Power Appl 2022;16:100–11. https://doi.org/10.1049/elp2.12137.

[73] Kuang Y, Chew ZJ, Ruan T, Lane T, Allen B, Nayar B, et al. Magnetic field energy harvesting from the traction return current in rail tracks. Appl Energy 2021;292. https://doi.org/10.1016/j.apenergy.2021.116911.

[74] Kuang Y, Chew ZJ, Ruan T, Zhu M. Magnetic Field Energy Harvesting from Current-Carrying Structures: Electromagnetic-Circuit Coupled Model, Validation and Application. IEEE Access 2021;9:46280–91. https://doi.org/10.1109/ACCESS.2021.3068472.

[75] Ptitsyna N, Villoresi G, Kopytenko YA. Railway-generated magnetic field: Environmental aspects. Railway Transportation: Policies, Technology and Perspectives, 2009, p. 87–140.

[76] Feliziani M, Campi T, Cruciani S, Maradei F. Chapter 5 - Magnetic couplers for automotive WPT systems. In: Feliziani M, Campi T, Cruciani S, Maradei F, editors. Wireless Power Transfer for E-Mobility, Academic Press; 2024, p. 129–84. https://doi.org/https://doi.org/10.1016/B978-0-323-99523-8.00005-9.

[77] Zhao H, Zhang X, Wang Y, Liu K, Tian Z, Cheng S, et al. Comprehensive Investigation on the Influence of Magnetic Materials on the Weight and Performance of Onboard WPT Systems. IEEE Trans Ind Appl 2022;58:6842–51. https://doi.org/10.1109/TIA.2022.3188611.

[78] Cheng W. Interpretation of Impedance in the Light of Energy Dissipation and Eddy Current Nondestructive Evaluation of Pipe Wall Thickness. IEEE Trans Instrum Meas 2022;71:1–11. https://doi.org/10.1109/TIM.2022.3147310.

[79] Tashiro K, Wakiwaka H, Hattori G-Y. Estimation of Effective Permeability for Dumbbell-Shaped Magnetic Cores. IEEE Trans Magn 2015;51:1–4. https://doi.org/10.1109/TMAG.2014.2359468.

[80] Zhou SH, Chen ZY, Feng SM. Improvement Methods of Apparent Permeability of Ferromagnetic Core. Adv Mat Res 2013;712–715:1876–80. https://doi.org/10.4028/www.scientific.net/AMR.712-715.1876.

[81] Goodenough JB. Summary of losses in magnetic materials. IEEE Trans Magn 2002;38:3398–408. https://doi.org/10.1109/TMAG.2002.802741.

[82] James RD. Magnetic alloys break the rules. Nature 2015;521:298–9. https://doi.org/10.1038/521298a.

[83] Alger PL, Wagoner CD, Proteus Steinmetz C, Alger PL, Caldecott Schenectady E, Brittain JE, et al. Charles P. Steinmetz and the Development of Engineering Science. vol. 13. EDUCATION; 1974.

[84] Zhang X, Xu H, Huang S. Steinmetz-equation of magnetic core materials. Proc.SPIE, vol. 13554, 2025, p. 135540B. https://doi.org/10.1117/12.3064994.

[85] Stoyka K, Capua GD, Femia N. A Novel AC Power Loss Model for Ferrite Power Inductors. IEEE Trans Power Electron 2019;34:2680–92. https://doi.org/10.1109/TPEL.2018.2848109.

[86] Mn-Zn Ferrite Material characteristics Ferrite for switching power supplies Ferrite for high-frequency power supplies Large size ferrite for high power. n.d.

[87] “Permalloy 80 - ESPI Metals.” https://www.espimetals.com/index.php/technical-data/175-Permalloy%2080 n.d.

[88] Xu Y, Bader S, Oelmann B. Design, modeling and optimization of an m-shaped variable reluctance energy harvester for rotating applications. Energy Convers Manag 2019;195:1280–94. https://doi.org/https://doi.org/10.1016/j.enconman.2019.05.082.

[89] Liu Z, Zheng L, Bao S, Yang A, Zhou D, Chu J, et al. Modeling and Optimized Design of the Free-Standing Magnetic Field Energy Harvester Based on Accurate Estimation of Effective Permeability. IEEE Trans Power Electron 2025;40:14014–26. https://doi.org/10.1109/TPEL.2025.3564377.

[90] Khan D, Basim M, Ali I, Pu Y, Cheol Hwang K, Yang Y, et al. A Survey on RF Energy Harvesting System with High Efficiency RF-DC Converters. Journal of Semiconductor Engineering 2020;1. https://doi.org/10.22895/jse.2020.0002.

[91] Beheshti Asl M, Zarifi MH. RF to DC micro-converter in standard CMOS process for on-chip power harvesting applications. AEU - International Journal of Electronics and Communications 2014;68:1180–4. https://doi.org/https://doi.org/10.1016/j.aeue.2014.06.008.

[92] Serov O, Chaari MZ. Unleashing the Potential: 2.45 GHz Energy Harvesting with a Rectenna and a 6-Stage Cockcroft- Walton Voltage Multiplier. 2024 International Technical Conference on Circuits/Systems, Computers, and Communications (ITC-CSCC), 2024, p. 1–6. https://doi.org/10.1109/ITC-CSCC62988.2024.10628272.

[93] Peters C, Kessling O, Henrici F, Ortmanns M, Manoli Y. CMOS Integrated Highly Efficient Full Wave Rectifier. 2007 IEEE International Symposium on Circuits and Systems, 2007, p. 2415–8. https://doi.org/10.1109/ISCAS.2007.377947.

[94] Roy S, Azad ANMW, Baidya S, Khan F. A Comprehensive Review on Rectifiers, Linear Regulators, and Switched-Mode Power Processing Techniques for Biomedical Sensors and Implants Utilizing in-Body Energy Harvesting and External Power Delivery. IEEE Trans Power Electron 2021;36:12721–45. https://doi.org/10.1109/TPEL.2021.3075245.

[95] Dwari S, Parsa L. Efficient low voltage direct AC/DC converters for self-powered wireless sensor nodes and mobile electronics. INTELEC 2008 - 2008 IEEE 30th International Telecommunications Energy Conference, 2008, p. 1–7. https://doi.org/10.1109/INTLEC.2008.4664097.

[96] Chen J, Peng H, Feng Z, Kang Y. A GaN BCM AC-DC Converter for Sub-1 V Electromagnetic Energy Harvesting with Enhanced Output Power. IEEE Trans Power Electron 2021;36:9285–99. https://doi.org/10.1109/TPEL.2020.3048195.

[97] Yiming Liu , Geng Tian , Yong Wang , Junhong Lin , Qiming Zhang , Hofmann Heath F. Active Piezoelectric Energy Harvesting: General Principle and Experimental Demonstration. J Intell Mater Syst Struct 2008;20:575–85. https://doi.org/10.1177/1045389X08098195.

[98] Edla M, Lim YY, Deguchi M, Padilla R V, Izadgoshasb I. An Improved Self-Powered H-Bridge Circuit for Voltage Rectification of Piezoelectric Energy Harvesting System. IEEE Journal of the Electron Devices Society 2020;8:1050–62. https://doi.org/10.1109/JEDS.2020.3025554.

[99] Noohi MS, Habibi M. An energy-efficient CMOS interface circuit with maximum power point tracking and power management capabilities for self-powered sensor node applications using 50/60 Hz transmission line magnetic field harvesters. Electrical Engineering 2023;105:1413–30. https://doi.org/10.1007/s00202-023-01740-7.

[100] Steigerwald RL. A comparison of half-bridge resonant converter topologies. IEEE Trans Power Electron 1988;3:174–82. https://doi.org/10.1109/63.4347.

[101] Mukherjee S, Barbosa P. Design and Optimization of an Integrated Resonant Inductor With High-Frequency Transformer for Wide Gain Range DC–DC Resonant Converters in Electric Vehicle Charging Applications. IEEE Trans Power Electron 2023;38:6380–94. https://doi.org/10.1109/TPEL.2023.3243807.

[102] Marvi F, Adib E, Farzanehfard H. Efficient ZVS Synchronous Buck Converter with Extended Duty Cycle and Low-Current Ripple. IEEE Transactions on Industrial Electronics 2016;63:5403–9. https://doi.org/10.1109/TIE.2016.2558483.

[103] Andersen TM, Zingerli CM, Krismer F, Kolar JW, Wang N, Mathuna C. Modeling and Pareto Optimization of Microfabricated Inductors for Power Supply on Chip. IEEE Trans Power Electron 2013;28:4422–30. https://doi.org/10.1109/TPEL.2012.2227815.

[104] Li Y, Yan Y, Yang H, Hu J, He Z. A Reconfigurable Rectifier-Based Power Improving Method of Free-Standing Two-Coil Magnetic Field Energy Harvesters Over a Wide Load Range. IEEE Trans Power Electron 2023;PP:1–6. https://doi.org/10.1109/TPEL.2023.3238763.

[105] Proynov PP, Szarka GD, Stark BH, McNeill N. Resistive matching with a feed-forward controlled non-synchronous boost rectifier for electromagnetic energy harvesting. 2013 Twenty-Eighth Annual IEEE Applied Power Electronics Conference and Exposition (APEC), 2013, p. 3081–6. https://doi.org/10.1109/APEC.2013.6520739.

[106] Li Y, Duan N, Liu Z, Hu J, He Z. Impedance-Matching-Based Maximum Power Tracking for Magnetic Field Energy Harvesters Using Active Rectifiers. IEEE Transactions on Industrial Electronics 2023;70:10730–9. https://doi.org/10.1109/TIE.2022.3219064.

[107] Tse KH, Chung HS. MPPT for Electromagnetic Energy Harvesters Having Nonnegligible Output Reactance Operating Under Slow-Varying Conditions. IEEE Trans Power Electron 2020;35:7110–22. https://doi.org/10.1109/TPEL.2019.2959625.

[108] Balato M, Costanzo L, Vitelli M. Maximization of the extracted power in resonant electromagnetic vibration harvesters applications employing bridge rectifiers. Sens Actuators A Phys 2017;263:63–75. https://doi.org/https://doi.org/10.1016/j.sna.2017.04.002.

[109] O'Connor T, Hyun JH, Ha DS. Power management circuit for kinetic energy harvesting from freight railcars. 2017 IEEE 60th International Midwest Symposium on Circuits and Systems (MWSCAS), 2017, p. 1426–9. https://doi.org/10.1109/MWSCAS.2017.8053200.

[110] Shi X, Cai M, Jiang Y. Key Role of Cold-Start Circuits in Low-Power Energy Harvesting Systems: A Research Review. Journal of Low Power Electronics and Applications 2024;14:55. https://doi.org/https://doi.org/10.3390/jlpea14040055.

[111] Carlson EJ, Strunz K, Otis BP. A 20 mV Input Boost Converter With Efficient Digital Control for Thermoelectric Energy Harvesting. IEEE J Solid-State Circuits 2010;45:741–50. https://doi.org/10.1109/JSSC.2010.2042251.

[112] Shrivastava A, Roberts NE, Khan OU, Wentzloff DD, Calhoun BH. A 10 mV-Input Boost Converter With Inductor Peak Current Control and Zero Detection for Thermoelectric and Solar Energy Harvesting With 220 mV Cold-Start and $-$14.5 dBm, 915 MHz RF Kick-Start. IEEE J Solid-State Circuits 2015;50:1820–32. https://doi.org/10.1109/JSSC.2015.2412952.

[113] Tao J, Wang Y, Cheng H, Mai R. Analysis and Design of Magnetic Field Energy Harvesting for Freight Train Sensors. IEEE Transactions on Transportation Electrification 2024;10:4503–12. https://doi.org/10.1109/TTE.2023.3314056.

[114] Yang H, Li Y, Liu Z, Luo H, Yan Y, He Z. An Accurate Power Model and High Power Density Design Method of Free-Standing Magnetic Field Energy Harvesters With H-Shaped Core. IEEE Transactions on Industrial Electronics 2023;70:7965–75. https://doi.org/10.1109/TIE.2022.3225854.